Photochemical & Photobiological Sciences

PERSPECTIVE

Cite this: *Photochem. Photobiol. Sci.*, 2019, **18**, 602

Ozone–climate interactions and effects on solar ultraviolet radiation

A. F. Bais, *[a] G. Bernhard, [b] R. L. McKenzie, [c] P. J. Aucamp, [d] P. J. Young, [e,f] M. Ilyas,[g] P. Jöckel [h] and M. Deushi [i]

This report assesses the effects of stratospheric ozone depletion and anticipated ozone recovery on the intensity of ultraviolet (UV) radiation at the Earth's surface. Interactions between changes in ozone and changes in climate, as well as their effects on UV radiation, are also considered. These evaluations focus mainly on new knowledge gained from research conducted during the last four years. Furthermore, drivers of changes in UV radiation other than ozone are discussed and their relative importance is assessed. The most important of these factors, namely clouds, aerosols and surface reflectivity, are related to changes in climate, and some of their effects on short- and long-term variations of UV radiation have already been identified from measurements. Finally, projected future developments in stratospheric ozone, climate, and other factors affecting UV radiation have been used to estimate changes in solar UV radiation from the present to the end of the 21st century. New instruments and methods have been assessed with respect to their ability to provide useful and accurate information for monitoring solar UV radiation at the Earth's surface and for determining relevant exposures of humans. Evidence since the last assessment reconfirms that systematic and accurate long-term measurements of UV radiation and stratospheric ozone are essential for assessing the effectiveness of the Montreal Protocol and its Amendments and adjustments. Finally, we have assessed aspects of UV radiation related to biological effects and human health, as well as implications for UV radiation from possible solar radiation management (geoengineering) methods to mitigate climate change.

Received 19th December 2018,
Accepted 19th December 2018

DOI: 10.1039/c8pp90059k

rsc.li/pps

1. Introduction

This paper is the first in a series,[1] and focuses on the effects of stratospheric ozone depletion, anticipated ozone recovery, and climate change on UV radiation reaching the Earth's surface, as well as the effects of other geophysical variables that affect UV radiation (Fig. 1). Before discussing new scientific findings attained since the previous Quadrennial Assessment report, a brief overview of the status of science at that time is provided, and then the main new findings related to ozone and climate science are briefly discussed. This background information is essential for understanding variations of UV radiation and assessing the contributions of the different factors that UV radiation depends on.

1.1 State of science in the 2014 EEAP report

The previous EEAP Assessment[2] reported that the Montreal Protocol was vital in protecting the ozone layer by reducing ozone-depleting substances (ODSs). As a result, any increases in UV radiation observed since the mid-1990s over northern mid-latitudes† remained small. Changes in UV radiation were predominantly caused by variability in cloudiness and aerosols rather than changes in ozone. At the time of the previous report, statistically significant decreases in UV-B radiation (280–315 nm) attributable to the beginning of ozone recovery had not been detected in any season and at any location. The absence of detectable trends was explained by the large

[a]*Laboratory of Atmospheric Physics, Aristotle University of Thessaloniki, Campus Box 149, 54124 Thessaloniki, Greece. E-mail: abais@auth.gr*
[b]*Biospherical Instruments Inc., 5340 Riley Street, San Diego, California, USA*
[c]*National Institute of Water & Atmospheric Research, NIWA Lauder, PB 50061 Omakau, Central Otago, New Zealand*
[d]*Ptersa Environmental Management Consultants, PO Box 915751, Faerie Glen, 0043, South Africa*
[e]*Lancaster Environment Centre, Lancaster University, Lancaster, UK*
[f]*Pentland Centre for Sustainability in Business, Lancaster University, Lancaster, UK*
[g]*School of Environmental Engineering, University Malaysia Perlis, Kangar, Malaysia*
[h]*Deutsches Zentrum fuer Luft- und Raumfahrt (DLR), Institut fuer Physik der Atmosphaere, Oberpfaffenhofen, Germany*
[i]*Meteorological Research Institute (MRI), Tsukuba, Japan*

†Throughout this document the latitude ranges for both the northern and southern hemispheres are defined as: polar latitudes (80°–90°); high latitudes (60°–80°); mid latitudes (30°–60°); tropics (0°–30°).

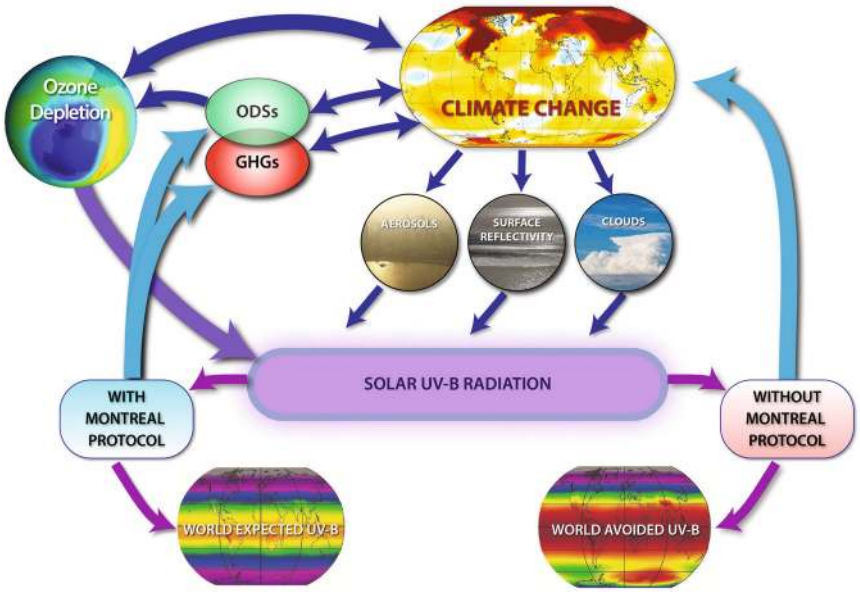

Fig. 1 Conceptual representation of the interactive effects of changes in greenhouse gases (GHGs) and ozone-depleting substances (ODSs) on climate and solar UV-B radiation at the Earth's surface. Increases of ODSs in the atmosphere have led to stratospheric ozone depletion and the ozone 'hole'. Actions prompted by the Montreal Protocol have resulted in decreasing ODSs and have helped to avoid large increases of solar UV-B radiation that would otherwise have occurred by the middle of the 21st century. Continued emissions of GHGs (*e.g.*, carbon dioxide, methane, and nitrous oxide) will change the climate and will also modify the recovery of stratospheric ozone, which is expected from decreasing concentrations of ODSs. Climate change will also affect clouds, surface reflectivity at high latitudes, where changes in sea ice and snow cover are expected, and aerosols near the Earth's surface. The combined effects of changes in ozone, aerosols, clouds, and reflectivity will determine future levels of UV-B radiation at the Earth's surface.

natural variability of UV-B radiation resulting from the many factors that influence it and the lack of suitable UV data prior to the 1990s.

Year-round increases in UV radiation were observed as early as the mid-1990s over some northern mid-latitude locations but were predominantly caused by reductions in cloudiness and aerosols. At several northern high-latitude sites, UV-B irradiance had decreased since the mid-1990s because of a reduction in snow- and ice-cover. These decreases were most prominent in the summer and autumn. However, large, short-term increases in the erythemal (sun-burning) UV dose had also been measured at several Arctic and Scandinavian sites in response to episodic decreases of stratospheric ozone, such as an event occurring in the spring of 2011[3] when the total erythemal UV dose accumulated over the low-ozone period of about 27 days increased by up to 50% at several sites in the Arctic and Scandinavia. Between February and April 2011, the total ozone at some locations was occasionally less than 50% of the climatological mean.

With continued effective implementation of the Montreal Protocol, future changes in UV-B irradiance outside the polar regions were projected to be dominated by changes in aerosols. These were projected to decrease significantly across the globe in the second half of the 21st century, particularly over heavily populated areas in Asia because of measures for improvement of air quality. However, confidence in the magnitude of the projected changes was low due to the uncertainty of future policies on emission controls.

Future levels of UV-B irradiance at high latitudes would be influenced by the recovery of stratospheric ozone and by changes in clouds and reflectivity of the Earth's surface. In Antarctica, reductions of up to 40% in noon-time erythemal UV radiation during spring were projected for 2100 because of the anticipated recovery of the stratospheric ozone. These projected reductions would be comparable in magnitude with the increases in UV radiation that had occurred in the past due to ozone depletion. Reductions in surface reflectivity due to ice-melt were projected to reduce UV-B irradiance by up to 10% in the Arctic, but confidence in the magnitude of these effects was low.

1.2 Current status of total and stratospheric ozone

The emissions and concentrations of ODSs in the atmosphere have been declining continuously since the mid-1990s because of the success of the Montreal Protocol. In response to this reduction in ODSs, global (60°S–60°N) column ozone is no longer declining. Small increases of 0.3 to 1.2% per decade since 1997 have been observed but are not statistically significant.[4] Different datasets of satellite and ground-based observations for the period 1997–2016 within 60°S–60°N show close to zero changes in total ozone for the tropics and the northern hemisphere (NH) and increases of 0.6% per decade for the southern hemisphere (SH). Generally, these changes are not statistically significant, except for two datasets showing small positive changes of 0.5 and 0.8% per decade in the tropics.[5] In recent years (2014–2017), total ozone has remained below the

average of the 1964–1980 period: about 2.2% for the global average (60°S–60°N), about 3.0% for the northern mid-latitudes (35°N–60°N), about 5.0% for the southern mid-latitudes (35°S–60°S), and less than 1% for the tropics (20°S–20°N).[4] These estimates are essentially the same as those reported in the previous report of the Scientific Assessment Panel.[6] The only exception is Antarctica, where statistically significant increases in total ozone inside the polar vortex have now been observed for the period 2001–2013 in austral spring (about 1.7% per year, statistically significant at the 95% confidence level) and summer (about 0.5% per year, statistically significant at the 90% confidence level).[4,7,8] Further evidence of decreasing depletion of stratospheric ozone over Antarctica has been reported[9] by analyzing ozone and inorganic chlorine measurements for the period 2005–2016 using data from the Microwave Limb Sounder onboard the Aura satellite.

Analysis of ozone-profile data from nine stations in Antarctica[7] has confirmed results from an earlier study,[8] which reported the first signs of recovery of Antarctic ozone based on data from only two stations. Statistically significant (95% confidence level) positive trends in ozone concentrations for 2001–2013 were found in the lower stratosphere (altitude 10–20 km) for austral spring. Of note, the second study[8] omitted data from 2015, which was influenced by aerosols from the eruption of the Chilean volcano, Calbuco,[10,11] and the long-lasting polar vortex,[12] both of which contributed to a record-sized ozone 'hole' that year. Subsequent studies have corroborated these conclusions with additional analyses of profiles from Antarctic ozonesondes[13] and multiple linear regression approaches with satellite data.[14]

There is some variation in trends in the ozone measured at different altitudes and latitudes, and these are generally consistent with our understanding of the physics and chemistry of ozone.[15,16] At mid-latitudes and the tropics, measured concentrations of ozone show an increase of 2–4% per decade in the upper stratosphere (altitude 35–45 km) since about 2000.[15] This increase is consistent with the projected recovery of stratospheric ozone resulting equally from decreasing concentrations of ODSs and increases in GHGs.[4] Increases of a similar magnitude were also reported from combined data of different satellites for the period 1998–2016.[17] However, that same study found that ozone concentrations in the lower stratosphere (altitudes below 24 km) of tropical and mid-latitudes (60°S–60°N) continued declining by about 1.0% per decade in the same period. For total ozone, there were no statistically significant changes. These results were not able to be reproduced by state-of-the-art models used in that study,[17] but more recent model studies, extended to 2017, suggest that the apparent decrease in ozone in the tropical and mid-latitude lower stratosphere is the result of interannual variability in atmospheric circulation.[18–20] A longer record of observations is required to conclusively determine whether this trend in lower stratospheric ozone is a forced response to changes in ODSs or climate, or whether it is part of natural variability.

In the remainder of the 21st century, we expect that the amounts of stratospheric ozone will be controlled by continuing decreases in ODSs and increases in GHGs. Decreasing ODSs will lead to increases in the concentrations of ozone at all altitudes and latitudes. Increasing GHGs will lead to cooling of the upper stratosphere and to increasing concentrations of ozone in the upper stratosphere at all latitudes because the rate of ozone destruction is slower at lower temperatures. Moreover, increasing GHGs will lead to changes in circulation resulting in decreases in concentrations of ozone in the lower stratosphere at low latitudes. At mid latitudes, the effect in the lower stratosphere depends on the assumed GHG emission scenario.[21]

Generally, total ozone is expected to increase above its levels in the pre-stratospheric ozone depletion period (1964–1980) at mid latitudes (termed "super recovery"), while in the tropics, total ozone will slightly decrease and remain below the levels observed during the 1964–1980 period. These small decreases in tropical total ozone are driven by decreases in ozone in the lower stratosphere and their magnitude is dependent on GHG emissions.[16,22]

In polar regions, cooling of the middle and upper stratosphere resulting from increased GHGs will drive increases in ozone in these atmospheric regions. For the lower stratosphere, the decline in ODSs will be the primary driver of increases in ozone over this century, with GHG-driven dynamical changes being additionally responsible for ozone increases in the Arctic (see also discussion in the following sections). However, the high interannual variability in stratospheric temperature in the Arctic means that individual years will likely continue to experience large losses of ozone throughout the 21st century.[4]

1.3 Benefits from the Montreal Protocol

1.3.1 Direct impacts. The implementation of the Montreal Protocol has already resulted in significant benefits for the stratospheric ozone layer and, consequently, for surface UV-B radiation. In the previous assessment, we discussed the direct environmental implications of the "world avoided" scenario, which describes a future without the Montreal Protocol where stratospheric ozone depletion had continued unabated.[23] By 2070, increases in UV-B radiation would have led to peak UV Index (UVI)‡ values greater than 35 in the tropics and 5–15 at the sunlit northern polar cap, the latter being similar to or larger than the values found in the subtropics and tropics in 2000.[24] At mid latitudes, peak UVI values would have been approximately 3 times as high as in the period prior to the onset of stratospheric ozone depletion.[25]

More recent calculations with a chemistry-transport model have shown that, without the Montreal Protocol, a deep Arctic ozone 'hole', with total ozone values below 120 Dobson Units (DU), instead of the usual 400–450 DU, would have occurred in 2011 given the meteorological conditions in that year.[26] The decline of stratospheric ozone over northern hemisphere mid-

‡The UV Index (UVI) provides to the public a simple, dimensionless quantity to report the levels of the erythemally-weighted (or "sunburning") irradiance. It is calculated by multiplying the erythemally weighted irradiance expressed in units of W m^{-2} by 40.

latitudes would also have continued, with depletion twice that actually experienced in 2013. In addition, the Antarctic ozone 'hole' would have been 40% larger in 2013 relative to the actual situation, with enhanced loss of ozone also at sub-polar latitudes of the SH. These large reductions in ozone since 1980 would have resulted in increases in springtime UV-B radiation at the Earth's surface of about 10% at mid-latitudes and over 20% at high latitudes of both hemispheres in 2013, with important implications for the health of humans (see ref. 27) and ecosystems (see ref. 28 and 29).

Scientific estimates of future ozone and UV radiation levels rely on scenarios of declining ODSs resulting from continued adherence to the Montreal Protocol and its Amendments. However, a recent study[30] reported unexpected and persistent increases in global emissions of CFC-11, questioning the existing ODS-reduction scenarios. Moreover, the continued growth in the atmospheric concentrations of dichloromethane (CH_2Cl_2), a chlorocarbon not controlled by the Montreal Protocol, could offset some of the future benefits of the Montreal Protocol and lead to a substantial delay (more than a decade) in the recovery of stratospheric ozone over Antarctica.[31] At present, effects on UV-B radiation due to the recently reported emissions in CFC-11 cannot be quantitatively estimated because the effects on ozone have not yet been quantified.

1.3.2 Indirect effects – the Montreal Protocol and climate. Chlorofluorocarbons (CFCs) and some of their replacements are potent GHGs. Therefore, by controlling them, the Montreal Protocol has not only been beneficial for stratospheric ozone and UV radiation at the Earth's surface, but also useful in mitigating global temperature rise and other effects associated with climate change. Measurements in discrete air samples at ground-based stations across North America and by aircraft in the remote atmosphere have shown that ODSs decreased by about 40% from 2008 to 2014.[32] However, the more recent emissions of most hydrofluorocarbons (HFCs; ODS replacements, which do not destroy ozone but have still considerable global warming potentials) have been increasing over the same period. The phase-out of HFCs by 2030, in accordance with the provisions of the Kigali agreement,[33] is projected to reduce the climate impacts of HFCs in the upper troposphere and stratosphere by 90% by the year 2050,[34] and to avoid additional warming near the Earth's surface of up to 0.5 °C by 2100.[35]

Large effects on climate near the Earth's surface that would have occurred in the absence of the Montreal Protocol have been estimated by several chemistry-climate model (CCM) studies.[24,36,37] These studies showed that the Montreal Protocol helped to avoid a further strengthening of the Southern Annular Mode (SAM)§ as well as further enhancement of the warming in the lee of the Antarctic Peninsula. In the Arctic, the avoided loss of stratospheric ozone due to implementation of the Montreal Protocol is associated with a warming of the Arctic Ocean and North America, and a cooling over Western Europe and Siberia. These projected changes are comparable with those expected by 2025 due to GHGs.[36]

More recent studies have investigated specific impacts on climate near the Earth's surface that have been mitigated by the Montreal Protocol. For instance, a single model study found that, without the Montreal Protocol, the additional radiative forcing (global warming) from CFCs and additional ozone depletion (stratospheric cooling) would have driven large changes in the hydrological cycle, with the sub-tropical dry zones becoming drier and the mid-latitude wet zones becoming wetter.[38] A related study with a similar model[39] projected that the intensity of tropical cyclones would have been three times as large by the year 2065 without the Montreal Protocol, although this effect was dominated by the global warming effect of CFCs, with a minor role for the (considerable) stratospheric cooling. Projections of climate change in the absence of the Montreal Protocol have shown an additional global mean warming of >2 °C by 2070, due to the large increases in radiative forcing from increasing ODSs.[24] These unintended benefits of the Montreal Protocol in mitigating climate change mean that some of the large economic costs from climate damage have been avoided.[40,41] However, some of the replacement compounds (HFCs) are also potent GHGs that are now controlled by the Kigali Amendment.

1.4 Climate and chemical effects on stratospheric ozone

Increasing concentrations of GHGs, and the resulting climate change, will affect physical and chemical processes important for stratospheric ozone, and therefore UV radiation at the surface. These processes will alter temperatures and abundance of trace gases and, in turn, reaction rates important for ozone levels, as well as the Brewer-Dobson circulation (BDC)¶, which controls the distribution of ozone.[4]

The middle and upper stratosphere cools in response to increasing concentrations of GHGs, in particular, carbon dioxide (CO_2), methane (CH_4), and nitrous oxide (N_2O), due to increased emission of long-wave radiation to space. Outside of the polar regions, this cooling leads to greater concentrations of stratospheric ozone because the rate of catalytic loss of ozone declines with decreasing temperature. For the period 2000–2016, model simulations suggest that increasing concentrations of GHGs account for about half of the observed positive trends in upper stratospheric ozone (35–45 km) of about 2–4% per decade.[4]

At polar latitudes, destruction of stratospheric ozone is drastically accelerated due to heterogeneous reactions on polar stratospheric clouds (PSCs), which form when temperatures in

§ The SAM is the leading mode of southern hemisphere extratropical climate variability, describing a see-saw of atmospheric mass between the mid- and high-latitudes, with corresponding impacts on the strength of the circumpolar westerly winds. A positive SAM index corresponds to a poleward shift of the maximum wind speed, which results in weaker-than-normal westerly winds in the southern mid-latitudes.

¶ The BDC describes a pattern of atmospheric circulation according to which tropospheric air enters the stratosphere in the tropics and then moves upward and poleward before descending in the middle and high latitudes. It explains why tropical air contains less ozone than polar air, even though most atmospheric ozone is produced in the tropical stratosphere.

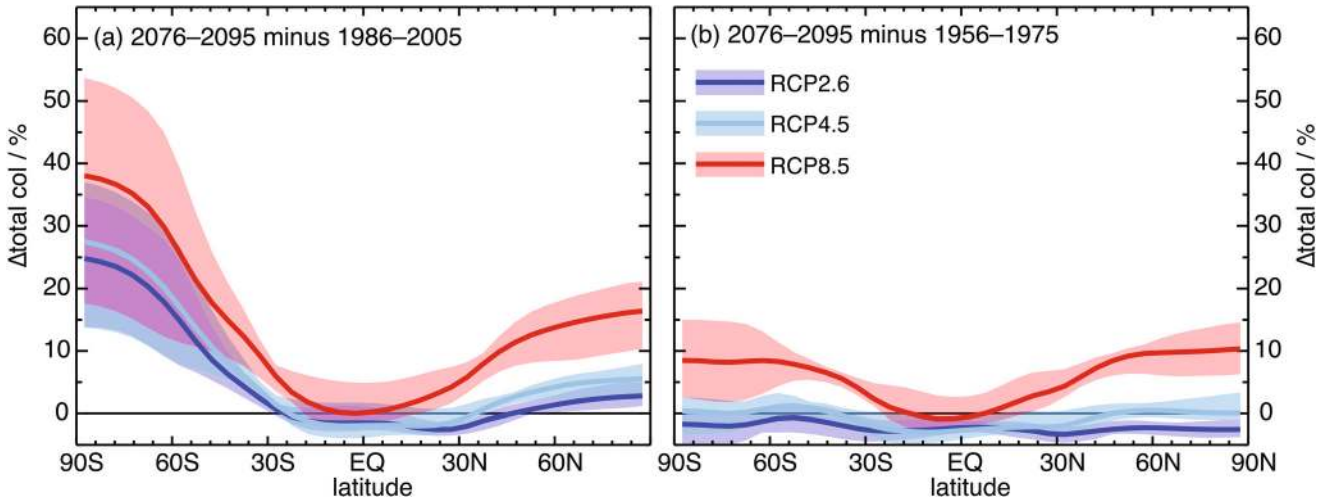

Fig. 2 Simulated relative change (in %) in total column ozone by the end of the 21st century (2076–2095 average) compared to (a) the strong stratospheric ozone depletion period (1986–2005), and (b) before the strong ozone depletion period (1956–1975). Results are for three RCP scenarios and five different CMIP5 models, showing both the mean change and the inter-model spread. The chosen CMIP5 models all have interactive chemistry and simulate throughout the depth of the stratosphere: CESM1-WACCM, GFDL-AM3, GISS-E2-H (p2), GISS-E2-R (p2) and MIROC-ESM-CHEM. Data are as per Butler *et al.*,[21] their Fig. 1.

the lower stratosphere drop below a critical threshold. At present, temperatures are generally higher in the Arctic stratosphere compared to the Antarctic, meaning that formation of PSCs is less extensive and less frequent in the Arctic. However, in the future, the region with temperatures below the critical threshold for formation of PSCs may increase significantly, leading to more rapid stratospheric ozone depletion while levels of chlorine remain elevated.[4]

Stratospheric temperatures in the Arctic are highly variable, with some years already experiencing temperatures low enough for formation of PSCs. Recent examples include the boreal winter/spring of 2010/2011,[3] November and December 2015,[42,43] as well as January 2016.[43] CCMs suggest that similarly large losses of ozone may sporadically recur until the middle of the 21st century during Arctic winters characterized by a cold and strong polar vortex.[44,45] Dynamical processes will continue to play an important role in determining levels of Arctic springtime ozone in the future, although halogen chemistry will remain a smaller contributor to stratospheric ozone depletion for many decades.

Model calculations suggest that increasing concentrations of GHGs will increase the strength of the BDC, leading to decreases of ozone in the tropical lower stratosphere and increases at higher (extra-tropical) latitudes.[46] The weight of evidence suggests that the shallow (lower stratosphere) branch of the BDC has strengthened over recent decades, but evidence for strengthening in the middle and upper stratosphere is less clear.[4] Decadal-scale variability in the strength of the BDC will also be important in driving medium-term (next few decades) trends in ozone.[20] Over this century, the magnitude and rate of ozone recovery will depend on the expected reduction in halogenated ODSs as well as on climate changes driven by GHG emissions, and especially through the strengthening of the BDC.[16,21,22] One model study has suggested that, by the end of the 21st century, stratospheric ozone over Antarctica may have recovered to levels greater than in 1960, due to an increased dynamical supply of ozone from a strengthened BDC.[22]

Projections of future changes in stratospheric ozone also depend on the direct chemical impacts of the GHGs, methane and N_2O. Increasing concentrations of N_2O destroy stratospheric ozone, while increasing concentrations of methane result in greater ozone production in the lower stratosphere and troposphere down to the surface.[4] Future global stratospheric ozone concentrations, and indirectly surface UV radiation (notwithstanding changes in clouds and aerosols in the troposphere), will be largely controlled by the abundance of N_2O and methane in the second half of the 21st century, when concentrations of ODSs are projected to become comparatively small.[21] Overall, the simulated magnitude of these impacts is dependent on the models used,[16,21,47] increasing the uncertainty in the projected changes in UV radiation.

Fig. 2 shows recovery of the total ozone column in the future as a function of latitude, as simulated by a selection of CCMs that were included in the fifth Coupled Model Intercomparison Project (CMIP5).[21] Increasing the concentrations of GHGs (RCP‖ 2.6 to RCP 4.5 to RCP 8.5)[48] results in a stronger BDC, which means larger increases in stratospheric

‖ Representative Concentration Pathways are greenhouse gas concentration (not emissions) trajectories adopted by the IPCC for its fifth Assessment Report (AR5) in 2014. The pathways are used for climate modelling and research. They describe four climate futures, which differ on how much greenhouse gases are emitted in years to come. The four RCPs, RCP 2.6, RCP 4.5, RCP 6, and RCP 8.5, are named after a possible range of radiative forcing values in the year 2100 relative to pre-industrial values (+2.6, +4.5, +6.0, and +8.5 W m^{-2}, respectively).

ozone at higher latitudes by the end of the 21st century (Fig. 2a). For the tropics, the change in total ozone column is a combination of temperature-mediated upper stratosphere ozone recovery (strongest in RCP 8.5) *versus* ozone decreases in the lower stratosphere due to a stronger BDC.[16,47] In addition, the tropospheric ozone column increases in RCP 8.5, but decreases in RCP 4.5 and 2.6.[47] For RCP 2.6 and 4.5, the ozone column recovers close to mid-20th century values (~1960; Fig. 2b), with RCP 8.5 exceeding those levels at the higher latitudes.

Climate changes at the Earth's surface may also be important for stratospheric ozone. Recent work has suggested that the loss of Arctic sea ice has contributed to a persistent late-winter shift of the Arctic vortex towards the Eurasian continent over the past three decades,[49] leading to decreases in total ozone over Eurasia and increases over North America, together with the suggestion that recovery of total ozone over Eurasia may be delayed during the first four decades of the 21st century.[50] However, further analysis of these changes in vortex patterns with climate models suggests that, while there may be a small anthropogenic component to the trend in vortex position, this is not linked to the decline of Arctic sea ice.[51] This analysis concludes that the recent trends in the vortex noted by ref. 49 may be primarily a result of unforced internal variability.

Finally, variability in atmospheric circulation patterns also affects the distribution of stratospheric ozone and therefore UV-B radiation. An understanding of the role of interannual variability–and natural variability on longer timescales–is necessary to ascertain when the ozone layer has recovered.[4] One driver of interannual variability is the quasi-biennial oscillation (QBO), which describes an east–west oscillation in tropical stratospheric winds. In the NH winter of 2015/2016 an unprecedented disruption of the QBO was detected,[4,52,53] and total ozone measurements by the satellite-borne Solar Backscatter Ultraviolet Radiometer (SBUV) revealed the development of positive anomalies of ozone in the equatorial stratosphere in May–September 2016 and a substantial decrease in ozone in the subtropics of both hemispheres.[54] As the understanding of factors affecting the QBO is incomplete, it is unclear whether recurrence of such a disruption is likely in a changed climate. In general, the magnitude of stratospheric ozone depletion in Antarctica will continue to exhibit variability at interannual time scales, until ODSs are removed from the stratosphere and the ozone layer has recovered.[4]

Variability in the propagation and dissipation of planetary waves will also alter stratospheric circulation, which affects the distribution and chemistry of ozone over the globe. For instance, the strength of the polar vortex in the SH, and resulting levels of polar stratospheric ozone depletion, have been shown to be coupled with anomalies in sea surface temperature (SST) in the maritime continent/East Asian marginal seas, which drive anomalous planetary wave behavior.[55] Furthermore, the overall warming of the surface of the ocean in this region could have driven a substantial fraction of the observed trend of loss of polar ozone in the SH (~17%) through the anomalously weak propagation and dissipation of planetary waves, and resulting stronger, colder vortex.[55] Variability in planetary waves is also associated with the El Niño-Southern Oscillation (ENSO) and has been shown to be coupled to the zonal distribution of the mid-latitude total ozone column (*e.g.*, increased ozone for the North Pacific, southern USA, northeastern Africa and East Asia, but decreased ozone over Europe and the North Atlantic during El Niño events).[56]

2 Effects of changes in stratospheric ozone on UV radiation and climate

Changes in stratospheric ozone have been a major driver of changes in clear-sky UV-B radiation, especially at high latitudes where ozone exhibits its highest variability. Depletion of stratospheric ozone resulting from emissions of ODSs into the atmosphere has led to latitude-dependent increases in UV-B radiation at the Earth's surface, particularly in the 1980s and 1990s. Such increases in UV-B radiation have been measured at various locations and have been extensively discussed in previous assessment reports.[23,57–60] Over some regions, direct correlations between ozone and UV-B radiation could not be detected in measurements because they were masked by other factors that are also strong attenuators of UV-B radiation, as discussed in section 3. The changes in ozone that have occurred over the past decades resulted in changes in UV-B radiation at the Earth's surface and in surface climate, with consequences for human health, marine and terrestrial ecosystems, as well as in tropospheric chemistry, biogeochemical cycles, and materials. These impacts are discussed in ref. 27–29 and 61–63. This section assesses the literature on the impacts of recent ozone changes on climate and UV radiation, whereas future projections are discussed later.

2.1 Effects of Antarctic stratospheric ozone depletion on climate

There is now general agreement that the recurrent ozone 'hole' in the Antarctic stratosphere in spring is a major driver of observed changes in atmospheric circulation in the SH summer.[4] These changes are affecting the climate near the surface in various ways, and future projections of their impact depend on the rate of recovery of ozone *versus* the rate of increase of GHGs. Increased concentrations of ODSs and depletion of ozone over Antarctica in the late 20th century have been recognized as important drivers of changes in climate in the SH, and have been suggested as explanations for the observed changes in circulation, temperature, and salinity of the Southern Ocean.[64,65]

2.1.1 Shifting of climate zones. Well-established changes in climate due to depletion of Antarctic ozone include a strengthening and poleward contraction of the westerly atmospheric circulation over the southern extratropics (all latitudes except the tropics) during austral spring and summer. This corresponds to a trend towards the positive index of SAM, leading to associated effects on temperature and precipitation in the mid-latitudes extending into the subtropics and even the

tropics. New studies have reconfirmed these overall effects using different approaches based on observations and models.[66,67]

Long-term data records show that changes in tropospheric circulation due to the ozone 'hole' have contributed to a decrease in summer temperatures over southeast and south-central Australia, and inland areas of the southern tip of Africa.[68] In the decades since the appearance of the ozone 'hole', anomalously high (or low) total ozone column amounts in the spring are significantly correlated with hotter (or colder) than normal summers over large regions of the SH. These patterns are related to the SAM.

Depletion of stratospheric ozone in Antarctica has been shown to explain more than half of the observed changes in precipitation between 1979 and 2013 in the subtropics of the SH, while increasing concentrations of GHGs have a weaker role.[69] This finding emerged from a statistical modelling approach (maximum covariance analysis) that was used to quantify the relative contribution of different climate forcing mechanisms, including stratospheric ozone depletion, changes in the sea surface temperature of the equatorial Pacific, and increasing GHGs. In a more recent study,[70] an analysis of observations and climate models demonstrated that depletion of stratospheric ozone has led to changes in springtime precipitation in the sub-tropical South Pacific Ocean, Australia, and New Zealand over the 1961–1996 period. These changes range from −25% to +40% depending on location. Despite the large variability in the magnitude of impact among climate models, they all indicate a consistent pattern of changes over this region. Furthermore, qualitative agreement between models and measurements suggests that these effects on precipitation will likely reverse when ozone recovers in the future.

South-eastern South America experienced the highest increase globally in extreme summer rainfall over the 20th century.[71] An analysis of an ensemble of 12 simulations by one climate model suggests that this increase in extremes of maximum precipitation, as well as a decrease in the extremes of maximum temperature, over the second half of the twentieth century were driven by the changes in tropospheric circulation induced by depletion of stratospheric ozone.[72] This supports previous studies,[73,74] and, although it is at odds with a similar study[75] in its attribution of the effect to stratospheric ozone depletion, it draws its evidence from a larger model ensemble and analysis of a period more appropriate to the impact of stratospheric ozone depletion.

Changes in the tropical atmospheric circulation caused by Antarctic stratospheric ozone depletion and increasing GHGs have resulted in a poleward shift of the boundaries of sub-tropical and tropical climatic zones. A recent modelling study[76] has confirmed previous work and showed that the observed poleward expansion of the Hadley** circulation cell is caused mainly by these two anthropogenic forcing mechanisms, rather than by natural forcing. As with the changes in SAM, the ozone depletion in the Antarctic ozone 'hole' was found to dominate the expansion of the southern Hadley cell in the austral spring and summer, with a smaller contribution from Arctic stratospheric ozone depletion for the northern cell in boreal spring.

Linkages between stratospheric ozone depletion and tropospheric changes have previously been reported for the austral summer months (December–February). A new study has shown that this effect persists through to the autumn.[77] This study reported a poleward shift in the position of the jet stream (*i.e.*, a positive SAM index) during May, driven by the stratospheric cooling associated with Antarctic stratospheric ozone depletion. However, mechanistic descriptions of the dynamical drivers for the trend, including why the significant trends favour particular months, remain to be provided.

The continued expansion of the Hadley cell expected from increases in GHGs will be slowed by recovery of stratospheric ozone. This modification of the Hadley cell will modify the boundaries of the climatic zones, leading to expansion of subtropical dry zones to higher latitudes, affecting terrestrial and aquatic ecosystems (see ref. 28).

2.1.2 Effects on Antarctic sea-ice-cover. Changes in sea ice are important for UV-B radiation. Increases in the extent of sea ice lead to increased UV-B radiation above the surface, but to decreased radiation penetrating the water under the ice, with implications for terrestrial and aquatic ecosystems. There is no consensus with respect to the contribution of the ozone 'hole' to the observed increase in the extent of sea ice around Antarctica between 1979 and 2014, which was followed by a dramatic decline between 2014 and 2017.[78] Preliminary data suggest that the extent of sea ice in 2018 was similarly low to that observed in 2016 and 2017 (https://neptune.gsfc.nasa.gov/csb/index.php?section=234). Climate model simulations with realistic stratospheric ozone depletion do predict decreases in sea ice,[64] but do not capture the regional patterns in trends.[79] Consequently, confidence in the ability of models to accurately simulate the response of sea ice to ozone depletion is low.[4]

There has been progress in our understanding of the physical processes that link stratospheric ozone depletion to sea-ice-cover trends. Based on analysis of idealized climate model simulations, two processes operating on different time scales have been proposed.[4,80] In the short-term (a few years to a few decades, depending on the model), changes in ocean circulation induced by depletion of stratospheric ozone cool the sea surface around Antarctica, leading to expansion of the sea ice, as well as to upwelling of warm waters in the region of the seasonal sea ice. This pattern is consistent with the well-known relationship between SAM and sea ice or ocean surface temperature. In the long-term (multiple decades), the effect resulting from upwelling of warm water begins to dominate, slowly leading to warming of the ocean and ultimately to long-term reduction of sea ice. The short/long-term behavior has been noted in other climate model studies,[65,81] although the characteristic time scales of each process vary greatly between

**The Hadley circulation is a large-scale atmospheric convection cell in which air rises at the equator and sinks at medium latitudes, typically at about 30° northern or southern latitudes.

different models.[82] The impact of SAM on sea ice remains unclear.

A more detailed discussion on the relevant physical mechanisms and model results for relationships between ozone and sea ice is presented in the WMO Scientific Assessment Panel Report.[4]

2.1.3 Direct effects on solar radiation at the Earth's surface. A modeling study[83] investigated the direct effect of the Antarctic ozone 'hole' on total solar radiation. Weaker absorption by the smaller amounts of ozone in the stratosphere leads to increased UV radiation at the Earth's surface. The contribution of the increased UV radiation to total solar radiation at the surface has been estimated to be 3.8 W m^{-2} (about 2%) in October–December. However, for the highly reflecting surface of Antarctica,[84] most of this excess radiation is redirected upwards and does not contribute significantly to increases in air-temperature near the surface.

2.2 Effects of recovery of Antarctic ozone on UV radiation

The beginnings of Antarctic ozone recovery have been reported and discussed in several studies,[4] and it is expected that UV-B radiation at the surface will decrease as ozone increases. However, so far there has been no evidence of reductions in UV-B radiation over Antarctica in response to ozone recovery. As noted in section 1.4, the magnitude of Antarctic stratospheric ozone depletion, and the corresponding effect on UV-B radiation, will continue to exhibit variability at interannual time scales until the ozone layer has recovered.[4] The enhanced ozone depletion seen in 2015 due to aerosols from the eruption of Calbuco in southern Chile[8,10,11] demonstrates the continued importance of episodic impacts on the Antarctic stratosphere while ODSs are still present.

2.3 Effects of Arctic ozone losses on UV radiation and climate

The recently observed transient depletion of stratospheric ozone in the Arctic led to increased UV-B radiation at the Earth's surface and may have contributed to changes in the surface climate of the NH. As discussed in the previous assessment report,[2] unprecedented decreases in stratospheric ozone for the region were observed over the Arctic in winter 2010/11 due to unique meteorological conditions,[3] and have influenced UV radiation in the summer of 2011.[85] Smaller decreases in ozone occurred again in the winter of 2015/16,[86] albeit with different timing. During the second half of February 2016, the total ozone column was reduced by more than 30% relative to the historical (2005–2015) mean over Northern Scandinavia and Northern Siberia. This led to an increased UVI at the surface of up to 60% over an area roughly matching the region where ozone was abnormally low. However, absolute increases remained below 1 UVI unit because the event occurred early in the year when solar elevation angles were low.[43]

Analysis of measurements of ozone in 1979–2012 revealed a statistically significant association (at the 95% level) between low concentrations of Arctic stratospheric ozone in March and changes in climate between 30 and 70°N in March and April.[87] The changes include a poleward shift of the North Atlantic jet stream, lower-than-normal surface temperatures over eastern North America, Southeastern Europe, and southern Asia, and higher-than-normal temperatures over northern and Central Asia. Another study[88] suggests that effects from variations in Arctic stratospheric ozone may extend even to the tropics and may be associated with El Niño Southern Oscillation (ENSO) events. However, neither study has demonstrated causality between the identified associations. Moreover, further investigation is needed to disentangle the role of sea-ice loss[89,90] and interannual variability[51] for northern mid-latitude changes associated with the jet stream and vortex.

3 Factors other than ozone that affect UV radiation

Apart from ozone, the important determinants for UV radiation at the Earth's surface are clouds, aerosols, and surface reflectivity. These factors are strongly related to anthropogenic activities that have led to increased emissions of GHGs and changes in particles released into the atmosphere, which are expected to change in the future. UV radiation is also determined by the 11-year solar cycle and long-term changes in solar activity, both directly and indirectly through influences in stratospheric ozone. The variability and importance of these factors for UV radiation reaching the Earth's surface have been discussed already in previous reports.[2,91] Here we present a summary of recent studies on key properties and mechanisms as they relate to effects on UV radiation, and are essential for estimating ambient levels of UV radiation.

3.1 Clouds

Clouds are by far the most important attenuators of solar radiation reaching the troposphere across all wavelengths. Thick clouds can diminish radiation to levels close to zero, while thin clouds can lead to reductions of at least a few percent. New studies have improved understanding of the effects of clouds on UV radiation and the physical mechanisms of the processes involved. The weak wavelength dependence of the optical depth of clouds predicted by theory has been confirmed with measurements.[92] In this study, the optical depth of clouds at a given instance was determined by iterative comparisons of the measured irradiance to estimates of irradiance from a model based on a range of optical depths of clouds. Measurements under overcast conditions at Valencia, Spain, indicate that the attenuation by clouds is 2% smaller for erythemal irradiance than for total solar irradiance. Even though the optical depth of clouds is almost independent of wavelength, the effect of clouds on solar irradiance reaching the surface is wavelength-dependent because of interactions of the cloud with the Rayleigh-scattering of radiation by the air-molecules.[93,94] Due to wavelength-dependent effects, clouds can modify the sensitivity of erythemal radiation to variations in total ozone. For example, a recent study for Granada, Spain,

reported that erythemal irradiance showed a greater sensitivity to ozone with increased cloudiness.[95]

There has been confusion in the recent literature about the magnitude and wavelength-dependence of the effects of clouds on UV radiation. To clarify this issue, high-quality spectral measurements obtained from instruments at several sites covering a wide range of altitudes (up to 3.4 km at Mauna Loa Observatory in Hawaii) were used to analyze the wavelength dependence of cloud effects on UV radiation.[96] During partly cloudy conditions when the sun is not obscured, radiation at the Earth's surface for all wavelengths can be significantly higher than for clear-sky conditions because bright clouds scatter more radiation towards the surface than the blue sky. Such events can last for a few minutes or even longer, depending on the type of cloud and speed of its movement. These enhancements of radiation by clouds tend to be smaller in the UV-B than in the UV-A (315–400 nm) or visible regions, mainly because the proportion of the direct radiation (which is responsible for the enhancement) in the UV-B is smaller than for the longer wavelengths. In snow-free conditions, enhancements greater than 20% are rare in the UV-B region, but can reach 40% in the UV-A region.[96,97] Enhancements by clouds can be even larger in the visible region, but they rarely exceed 50%.[96–98] These results are consistent with earlier studies.[99,100] "Cloud enhancement" events can substantially increase exposure to UV radiation for short periods, so can be important for exposure of humans and ecosystems. However, over longer periods (*e.g.*, over the course of a day), the presence of clouds usually reduces the total dose of UV radiation.

Clouds scatter back (upwards) a large portion of the incoming solar radiation. The effective albedo caused by clouds below a mountain summit has been quantified using measured and modeled UV irradiance data from the Izaña observatory (28°N, 2400 m above sea level).[101] The largest observed effective albedo value in the UV was found to be 0.58 (*i.e.*, 58% of incident radiation is reflected upwards). More typical values range between 0.2 and 0.5 and are about 10 times larger than the local surface albedo (0.02–0.05).

Measurements combined with radiative transfer modeling confirmed theoretical predictions from Mie theory that clouds composed of small water droplets attenuate UV radiation more efficiently than clouds composed of large droplets, for the same liquid water content.[102] The magnitude of this effect depends on the solar zenith angle and liquid water content, which determine the optical thickness of the cloud in the path of the radiation. Clouds in highly polluted atmospheres tend to consist of more, smaller cloud droplets (compared to clean atmospheres) and can last longer because they are less likely to produce rain.[103]

Better understanding of the wavelength-dependent effects of clouds on radiation received at the ground will allow more accurate quantification of how different biological or chemical weightings of radiation respond to changes in cloudiness. This may be important in the coming decades, as global cloud patterns and characteristics are projected to change due to climate change.[48]

3.2 Aerosols

3.2.1 Effects of aerosols on UV radiation. Aerosols (solid and liquid particles suspended in the atmosphere (see ref. 62)) play a significant role in attenuating UV radiation and in modifying the fraction of its diffuse component. The optical properties of aerosols depend on their size, shape, and chemical composition. Quantifying the effect of aerosols on UV radiation at the Earth's surface requires knowledge of the total aerosol optical depth (AOD or τ; dimensionless) and its absorption efficiency (SSA).†† The dependence of UV irradiance on AOD, SSA, wavelength and measurement geometry (horizontal, spherical, vertical cylinder) was discussed in detail in the last assessment.[2]

Measurements of SSA at wavelengths in the UV-B are difficult because aerosol absorption must be separated from the absorption by gases, including ozone, as well as nitrogen dioxide (NO_2) and sulfur dioxide (SO_2), which are typically also abundant in polluted regions. The dearth of observations of SSA and its wavelength dependence is therefore one of the largest uncertainties in estimating surface UV irradiance or projecting future levels of UV radiation in regions with high levels of air pollution.

Fig. 3 shows measurements of the SSA at Santa Cruz, Bolivia.[104] The decrease of SSA towards wavelengths in the UV-B is qualitatively similar to that reported in our last assessment[23] and recent measurements at Athens, Greece.[105] However, measurements of SSA in the UV-B like those reported in these two studies[104,105] are rare, and absolute values of SSA can vary significantly depending on the chemical composition of aerosols. For example, organic aerosols (*i.e.*, aerosols that contain organic carbon material) exhibit a large wavelength dependence in the UV-B compared to other aerosol types.

The highly non-linear changes in SSA with wavelength have important implications for calculating the effect of aerosols on UV radiation. Their effect will be seriously underestimated if SSAs measured at longer wavelengths are simply extrapolated into the UV-B region. As discussed in the previous report,[2] at least 20% of the observed difference in UV-B radiation between New Zealand and rural USA was attributable to aerosol effects, despite the relatively small difference in AOD between the sites.

Most pronounced effects of aerosols occur near the sources of emission, but significant influences have been identified on regional and global scales due to transport of aerosol. Changes in the amount and optical properties of anthropogenic aero-

†† The AOD is the sum of the absorption optical depth τ_{abs} (which quantifies the attenuation of the direct solar beam due to absorption of photons) and the aerosol scattering optical depth τ_{sca}: ($\tau = \tau_{sca} + \tau_{abs}$). The wavelength dependence of τ is often parameterized by a simple power model: $\tau \propto \lambda^{-\alpha}$, where the Ångström exponent α quantifies the wavelength dependence of τ. The value of α is often determined from measurements in the visible, and extrapolation to UV wavelengths is subject to uncertainties. Instead of specifying τ and τ_{abs}, the single scattering albedo (SSA) is often reported: $\mathrm{SSA} = \frac{\tau_{sca}}{\tau_{sca} + \tau_{abs}} = \frac{\tau_{sca}}{\tau}$, resulting in: $\tau_{abs} = (1 - \mathrm{SSA}) \times \tau$. A decrease in SSA, therefore, corresponds to an increase in absorption of radiation.

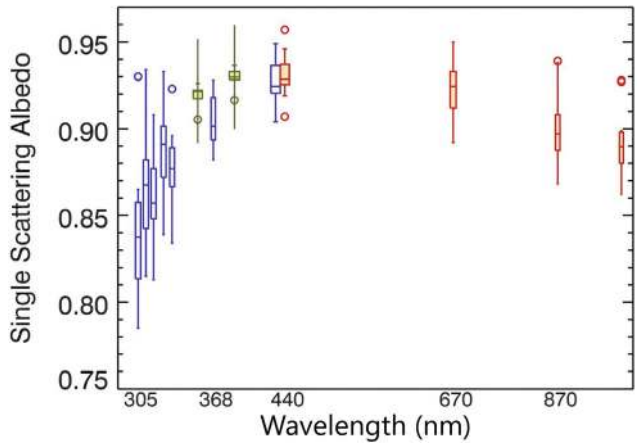

Fig. 3 Spectral dependence of smoke aerosol single scattering albedo (SSA) derived from ground-based and satellite observations during the field campaign in Santa Cruz, Bolivia, in September–October 2007. Data are from a UV-MFRSR instrument (blue), AERONET (red), and OMI (green). All data are shown as box-whisker plots. Boxes are the inter-quartile range (IQR; 25 to 75 percentiles) and whiskers are stretched to the maximum and minimum within 1.5 times the IQR. The circles show the outliers (adapted from Mok *et al.*[104]). Measurements of SSA from the ground (UV-MFRSR, AERONET) are more reliable than measurements from space (OMI) because of the difficulty of probing the lower troposphere with satellites.

sols have been observed at multiple locations worldwide. Data from the AERONET network revealed decreases in the amount and absorption efficiency of aerosols (quantified by the SSA) at most stations since 2000.[106–109] These changes were caused by decreases in air pollution which would be expected to have led to increases in UV radiation at the surface. However, at most locations, no UV radiation data are available to assess these effects quantitatively.

Measurements at seven stations in the USA over 1995–2010 indicated a positive trend in diffuse irradiance, despite there being no trend in clear-sky direct solar irradiance.[110] It was hypothesised that this finding was a result of growth in air traffic over the USA, which increased the amount of cirrus clouds.

As changes in total ozone over mid-latitudes have been generally small since the onset of stratospheric ozone depletion, changes in the attenuation of UV-B radiation under cloud-free skies in most populated areas are mainly controlled by the concentrations of aerosols and the wavelength dependence of their optical properties. Data from a multi-filter shadow-band radiometer and a sun-photometer have been combined to quantify the absorption efficiency of aerosols over Athens, Greece, at selected wavelengths in the UV-A, visible and near-infrared ranges (332–1020 nm). The largest absorbing efficiency was found for organic and dust aerosols,[105] confirming the results of a previous study,[111] which showed that desert dust can attenuate the direct UV irradiance at 400 nm by up to 55% and increase the diffuse irradiance by up to 40%.

At many locations over China, the amounts of aerosol remain high. The AOD at 440 nm has ranged between 0.3 and 1.0, and has exceeded 5.0 during extreme events in some locations, but with no significant trend since 2002.[112] Analysis of recent ground-based and satellite observations over East China for 2005–2015[113] suggests that the AOD was decreasing over this period, leading to increases in total solar radiation. Data from XiangHe in North China suggest that decreases in the optical depth and increases in the single scattering albedo (smaller absorbing efficiency) of aerosols have contributed to the observed increases in the direct and diffuse solar radiation. It is difficult to extrapolate these findings to the UV region, since scattering by aerosols affects UV radiation differently than visible.[23]

A climate-change-driven increase in the frequency and extent of wildfires[114–117] could be an important source of aerosols, with significant effects on surface UV radiation. Carbonaceous aerosols resulting from combustion include black carbon (BC), which is primarily released at elevated temperatures, and brown carbon (BrC), which is produced by the burning of organic matter at lower temperatures such as in forest fires (see ref. 29 and 61) Both aerosol types can strongly absorb UV-B radiation. By considering the different fractions of BC and BrC over Santa Cruz, Bolivia, it was found that absorption by BrC caused a further 20–25% reduction in irradiance at 305 nm compared to the BC-only absorption.[104] If confirmed, unaccounted reduction in surface UV-B irradiance by BrC could be important when assessing health risks due to exposure to UV-B radiation. The wavelength dependence of the absorption of UV and visible radiation by BC was previously believed to be relatively small, decreasing proportionally to the reciprocal of wavelength ($1/\lambda$).[118] However, measurements from the ground and space for Santa Cruz, Bolivia, indicate that the absorption by BrC has a strong wavelength dependence in the UV with the largest absorption observed at the shorter UV-B wavelengths.[104] Greater effects of aerosols on UV than on visible radiation were also shown by measurements influenced by the smoke plume of the California Rim Fire (encompassing Stanislaus National Forest and Yosemite National Park) on 27 August 2013.[119] Measurements at Lake Tahoe (located 120 km away from the wildfire) showed that, over a period of about 10 days, UV-B radiation was more strongly reduced than visible radiation, albeit with high variability due to changes in wind direction and thickness of the smoke plume. At times, the UV-to-visible ratio was reduced by almost 50%. Such events, which may become more frequent in a warmer and drier climate,[114–117] are important because by attenuating the UV and visible radiation received at the ground and by regulating the ratio of UV-to-visible radiation in the environment they can affect important biological processes, for instance, the emissions of biological volatile organic compounds (see examples in ref. 27–29 and 61).

Modeling studies have projected that, due to climate change, summertime concentrations of BrC aerosol over the western United States will increase by 40–70% and concentrations of BC aerosol by 20–27% by 2050, relative to the present.[120,121] Most of this increase (75% for BrC and 95% for BC) is caused by larger emissions from wildfires. Such

increases in carbonaceous aerosols would lead to significant reductions in surface UV radiation. For instance, a recent study has shown that wildfires in Russia in 2010 caused reductions of up to 50% in the daytime averaged photolysis rates of NO_2 and ozone along the aerosol plume, driven by reduced UV radiation.[122] Both types of carbonaceous aerosol can be transported across the globe and persist in the atmosphere for days to weeks (see ref. 61 and 62). Inclusion of emissions from fires in climate models increased the predicted global mean annual aerosol optical depth at visible wavelengths by 10%.[123]

Besides their role as condensation nuclei in the formation of clouds, aerosols may also interact with cloud droplets resulting in changes in the albedo of clouds, which in turn affects the fraction of solar radiation scattered upwards. Model results have shown large increases in the albedo of clouds with increasing concentration of aerosols that are related to changes in the water content of clouds and in the size distribution of cloud droplets.[124] With respect to the origin of aerosols, anthropogenic sulfate aerosols had a greater effect on the albedo of clouds than non-sulfate aerosols.

Future changes in concentrations of atmospheric aerosols used in climate modeling studies depend on the assumed RCP scenario. For the RCPs 8.5, 4.5 and 2.6, the aerosol content is projected to decline strongly and monotonically during the 21st century, after peaking around 2010, while for RCP 6.0 the peak occurs later, around 2050.[125] Consequently, the importance of aerosols in modifying solar UV radiation will become weaker during the 21st century for RCPs 8.5, 4.5 and 2.6. For RCP 6.0, the greater projected AOD for the future would result in reduced UV radiation compared to other RCPs. The aerosol optical properties, such as SSA, asymmetry factor and Ångström exponent might also change in the future, but this information is not included in the RCPs. Lack of information on how these optical properties of aerosols will change over time increases the uncertainties of simulations of UV radiation for the future, which are further affected by the poor knowledge of the wavelength-dependence of SSA.

3.2.2 Advances in the monitoring of aerosols. The tools available for quantifying concentrations of aerosols and the wavelength dependence of their optical properties are still inadequate. The need for development of methods and instrumentation to quantify the absorption efficiency of aerosols at UV wavelengths has already been discussed in previous assessments.[23,59] Algorithms to calculate the AOD from measurements of instruments of the European Brewer Network have recently been improved and harmonized.[126] Results from two intercomparison campaigns suggest that a well-maintained and calibrated Brewer instrument is capable of measuring AOD with a precision of 0.005 and an uncertainty of 0.04 in the UV range from 310 to 320 nm, with the corresponding values for 306 nm being slightly worse, 0.01 and 0.05, respectively.

A new sun-photometer (ultraviolet precision filter radiometer, UVPFR) developed at PMOD/WRC Davos, Switzerland has been extensively evaluated during two campaigns in Izaña-Tenerife, Spain, in 2015 and 2016, and compared with a Brewer spectrophotometer. It was found that both instruments can measure the aerosol optical depth (AOD) with 0.01 precision at UV-B wavelengths between 305 and 320 nm.[127] Further, a new method has been proposed to enable more accurate calibration of AOD sun-photometers at locations with high and variable aerosol load.[128] Finally, in an intercomparison campaign held in Davos, Switzerland, in autumn 2015, most of the instruments measuring the AOD at visible wavelengths (500 and 865 nm) agreed to within 0.005 units of AOD, while two thirds of the instruments reporting AOD in the UV-A (368 and 412 nm) achieved that goal.[129] Such improvements in instrumentation and methods will facilitate clearer separation of the effects of ozone and aerosols on UV-B radiation.

3.3 Surface reflectivity

Variations in the reflectivity of the Earth's surface (over land and ocean) can lead to variations in incident downwelling irradiance because a fraction of photons that are reflected upward by the reflecting surface is scattered downward by air molecules, aerosols, and cloud droplets. This effect is more pronounced when the surface is covered by fresh snow or ice.

At Barrow, Alaska (71°N), changes in snow cover observed during the last 25 years have had a profound effect on surface UV radiation as illustrated in Fig. 4. At this site, there are indications that the onset of persistent snow cover at the beginning of winter has advanced by 8 ± 7 (±2σ) days per decade (blue dataset in Fig. 4, plotted on an inverted scale). In response, the monthly mean UV-A irradiance for October (red dataset in Fig. 4) has decreased by 8 ± 4% per decade. This decrease cannot be attributed to changes in ozone and is largely the result of a longer snow-free period in October.[130] For the period 1995–2014, there is a significant anti-correlation (R^2 = 0.56) between the onset of persistent snow cover and monthly mean UV-A irradiance.

Based on data from different satellites, statistically significant (at the 95% level) negative trends in UV reflectivity were

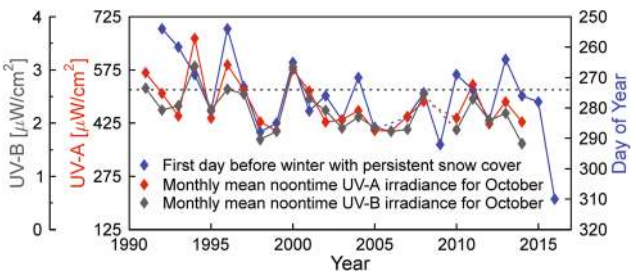

Fig. 4 Comparison of UV-B (grey symbols) and UV-A (red symbols) irradiance at Barrow with the timing of snow cover onset (blue symbols, right axis), defined as the first day before winter when the surface albedo becomes larger than 0.6 and stays above 0.6 for the rest of the winter. Note that the right axis is inverted. The dotted horizontal line indicates 1 October. The figure is adapted from Bernhard[130] and updated with data from 2010–2016. Surface albedo was measured with pyranometers that are part of the Baseline Surface Radiation Network (BSRN). UV measurements are not available for 2009, 2015, and 2016.

found for areas in the Bellingshausen/Amundsen Seas near Antarctica, with sea-ice coverage greater than 30%.[131] Although these estimates include radiation reflected by clouds, the air molecules and the surface, reflection by bare or snow-covered sea ice was the main driver of the observed variability in reflectivity. This study reported a reduction in UV reflectivity of up to 3.6 ± 1.0% per decade due to reduction in the concentration of sea ice for the period 1980–2012 in March. On the other hand, positive trends were found for ice-free areas and for areas with low ice-coverage for the entire Southern Ocean. Since the trend in reflectivity in ice-free regions within the 50°–60°S latitudinal band is also generally positive, it is possible that a small increase in cloud amount and/or opacity occurred in the Southern Ocean during the examined period. Finally, the trends over areas with high concentrations of sea ice over this latitude band are mostly negative, although often not statistically significant at the 95% level.

The observed biases in the representation of variations in the surface albedo in the CMIP5 climate models when compared to measurements raise doubts about the reliability of future projections by these models with respect to responses due to the development of sea ice.[132] This conclusion arose from a study focused on the evaluation of spatial and temporal variations in the albedo of ice in the CMIP5 models during the Arctic summer against satellite observations (CLARA-SAL) of surface albedo for the period 1982–2005.[132] Although many individual models show large biases, the mean values of CMIP5 ensemble agree relatively well with the satellite data. However, the good agreement may be serendipitous considering that the discrepancy between individual models and the observations is not well understood.

Over areas currently covered by ice or snow, particularly over high latitudes and high altitudes, reduction of reflectivity of the Earth's surface in the future will lead to decreases in downwelling UV radiation. Local ecosystems should receive less UV radiation in the future, but current models are unable to provide accurate projections of changes in reflectivity.

3.4 Solar activity

The previous EEAP Assessment concluded that the direct influence of solar activity on the UV-B radiation at the surface is small, but indirect effects, through changes in the formation of ozone initiated by the absorption of solar UV-C (100–280 nm) radiation in the upper stratosphere could be more important. Furthermore, it was suggested that a grand solar minimum that might occur in the future could influence the global climate and the ozone layer, leading to increases in UV-B radiation at the surface. A new modeling study for the period 2000–2199, investigated the influence on ozone and climate by a hypothetical strong decline in solar activity that would last until 2199.[133] It was found that a reduction of about 15% in solar UV-C radiation would lead to a decrease in formation of ozone by up to 8%, which would overcompensate the anticipated increase in stratospheric ozone due to reduced stratospheric temperature and acceleration of the BDC. This would lead to a delay in the recovery of total ozone from ODSs, with global ozone not returning to pre-ozone-'hole' values before the end of the grand solar minimum. Although UV-B radiation at the top of the atmosphere is expected to decrease slightly during a grand solar minimum due to weaker emission from the sun, the effect on UV-B radiation from decreasing total ozone is stronger, resulting in an overall increase of UV-B radiation at the surface. Moreover, during a grand solar minimum, the flux of energetic electrons would diminish, leading to less destruction of ozone by NO_x in polar regions.[134] The effects of changes in high energy electrons due to reduced solar activity have not been fully evaluated yet.[133]

3.5 Effects of climate change on surface UV radiation

Climate change affects surface UV radiation by altering the amount and distribution of ozone, cloud cover and type, aerosol abundance, and surface reflectivity. This section assesses the impact of climate change on drivers other than ozone, which was discussed earlier.

In agreement with simulations from climate models, several independent satellite records indicate that changes in large-scale patterns of clouds have already occurred between the 1980s and 2000s.[135] Between latitudes of 60°S and 60°N, observed and simulated changes in cloud patterns are consistent with poleward retreat of mid-latitude storm tracks, widespread reduction in cloudiness at mid-latitudes between about 30° and 50° of both hemispheres (presumably leading to increases in UV radiation at the surface), and expansion of subtropical dry zones, as discussed in section 2.1.1 and in ref. 28. The primary drivers of these changes in clouds are increasing concentrations of GHGs. Over the Arctic ocean, cloud cover increased rapidly during the last 20 years due to warming of the lower troposphere and large reduction of sea-ice cover, which led to enhanced upward transport of moisture.[136] During the period of winter darkness in the Arctic, increased cloud-cover warms the troposphere, and may accelerate the retreat of sea ice, enhancing the feedback processes of Arctic warming.[137]

Apart from their effects on clouds, reductions in ice- and snow-cover, as well as changes in their characteristics (*e.g.*, thickness of ice, depth of snow), influence the exposure of ecosystems to solar UV radiation. Less snow- and ice-cover reduces UV radiation at the surface (due to the lower surface reflectivity) but leads to greater exposure to UV radiation for organisms usually protected under snow and ice. Between 1979 and 2016, the extent of sea ice in the Arctic has decreased at rates of 2.7% and 13.3% per decade in March and September, respectively.[138] Due mostly to later autumn freeze-up, the Arctic sea-ice-free season has lengthened between 1979 and 2013 at a rate of 5 days per decade on average, but with a maximum rate of 11 days per decade in some regions.[139] Over Arctic land areas, the snow cover in June was less than 4 million km^2 only once in the period 1967–2008, but has been below this value every year since 2008.[140]

In the SH, while Antarctic sea ice has been increasing since the start of satellite monitoring in 1978 until 2014, sea-ice-cover decreased dramatically in the last three years, shrinking

to a historic low on 1 March 2017.[78] Climate change will also change the extent of ice-free areas on the Antarctic continent, yet the distribution and severity of these effects remain unclear.[141] A previous study[141] suggests that melting across the Antarctic continent will lead to the emergence of between about 2100 (RCP 4.5 scenario, lower bound) and 17 000 km^2 (RCP 8.5 scenario, upper bound) of new ice-free area by the end of this century; the upper bound representing nearly a 25% increase. Most of this reduction is projected to occur on the Antarctic Peninsula where the total ice-free area could increase by a factor of three.

Lastly, climate change will affect the abundance of aerosols in the air. For example, the observed increasing frequency and extent of wildfires due to climate change,[117] is an important source of aerosols with significant effects on UV radiation at the Earth's surface. Despite strong correlation between increased drought frequency and occurrence of wildfires,[119] projections of changes in wildfires and associated emissions of compounds and aerosols into the atmosphere are limited in accuracy by the complexity of the processes.[114]

The direct and indirect effects of climate change discussed above do not change UV radiation in simple ways but depend on latitude, season, location, and emission scenario. Projections that take these factors into account are discussed in section 5. Impacts of changes in UV radiation due to these factors are discussed in ref. 27–29 and 61–63.

4 Variability in UV radiation and trends from observations

4.1 Variations of UV radiation in space and time

UV radiation at the Earth's surface is mostly controlled by the solar zenith angle (SZA), which varies with the time of day, latitude, and season. Seasonal variations in Sun–Earth separation are also significant. Absorption and scattering processes in the atmosphere result in additional variation, as discussed in section 3.

In the previous assessment,[23] latitudinal variations in annual doses of UV-B and UV-A radiation were discussed. These were derived from high-resolution measurements with ground-based spectroradiometers that comply with the quality standards of the Network for the Detection of Atmospheric Composition Change (NDACC).[142] This study has recently been expanded to also include latitudinal variations in the annual erythemal dose.[143] Because UV-B radiation contributes approximately 90% to the erythemal weighting, latitudinal differences in UV-B and erythemal dose show similar patterns, but gradients are larger than for the UV-A dose.

The annual erythemal dose is approximately a factor of four larger in the tropics than at high latitudes.[143] In the tropics, the annual dose reaches about 1.75 MJ m^{-2} near sea-level, which corresponds to an average daily dose of 4.8 kJ m^{-2}. At high altitude sites, much higher doses were measured at the Atacama Desert, Chile (5.2 km altitude),[144] which correspond to about 2.4 MJ m^{-2} of erythemal irradiance. For fair-skinned individuals (skin type-I), the minimal erythemal dose (MED) leading to reddening of the skin is about 0.2 kJ m^{-2}.[145] The average daily dose at the equator is therefore about 24 MED for a person with type I skin. The maximum daily erythemal dose ever observed at the Mauna Loa observatory, Hawaii, located at 3400 m altitude, is 9.5 kJ m^{-2} (or 47.5 MED for a person with type 1 skin).[146]

Despite low solar elevations at high latitudes, annual erythemal UV doses in Antarctica are still significant and can reach nearly half the values at mid-latitudes because of high surface albedo, 24 hours of sunlight in the summer (which occurs when the Earth–Sun separation is at its minimum), the effect of the ozone 'hole', and high surface elevation.[147] For example at the South Pole, the average daily erythemal dose is 1.3 kJ m^{-2} or almost one third of the dose measured in the tropics.[143] However, during the ozone 'hole' periods the maximum dose at the South Pole can reach 7.8 kJ m^{-2} which is similar to that at mid- to low-latitudes.[147]

Vitamin D_3-weighted UV doses (*i.e.*, UV doses relevant for the synthesis of vitamin D in human skin) during winter months in Northern Germany (52°N) and New Zealand's South Island (45°S) have recently been compared.[148] A strong latitudinal effect is expected due to the lower sun elevations at higher latitudes. When corrected for the difference in latitude, the vitamin D_3-weighted exposure in New Zealand during winter is a factor of 2 higher than in Germany, mainly because of greater cloudiness in Northern Germany. However, the attenuation by clouds at European stations at latitudes less than 48° N is smaller than Northern Germany, implying that the difference in UV levels between Europe and New Zealand is less pronounced for these more southern European locations.

Year-to-year variability in UV irradiance at a given location is controlled mainly by variations in ozone concentrations, cloud cover, and aerosols. Variations in ozone and their effect on UV irradiance at the surface are most pronounced at high latitudes. Despite recent evidence that stratospheric ozone concentrations are recovering, the ozone-induced variability of UV-B radiation in Antarctica remains very large, with near record high UVI observed at the South Pole in spring 2015 and below average UVI in spring 2016 and 2017 (Fig. 5). The relatively high UVI values observed in the spring of 2015 were partly caused by a large and long-lasting ozone 'hole'. Chemical depletion of ozone was enhanced in that year by heterogeneous processes associated with the volcanic aerosols that were injected into the stratosphere by the eruption of the Calbuco volcano in Chile,[8,10] as well as by an unusually cold and undisturbed polar stratospheric vortex.[12]

4.2 Observed long-term changes in UV radiation

Long-term changes in UV radiation have historically been calculated from measurements performed from space and at the ground. Satellite sensors suitable for estimating the UV irradiance at the Earth's surface only became available in the late 1970s. The number of reliable ground-based stations was also small before the ozone 'hole' was discovered. Trend calculations based on direct observations are therefore limited to only the last 38 years or so, with few exceptions.

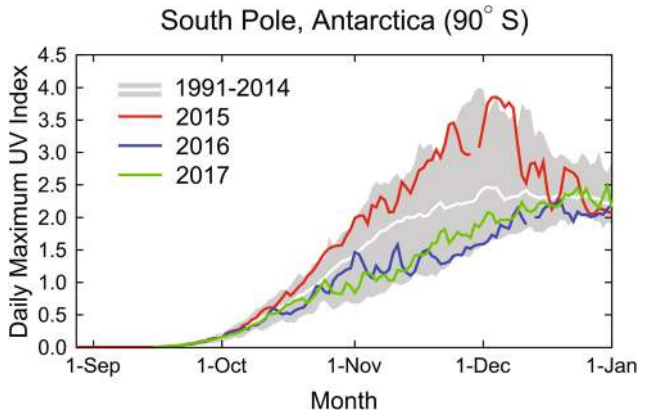

Fig. 5 Daily maximum UVI measured at the South Pole in 2015 (red line) and 2016 (blue line) and 2017 (green line) compared with the average (white line) and the lowest and highest values (grey shading) of observations of the years 1991 to 2014. Note that the ozone 'hole' first occurred in the 1970s and the reference range of 1991–2014 therefore only includes years when the 'hole' was established. The UVI was calculated from spectra measured by a SUV-100 spectroradiometer located at the South Pole. Up to 2009, the instrument was part of the NSF UV monitoring network[149] and is now a node in the NOAA Antarctic UV Monitoring Network (https://www.esrl.noaa.gov/gmd/grad/antuv/). Consistent data processing methods were applied for all years.

Changes in UV radiation since 1979 have been derived from a series of polar orbiting satellite instruments for the latitude range of 55°S to 55°N and results were summarized in the last assessments.[2,91] The UV data are derived mainly by radiative transfer calculations using total ozone, SZA, and information related to surface reflectivity and aerosols. For the period 1979–2010, increases in UVI, evaluated as a function of month and latitude belt (zonal average for every 5° of latitude from 50°S to 50°N), ranged between 0 and +5% per decade. Changes were dominated by increases in the UVI that occurred in the first half of this period when stratospheric ozone depletion was progressing. Most of the increases are significant at the 95% level except those calculated for winter months of both hemispheres and the equatorial zone where changes are close to zero. The largest positive trends were observed during the spring and summer at mid-latitudes of the SH, where the greatest decrease of ozone within the latitude range 50°S–50°N was observed. Unfortunately, these trend estimates cannot be confirmed with ground-based measurements because observations of UV radiation in the SH started only in 1990, while the largest depletion of stratospheric ozone at southern mid-latitudes had occurred already in the 1980s. Since the late 1990s, when ground-based measurements at several sites became available, changes in the total column ozone have been small. Reflectivity data from several satellites between 1979 and 2012 suggest that decreases in sea ice and small increases in the amount of clouds over the region of the Southern Ocean around the Antarctic Peninsula have resulted in decreases in UV-B radiation at the surface,[131,150] opposing the effects due to decreasing total ozone.

Satellite-based trend estimates of UV radiation at the Earth's surface have not been updated during the last four years. Therefore, only changes in UV radiation derived from ground-based measurements and attribution to different factors are discussed in the following:

Time series of UVI in the period 1979–2017, derived from the TUV radiative transfer model,[151] are compared with measurements at Arrival Heights, Antarctica, under all-sky conditions (Fig. 6). The column amount of atmospheric ozone was the only input parameter allowed to change in the model, with no account being taken of possible changes in aerosols, or surface albedo. Despite that limitation, the clear-sky envelope of measurements of UVI closely follows the model for the years where both are available. The largest changes in the UVI over this station occurred in the 1980s, when no measurements were available to verify the effects of stratospheric ozone depletion on UV radiation and to assess the variability of UV radiation during this period. Since the 1990s, there has been high variability in UV radiation, which precludes trend detection. Factors other than ozone (*e.g.*, changes in sea-ice- and snow-cover) may explain the small differences between measurement and model.

Changes in solar UV irradiance at 305 nm (a wavelength strongly affected by ozone absorption) and 325 nm (a wavelength only weakly affected by ozone absorption) have been analyzed to estimate trends in the period 1994–2011 for four northern (59°–71°N) and three southern (55°–69°S) high-latitude locations.[152] Although data from as early as 1990 are available, the first few years were excluded from the trend analysis to minimize the influence from aerosols of the eruption of Mt. Pinatubo in 1991, which reduced stratospheric ozone concentrations in the NH between 1991 and 1993. For the northern sites (59°–71°N), trends of spectral irradiance at 305 nm ranged between −8% and +0.4 per decade. The trend averaged over the four sites is −3.9% per decade and is significant at the 95% confidence level. This negative trend agrees with a statistically-significant upward trend in satellite-derived total ozone of about 1.5% per decade. The corresponding trend of spectral irradiance at 325 nm is −0.4% per decade and is not statistically significant, which is consistent with the absence in observed trends of aerosol optical depth and cloud fraction at the four sites. For the three southern sites (55°–69°S), no significant long-term trends were observed for spectral irradiances at 305 and 325 nm as well as for total ozone, aerosol optical depth, and cloud fraction, throughout the entire period of record.

This study[152] is the first suggesting that statistically significant decreases in UV-B radiation at the Earth's surface over northern high latitudes have occurred in response to the recovery of stratospheric ozone. However, this finding has yet to be confirmed with observations at other locations to become more robust. In general, it is more difficult to detect trends in UV radiation than in total ozone because ozone-related changes in UV radiation are often masked by varying attenuation of UV radiation by clouds, aerosols, and other factors. For example, changes in solar UV radiation observed in north-

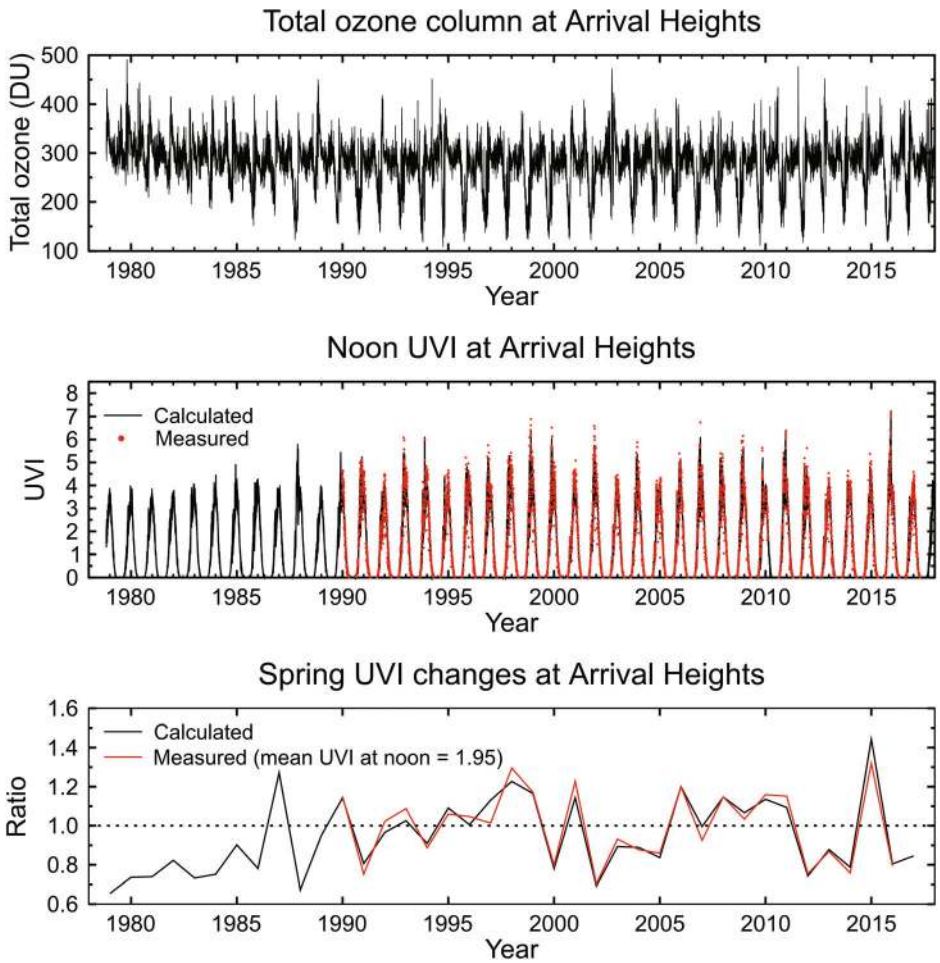

Fig. 6 (Top panel) Time series of daily total ozone at Arrival Heights (77.8°S, 166.7°E), Antarctica, derived from satellites for the 1979–2017 period. (Middle panel) Time series of daily noon UVI from measurements under all skies and model calculations based only on total ozone data. The measured UVI data (red symbols) are derived from spectra measured close to local noon by a SUV-100 spectroradiometer. Up to 2009, the instrument was part of the NSF UV monitoring network[153] and is now a node in the NOAA Antarctic UV Monitoring Network (https://www.esrl.noaa.gov/gmd/grad/antuv/). (Lower panel) Changes in noon UVI for spring (September–November), relative to the long-term mean over the same season, derived from measurements and model calculations.

ern mid-latitudes during the last two decades have been mainly controlled by clouds and aerosols rather than by ozone.

A study of a 20-year record (1994–2014) of spectrally resolved UV irradiance in Thessaloniki, Greece,[154] revealed increases in annual mean UV irradiance of 2–6% per decade. Updated time series of the anomalies of spectral irradiance at two wavelengths (307.5 nm and 350 nm representative of UV-B and UV-A irradiance, respectively) up to the end of 2017 are shown in Fig. 7 for cloud-free conditions. In the June–November period, the increases in irradiance are about 5% per decade for UV-B and 2.5% per decade for UV-A radiation and are caused predominantly by decreasing AOD. The greater increase in UV-B radiation is due to slightly decreasing total ozone in this season and the greater effect of decreasing AOD on UV-B radiation compared to UV-A wavelengths. During the last decade of the record (since the mid-2000s), the UV-A irradiance is no longer increasing, despite the continuing decrease of the AOD. This may be due to the weaker effect of aerosols on longer wavelengths. Ozone effects are largely manifested in the short-term (year-to-year) variability of UV irradiance. In another study, the day-to-day variability of noon-time clear-sky UVI at Thessaloniki was found to be influenced more by aerosols than total ozone, even on days with extremely high total ozone values.[155] These results are consistent with results for other locations discussed previously.[2]

Decreasing cloudiness with corresponding increases in UV radiation is part of a larger-scale phenomenon. For example, decreases in cloudiness over Europe have been confirmed with satellite data for the period 1983–2010.[156] According to this analysis, the annually averaged solar irradiance has increased by about 2 W m^{-2} per decade over Central and Eastern Europe. Depending on location, this change corresponds to a 1–2% increase in UV irradiance attributable to changes in cloudiness. At Chilton, United Kingdom (51°N), the variability in the erythemal annual dose has been investigated based on 25 years of data (1991–2015).[157] A large increase of 4.4% per year

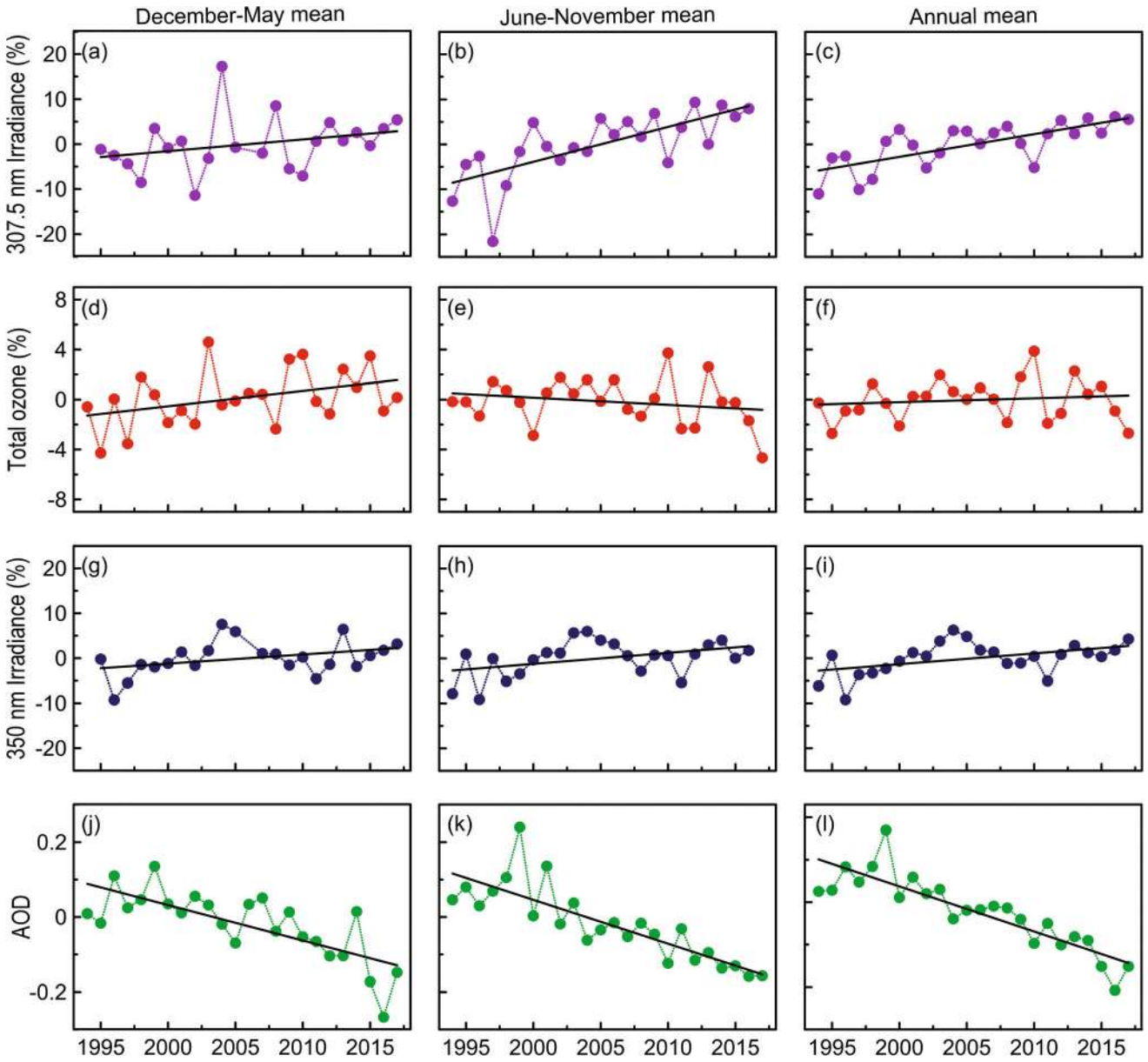

Fig. 7 Seasonal and yearly mean anomalies in percent relative to the long-term mean for clear-sky irradiance at 64° solar zenith angle for 307.5 nm (a, b, c) and 350 nm (g, h, i), total ozone column (d, e, f) and aerosol optical depth at 320 nm (j, k, l) for December–May (left panels), June–November (middle panels) and for the entire year (right panels). The AOD anomalies are expressed in absolute units. Linear trends are shown in each panel (black lines). The figure is adapted from Fountoulakis *et al.*[154] and updated to include data for 2015–2017. Data were recorded at Thessaloniki, Greece.

was found between 1991 and 1995, attributed to effects on total ozone from the eruption of Mt. Pinatubo in 1991 and an increase in total annual sunshine hours over this 4-year period. From 1995 to 2015, the dose decreased at a rate of 0.8% per year, and for the period 2000–2015, the decrease is slightly faster at 1.0% per year. Trends for all periods are significant at the 95% confidence level; however, no ozone measurements were included in that study, so an unambiguous attribution of the observed changes is not possible.

As discussed above, in densely populated or urban areas, changing aerosol effects can mask changes in UV-B radiation that arise from changes in ozone. Despite increasing total ozone over the 1991 to 2013 period, erythemally-weighted irradiance at Uccle, Belgium, increased by 7% per decade due to a combination of decreasing aerosol and cloud amounts, which more than counteracted the effect of ozone.[158] Their statistical analysis showed that trends in UV-B irradiance and total ozone changed in the late 1990s, consistent with the recovery of stratospheric ozone starting at about the same time.

4.3 Reconstruction of past changes in UV radiation from proxy data

Long-term datasets of surface UV radiation from ground-based instruments are sparse and only a few datasets adequately

cover the period since the onset of stratospheric ozone depletion. In the absence of direct measurements, empirical models have been used in combination with total ozone measurements and proxy data to reconstruct past UV irradiance levels. Changes in UV radiation due to clouds are frequently estimated from short-wave irradiance measured with pyranometers or instruments that record sunshine duration. These reconstructions are often limited by the availability of ozone data derived by satellites, which started operating only in the late 1970s. However, total ozone has been measured from the ground at a few research stations starting as early as 1926, and these data have been used to estimate longer-term historical levels of UV radiation.[159]

Two of the longest series of erythemal irradiance dating back to 1964 were reconstructed for two locations in Central Europe; in Belsk (52°N), Poland[160] and in Hradec Králové (50°N), Czech Republic.[161] The reconstruction for Belsk was based on a statistical model using aerosol extinction and total ozone data.[160] Increasing aerosols caused a decline in clear-sky UVI of up to 6% between 1964 and the mid-1970s, while increases in the UVI of about 5–6% per decade in 1974–1996 were caused in equal parts by stratospheric ozone depletion and decreasing aerosols. Since 1996, monthly-mean UVI at local noon has not changed substantially, as there have been no systematic changes in aerosol concentrations and total ozone over this period.

In Hradek Králové, the time series of erythemal irradiance was reconstructed using a radiative transfer model and additional empirical relationships.[161] Increases in daily doses of erythemal irradiance of up to 15% per decade were found in the 1980s and the 1990s, which were linked to the steep decline in total ozone of about 10% per decade. In the 1960s, the 1970s and the 2000s, the major driver for the observed changes in daily doses was the change in cloud cover, with mean annual doses in the most recent period (2004–2013) declining by about 5%.

UV radiation for the period 1950–2011 was reconstructed from a variety of proxy data for nine locations in Spain.[162] Erythemal irradiance increased over this time by about 13%, of which half was due to decreases in ozone. On a shorter timescale, 1985–2011, an increase of about 6% was calculated, mostly due to decreasing amounts of aerosols and clouds.

Measured and reconstructed data (using total ozone, snow depth, and daily sunshine duration as proxies) for the Polish Polar Station, Hornsund (77°N), have revealed no statistically significant trend for the period 1983–2016. However, statistically significant decreases in monthly doses of erythemal irradiance of about 1% per year were detected in May and June for the period 1996–2016.[163] This trend could not be attributed to observed increases in total ozone. Instead, cloud cover changes were identified as the main driver of the long-term UV changes at the site.

Statistically significant decreases in daily surface UV radiation from 1961 to 2015 were reported over most regions of China, ranging between 0.27 and 0.63 kJ per m^2 per year (0.15 and 0.37% per year).[164] These trends were derived from reconstructed data based on a model and proxy data from 724 weather stations, and are caused mainly by changes in aerosols and clouds. Unfortunately, no measurements of UV-B radiation were available at these stations, but trends in UV-B radiation are expected to be at least as large as those for total UV.

In conclusion, these reconstructions confirm that long-term changes in UV radiation over northern mid-latitudes since the onset of stratospheric ozone depletion in the mid-1960s have been mainly caused by changes in aerosols and clouds. Decreasing stratospheric ozone played a role at mid-latitudes only up to the mid-1990s.

5 Projections of UV radiation

Model-derived projections of UV radiation for the future have been extensively discussed over the last decade and presented in previous assessment reports.[23,59,165] These projections were based on variables affecting UV radiation which were derived from climate models and were updated as new improved climate models became available. In the following, we summarize new model results that update our assessment of changes in UV radiation for the next few decades and for the end of the 21st century.

Levels of UV-B radiation at the Earth's surface have been influenced by declining total ozone since the 1960s, particularly over the high latitudes of the SH including Antarctica. As concentrations of ODS started decreasing from the late 1990s, factors other than ozone have become the dominant drivers of changes in UV radiation, particularly outside Antarctica. These factors are influenced by increasing concentrations of GHGs and include clouds, aerosols, surface reflectivity, and UV radiation-absorbing air pollutants. Projected levels of UV-B radiation for the future depend on how these factors, including stratospheric ozone, will change in the next decades, and ultimately on the GHG scenario assumed in the respective CCMs.

Several new studies have investigated the dependence of total ozone projections by CCMs forced by different GHG emission scenarios (RCPs),[16,21,22,47] and, subsequently, the dependence of UV radiation projections under clear skies:[21,22]

Model simulations suggest that stratospheric ozone in the period 2075–2095 will exceed its pre-ozone-depletion (1955–1975) levels at all latitudes outside the tropics, if emissions of CO_2, CH_4 and N_2O continue unabated according to emissions scenario RCP 8.5. All else being equal, this would lead to reduced UV-B radiation over the same time frame.[21] The estimated decreases of noon UVI at northern mid-latitudes in 2075–2095 relative to 1955–1975 range between about 5 and 15%, with the largest decreases projected for the winter months, thus limiting UV radiation available for synthesis of vitamin D during winter even further (see ref. 27) For the southern mid-latitudes, the estimated decreases in UVI are smaller, ranging between about 3 and 10%. Noon UVI is projected to decrease in the Arctic by up to 20% in spring and to increase in Antarctica by up to 3% at the same season. In contrast, if actual emissions of CO_2, CH_4 and N_2O could be aggres-

sively reduced according to the RCP 2.6 scenario, by the end of the 21st century, UVI would increase relative to the 1960s (in response to slower recovery of ozone than for other RCPs) by up to 5% at all latitudes, except in the spring at high latitudes.[21] In the Arctic spring, noon UVI is projected to decrease by up to 5%, while over Antarctica remaining halocarbons would continue to deplete polar ozone and, together with changes in circulation, would increase the UVI by up to 20%. Note that these projections for UV radiation were based on an approximated relationship between UVI and total ozone, thus have not taken into account changes in clouds, aerosols, or surface reflectivity. Changes in UV-B radiation due to these factors are expected to be of comparable magnitude with, or in some cases, even greater than those related to changes in ozone.[2]

In another study,[22] simulations with a CCM were forced by three different GHG emission scenarios: RCP 4.5, RCP 6.0 and RCP 8.5. In the tropics, significant increases in DNA-weighted UV radiation by the end of the 21st century relative to the 1960s were found for all scenarios. These increases are driven by the respective projected decreases in total ozone. The largest increases were found for RCP 6.0, reaching 15% in specific tropical regions (*e.g.*, in South America, south Asia and over large parts of the Pacific Ocean). The average increase in DNA-weighted irradiance over the tropics ranges between 1 and 5% for different RCPs. In this study, cloud effects were considered internally in the CCM calculations. Of note, the action spectrum for DNA damage is shifted towards shorter wavelengths compared to the action spectra for erythema. DNA-weighted irradiance is therefore more sensitive to changes in ozone compared to erythemal irradiance quantified with the UVI, resulting in greater changes for the same change in ozone.

In a third study, focusing on the Arctic and northern high latitudes,[166] UV-B radiation is projected to decrease in 2090–2100 relative to 2000–2015 for both the RCP 4.5 and RCP 8.5 scenarios. These projected decreases are due to the recovery of total ozone, increases in cloud cover, and reduction of surface reflectivity caused by the shrinking of sea-ice- and snow-cover. Over land, the greatest reductions are projected for spring (April), under all-sky conditions and for RCP 8.5, locally reaching about 30% for the noon UVI and about 50% for the noon effective dose required to generate vitamin D. For RCP 4.5 these decreases are about 10% smaller than for RCP 8.5.

From these studies, it is evident that projections of UV-B radiation are very sensitive to the assumed scenarios for GHG emissions, which influence all factors that affect UV radiation, including ozone, especially with the recent finding that there has not been universal compliance to the Montreal Protocol.[4,30] Furthermore, sensitivity studies with models that participated in the IGAC/SPARC Chemistry-Climate Model Initiative (CCMI) concluded that concentrations of ozone derived from these models are subject to considerable uncertainties arising from the range of anthropogenic forcings specified in these models.[167] In addition, the processes that affect UV radiation and the interactions among the different factors that drive changes in UV radiation are not sufficiently well known. The overall uncertainties in projections of future UV radiation are therefore difficult to quantify.

Our previous assessment report[2] discussed the attribution of projected changes in UVI for the future to changes in total ozone, AOD, surface reflectivity and clouds, whereas the total ozone projections were provided by the CCMval models.[168] In this report, updated estimates of projections for the noon UVI are presented, following the same methodology but based on more recent projections of ozone, reflectivity, and clouds, obtained from the CCMI models.[167] Input data from only four of these models were used‡‡, because only these provided projections for both total ozone and surface reflectivity. These new model simulations are different from the former CCMval simulations because different scenarios for future concentrations of ODSs and GHGs were used. Projections for the period 1960–2100 were provided by the "REFC2" simulations of the CCMs, which assumed changes in GHGs according to the RCP 6.0 scenario[169] and changes in ODSs according to the A1[58] scenario.[167] Under the RCP 6.0 scenario, total ozone outside the tropics is projected to increase above its historic levels by the end of the 21st century. For RCP 8.5 this increase is larger.[16]

For the aerosol effects on UV radiation, AOD at 550 nm was derived according to RCP 6.0. The average AOD from nine models participating in CMIP5§§ was used.[170] Finally, the effects of clouds were quantified with the cloud modification factor (CMF) that is used to derive the UVI under all-sky conditions from the UVI under clear skies. The CMF was derived from simulations provided by two of the CCMI CCMs (HadGEM3-ES and MRI-ESM1r1) that had data available for the calculation of the CMF. The calculation of the wavelength-dependent effects of aerosols and clouds on UVI follows the methodology of the previous assessment report.[2]

Based on monthly values of these projected variables, the noon UVI under clear skies was calculated for each climate model, using the UVSPEC/libRadtran radiative transfer model.[171] Results are presented for two 10-year periods representing the present decade (2010–2020) and the future (2085–2095). Multi-model average differences in noon UVI for four months are shown in Fig. 8. The projected changes in UVI are sensitive to latitude and season, and can be attributed to different factors (ozone, aerosols, surface reflectivity, and clouds) that also exhibit a latitudinal and seasonal variability. The contribution of changes in these factors to the projected changes in UVI is shown in Table 1 for seven latitude bands and for four months.

The most important projected changes in UV radiation by the end of the 21st century compared to the present decade are:

(i) The large decreases at high and polar latitudes (>60°), with UVI values decreasing on average by 33–44% in the SH

‡‡ CCMI models: EMAC-L47MA, EMAC-L90MA, MRI-ESM1r1, HadGEM3-ES.
§§ CIMIP5 models: CESM1-CAM5, CSIRO-Mk3-6-0, GISS-E2-H, GFDL-ESM2M, HadGEM2-ES, MIROC-ESM-CHEM, IPSL-CM5A-MR, MRI-CGCM3, NorESM1-ME.

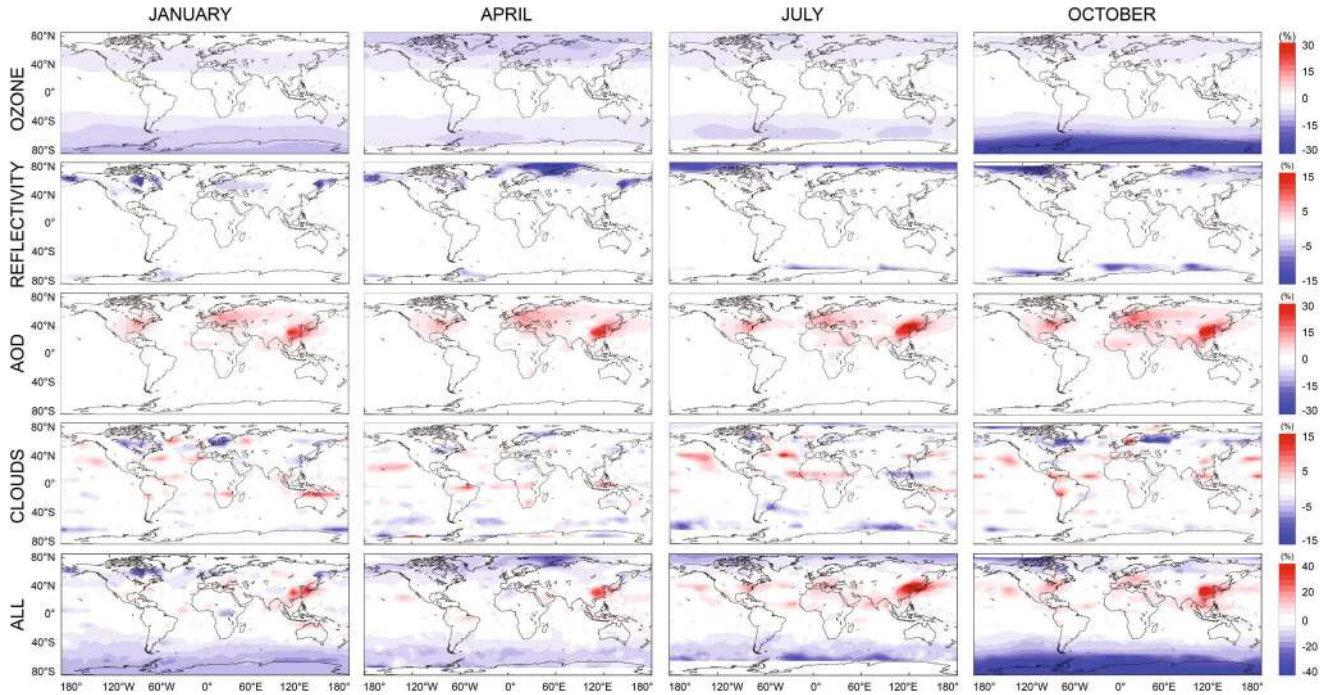

Fig. 8 Average changes in noon-time UVI calculated from CCMI simulations, between decadal averages for the present day (2010–2020) and at the end of this century (2085–2095; RCP6.0 scenario) for four months, calculated from projections by CCMs, including effects of changes in ozone, surface reflectivity, aerosols, and clouds. Also shown for each month are individual changes in UVI due to changes in each of these factors, while the others are kept constant. Note that the scale of the color coding is different for each factor.

during spring and by 5–15% in the NH during summer and autumn. These are due mainly to the projected increases in total ozone column and, for the NH, decreases in surface reflectivity.

(ii) The large increases at some northern mid-latitude regions, locally reaching 40% higher UVI values. These increases are due mainly to projected reduction in aerosol optical depth over densely populated and industrialized regions like East Asia, Central Europe and Eastern USA. In some of these areas, decreasing or increasing cloudiness modifies the effects of aerosols, leading to enhanced or reduced UV radiation levels.

For the southern polar latitudes, decreases in UVI of about 44% in October and 13% in January are almost entirely due to the projected recovery of stratospheric ozone by the end of the century and the disappearance of the Antarctic ozone 'hole'. The effect of ozone is rather uniform in the entire area, as manifested by the small range of the changes, while the contribution of the other factors is negligible.

For the SH high latitudes, the pattern is similar to the polar region but decreases in UVI are smaller in all months ranging from about 10% in April to 33% in October. In this latitude band the changes in UVI due to changes in reflectivity and clouds become more important, despite the small average values that do not exceed 3% across all seasons. The spread of the changes due to these factors is large, ranging from −12 to +2 for the reflectivity and from −14 to +16% for the clouds. This variability leads to a less uniform pattern of the changes in UVI.

Average projected changes in UVI at SH mid-latitudes are negative and similar across seasons (range −6 to −9%), while their spatial variability is large, ranging between 6 and −21%. Main contributors to these changes are increases in stratospheric ozone (−1 to −12% change in UVI) and changes in cloudiness (−9 to +5% change in UVI). Concentrations of aerosols over the SH at mid-latitudes to the pole are already low; therefore, their effects on average changes in UVI are negligible.

In the tropics, average projected changes in UVI are small (about 1%) for all variables, leading to small average increases of 0–2%. However, the large spread of the effects of aerosols (−6 to +21%) and clouds (−8 to +12%) leads to a large spread of the changes in UVI ranging spatially between −19% and +26%. Taking into account the large uncertainties in the projections of clouds, the magnitude of this large spatial variability is highly uncertain. However, the tropics include some areas that are projected to have fewer aerosols in the future, such as southeastern Asia, which explains the large projected increases in UVI. The greatest decrease in UVI is projected in January for Central Africa due to a projected increase in future aerosols.

At NH mid-latitudes, changes in UVI are dominated by large increases driven by the projected decreases in AOD. Increases in UVI are found for all seasons, locally reaching 54%, while on average the effect is much smaller, close to 5%. The largest increases are projected for China, Europe and Eastern USA, so that the UVI will increase to levels comparable with those at cleaner urban areas at similar latitudes. Reduced

Table 1 Average percentage changes in noon-time UVI calculated from CCMI simulations, between decadal averages for the present day (2010–2020) and at the end of this century (2085–2095; RCP 6.0 scenario), for seven latitude bands and four months. Also shown are contributions to changes in UVI from changes in total ozone, surface reflectivity, aerosol, and clouds. The mean and spread (standard deviation; SD) of the model results from all grid points in each latitude band are shown, as well as the minimum and maximum percentage change in UVI. Data for April and July in south polar latitudes and for January in northern polar latitudes are missing as solar radiation is close to zero in these months

		January			April			July			October		
		Avg. ± SD	Min.	Max.	Avg. ± SD	Min.	Max.	Avg. ± SD	Min.	Max.	Avg. ± SD	Min.	Max.
N. Polar	Ozone				−8 ± 1	−9	−7	−6 ± 0	−6	−5	−3 ± 0	−4	−3
>80°N	Reflectivity				−3 ± 5	−21	0	−8 ± 3	−11	−1	−7 ± 6	−20	0
	Aerosol	POLAR NIGHT			2 ± 0	0	2	−1 ± 1	−2	1	0 ± 1	−1	1
	Clouds				0 ± 0	−1	1	−2 ± 2	−8	2	−3 ± 5	−18	5
	UVI				**−9 ± 6**	**−27**	**−3**	**−14 ± 3**	**−19**	**−6**	**−14 ± 11**	**−36**	**5**
N. High	Ozone	−3 ± 1	−5	−2	−7 ± 1	−9	−5	−5 ± 1	−6	−4	−4 ± 1	−6	−3
60°N–80°N	Reflectivity	−2 ± 3	−16	1	−3 ± 3	−16	0	−1 ± 2	−11	0	−3 ± 3	−17	0
	Aerosol	2 ± 2	0	7	2 ± 2	0	9	1 ± 1	−1	5	2 ± 2	0	10
	Clouds	−1 ± 3	−10	8	0 ± 1	−7	3	0 ± 2	−8	6	−1 ± 4	−16	15
	UVI	**−6 ± 8**	**−35**	**11**	**−8 ± 5**	**−27**	**2**	**−5 ± 4**	**−16**	**4**	**−7 ± 5**	**−22**	**7**
N. Mid	Ozone	−4 ± 1	−6	−1	−5 ± 2	−8	−1	−3 ± 1	−5	−1	−2 ± 1	−4	0
30°N–60°N	Reflectivity	−1 ± 2	−16	1	0 ± 1	−15	0	0 ± 0	−2	0	0 ± 0	−4	0
	Aerosol	4 ± 4	−1	26	5 ± 4	−1	28	5 ± 5	1	38	5 ± 5	1	38
	Clouds	0 ± 2	−10	7	0 ± 1	−6	6	1 ± 2	−4	15	0 ± 2	−10	9
	UVI	**0 ± 7**	**−27**	**34**	**−1 ± 6**	**−17**	**32**	**5 ± 8**	**−6**	**54**	**5 ± 7**	**−8**	**53**
Tropics	Ozone	−1 ± 1	−3	0	0 ± 1	−2	0	−1 ± 1	−3	0	−1 ± 1	−3	0
30°S–30°N	Reflectivity	0 ± 0	0	0	0 ± 0	0	0	0 ± 0	0	0	0 ± 0	0	0
	Aerosol	1 ± 2	−4	19	1 ± 2	−5	21	1 ± 2	−6	16	1 ± 3	−4	21
	Clouds	0 ± 2	−5	12	0 ± 2	−5	12	0 ± 2	−8	8	0 ± 2	−4	11
	UVI	**0 ± 4**	**−19**	**17**	**1 ± 3**	**−8**	**23**	**1 ± 3**	**−8**	**19**	**2 ± 4**	**−8**	**26**
S. Mid	Ozone	−5 ± 2	−8	−2	−4 ± 1	−6	−1	−5 ± 1	−7	−1	−6 ± 3	−12	−1
30°S–60°S	Reflectivity	0 ± 0	0	0	0 ± 0	0	0	0 ± 0	−1	0	0 ± 0	−2	0
	Aerosol	0 ± 0	−1	5	0 ± 0	0	6	0 ± 0	0	5	0 ± 0	−1	5
	Clouds	0 ± 1	−4	4	−1 ± 2	−6	5	−1 ± 2	−9	3	0 ± 1	−3	5
	UVI	**−7 ± 3**	**−14**	**2**	**−6 ± 3**	**−15**	**3**	**−7 ± 4**	**−20**	**6**	**−9 ± 5**	**−21**	**2**
S. High	Ozone	−8 ± 1	−10	−7	−6 ± 1	−7	−5	−6 ± 0	−6	−5	−23 ± 8	−35	−9
60°S–80°S	Reflectivity	−1 ± 1	−5	0	−1 ± 1	−7	1	−2 ± 3	−10	2	−2 ± 3	−12	1
	Aerosol	0 ± 0	−1	0	0 ± 0	0	0	0 ± 0	−1	0	0 ± 0	−1	1
	Clouds	−1 ± 2	−12	2	−1 ± 3	−14	16	−3 ± 3	−12	7	−1 ± 2	−9	3
	UVI	**−14 ± 2**	**−21**	**−9**	**−10 ± 4**	**−31**	**4**	**−17 ± 7**	**−34**	**−3**	**−33 ± 8**	**−48**	**−14**
S. Polar	Ozone	−10 ± 0	−10	−9							−35 ± 1	−37	−33
>80°S	Reflectivity	0 ± 0	−2	0							0 ± 0	0	0
	Aerosol	0 ± 0	0	0	POLAR NIGHT			POLAR NIGHT			0 ± 0	0	0
	Clouds	0 ± 0	0	1							0 ± 1	−1	3
	UVI	**−13 ± 1**	**−15**	**−12**							**−44 ± 1**	**−48**	**−41**

concentrations of aerosols have already been observed during the last two decades over urban areas in Europe and Eastern USA (see ref. 62) At some of these locations, where measurements of UV irradiance were available, the reduced aerosols have led to increases in UV radiation, as discussed in section 4. The effect of the projected increases in total ozone above the pre-ozone-depletion levels due to increasing GHGs contributes from 0 to −8% to the projected decreases in UVI. Clouds are also important contributors inducing regional positive or negative changes in the UVI in the range −10 to +15%. Finally, in the northernmost mid-latitudes, projected reductions in surface reflectivity in January and April lead to decreases in UVI of up to 16%, particularly over areas presently covered by sea ice or snow, which are projected to decrease dramatically in the future (*e.g.*, Sea of Okhotsk, Russia, and Alaska).

At NH high latitudes, projected increases in ozone have similar effects to those at NH mid-latitudes. Reduction in surface reflectivity across all months is the dominant factor for the projected average decreases in UVI of about 6%. The large spatial variability of projected surface reflectivity and cloudiness which, as noted above, are associated with large uncertainties, leads to a very large spread in the projected changes in UVI ranging from −35 to +11%. The effects of changes in aerosol in this region are small, leading to average increases in UVI of less than 2%.

Finally, at the polar latitudes of the Arctic, the UVI is projected to decrease by the end of the 21st century relative to the present, on average by about 9% in April and about 14% in July and October. Regional changes in UVI of −36 to +5% are projected due to projected increases in total ozone (effect on

UVI: −9 to −3%), decreases in reflectivity (effect on UVI: 0 to −21%), and changes in cloudiness with effects on UVI of −18 to +5%.

The estimated changes in the UVI between the present decade and the end of the 21st century are associated with large uncertainties arising from the uncertainties of the projections of all factors, in addition to the effect of the assumed RCP scenario, which was discussed above. We estimate up to 30% uncertainty in the UVI calculations due to uncertainty in the aerosols, and particularly in the SSA. Variations of projections of different CCMs are also important. For April and July, only 50% of the projected changes in UVI over all latitudes are larger than the corresponding inter-model standard deviation. This percentage is even smaller (about 30%) for January and October. Therefore, our confidence in these estimates for the future is low (especially given the possible non-compliance issues discussed earlier). However, these estimates represent our best knowledge for the projected levels of UV radiation at the Earth's surface that are currently available. For regions and seasons where the projected changes in UVI are large (*e.g.*, greater than 5%) at least the direction of the changes is more certain.

The conclusions from the new UVI simulations do not substantially change our understanding of the projected changes in UVI by the end of the century relative to the present decade, as discussed in the previous assessment, where we found that UV is expected to increase in the tropics, where it is already too high for optimum health; and to decrease elsewhere, where it is sometimes too low for optimum health.[2] The magnitude of changes is somewhat smaller, owing to differences in the projections of the factors affecting the surface UV radiation, and the scenarios considered for their changes in the future. The latter is probably the most important source of the uncertainties for the UV radiation projections.

6 Implications of geoengineering for UV radiation

Solar Radiation Management (SRM) (also known as "geoengineering") has been suggested for counteracting the warming from increasing GHG by reducing the amount of solar radiation absorbed by the Earth's surface. Proposals for SRM include space reflectors, increasing of marine clouds, and injection of sulfuric aerosols into the stratosphere.[172,173] Since then, several studies have discussed potential implications of such actions for the atmosphere and the biosphere, including side effects on stratospheric ozone and solar UV radiation.[6,23,48,174] Impacts on stratospheric ozone would occur through: (i) chemical effects of the increased aerosol loading, (ii) resulting changes in temperature and scattered solar radiation in the stratosphere, with corresponding changed photolysis rates, both of which will impact ozone chemistry, and (iii) resulting changes in stratospheric circulation and transport. Recent studies have concluded that, despite progress in understanding the potential environmental, political, and societal risks and benefits of solar geoengineering, the current state of knowledge remains insufficient for conducting a comprehensive assessment that would be required for making future decisions on deployment.[175–177] Here we assess only effects of geoengineering on UV radiation. A more comprehensive discussion is included in the report of the Science Assessment Panel.[4]

Increased concentrations of sulfate aerosols from the continuous injection of SO_2 into the tropical stratosphere would have an effect similar to that from large volcanic eruptions. Model simulations of such solar geoengineering actions estimate losses in stratospheric ozone in most latitudes, which would lead to increases in UV-B radiation at the surface. However, the additional aerosol in the stratosphere would decrease UV radiation (both UV-B and UV-A) and increase the proportion of diffuse to direct solar radiation due to increased scattering by the aerosols.[178,179] Such increased diffuse radiation may influence the growth of plants since diffuse radiation is received and absorbed more effectively than direct radiation (see ref. 28 and 180). The estimated mean increase of diffuse radiation averaged over the UV-visible range (300–700 nm) is 11%.[181] However, because of commensurate losses in the direct beam component, the increase in global radiation (direct plus diffuse) would be smaller. Exposure of humans and ecosystems to enhanced UV-B diffuse radiation could have many important implications (as discussed above and detailed in ref. 27–29).

7 Advances in UV monitoring and modeling

In this section we discuss advancements in measuring UV radiation from the ground and space, as well as methods to determine personal exposure. Advancements in instrumentation to measure aerosol properties have been discussed in section 3.2.

7.1 Ground based systems

UV radiation at the Earth's surface has historically been measured with scanning spectroradiometers, broad-band instruments with a response function mimicking the erythemal response, and multi-filter instruments, which measure the spectral irradiance at several wavelengths (typically 4–7) in the UV range.[23] Spectroradiometers using double-monochromators are the most accurate instruments because of their ability to suppress stray light from the visible range that would otherwise be detected as wavelengths in the UV-B.

In the past, the quality of spectral UV measurements has been assessed with intercomparison campaigns, which bring together instruments from various networks to perform measurements side by side that are subsequently analyzed. In 2015 and 2017 two such campaigns were organized in the framework of the EUBREWNET COST action ES1207 (http://rbcce.aemet.es/eubrewnet) in El Arenosillo, Spain, with participation of more than 20 Brewer spectrophotometers.[182] An

intercomparison campaign of erythemal detectors took place in summer 2017 at PMOD/WRC in Davos Switzerland.[183] Finally, three spectroradiometers representing different networks in Australia and New Zealand took part in a two-month campaign in Melbourne, Australia, in autumn 2013.[184]

The alternative to these campaigns is the use of a reference instrument that is transported to UV monitoring locations, to operate synchronously and be compared with the local instrument(s). In the early 2000s, a portable reference spectroradiometer known as QASUME (Quality Assurance of Spectral solar UV Measurements in Europe) was developed and has performed more than 65 site visits to 33 European stations since 2001.[185] A comprehensive analysis of the instrument's uncertainties has recently been completed and a new reference spectroradiometer, named QASUMEII, was constructed, taking advantage of improvements in measuring techniques during the last decade.[185] For example, QASUMEII uses a hybrid detection system, which combines the high sensitivity of a UV-optimized photo counter with the good stability of silicon photodiodes. For wavelengths between 310 and 400 nm and SZAs smaller than 75°, measurement uncertainties at the 95% confidence level are 3.08% and 2.02% for QASUME and QASUMEII, respectively. Compared to QASUME's uncertainty of between 4.6% and 8.8%, depending on SZA, assessed in 2005,[186] improvements implemented during the last decade have reduced the instrument's uncertainty by more than half.

Despite their advantages in terms of measurement accuracy, scanning spectroradiometers are expensive to procure and operate, and scan-rates are comparatively slow. It may take more than 10 minutes to measure a spectrum in the UV range,[185] which makes it difficult to assess the effects of fast changes in intensity, for example, due to moving clouds. During the last decade, array spectroradiometers (ASRMs) have been increasingly introduced for spectral irradiance measurements in the UV. These instruments typically use a charge-coupled device (CCD) detector, which records the entire UV spectrum within seconds. However, for physical reasons they cannot use double-dispersion as with scanning spectroradiometers, and measurement errors caused by insufficient suppression of stray light typically limit the useful spectral range of these devices to wavelengths longer than about 305 nm, in particular for large SZAs.[184] For example, in 2014, solar measurements of 14 commercially available ASRMs were compared against QASUME during a campaign in Switzerland.[187] Almost all instruments applied a state-of-the-art numerical stray light correction.[188] Despite this correction, almost all measurements were affected by stray light at wavelengths shorter than 310 nm and overestimated the global spectral irradiance below this wavelength for all SZAs. However, some well-characterized instruments were able to determine the UVI to within 5% of QASUME measurements for SZAs less than 50°. For larger SZAs, the measurement accuracy deteriorated for all ASRMs participating in this campaign.

Recently, a radiometer was introduced that uses an array spectroradiometer in combination with several interference filters mounted in a filter wheel to reduce the effect of stray light.[189] A comparison of data from this instrument against a research grade spectroradiometer showed agreement within 10% for wavelengths larger than about 305 nm.[190]

We conclude from these results that the accuracy of currently available ASRMs is not sufficient to detect and quantify the small changes in surface UV radiation expected at mid-latitude locations caused by stratospheric ozone depletion and, eventually, by ozone recovery. However, the instruments are useful for monitoring the spectrum of radiation in situations when the radiation field changes rapidly (*e.g.*, partly cloudy conditions or under tree canopies). ASRMs have been widely used to study the effects of solar UV-B radiation in terrestrial ecosystems.[191]

Lack of proper quality control of data from radiometers of any type can lead to erroneous data and false conclusions, as for example the extremely high UVI of 43.3 at the tropical Andes reported by Cabrol *et al.*[192] A recent study where the data and methods were critically reviewed and incorrect data were identified, suggests that the maximum UVI at this location was in the range of 25 ± 5.[193]

The number of stations with high-quality spectral UV measurements is currently declining¶¶ and future funding for many of the remaining stations is uncertain.[194] If this trend continues, the scientific community may lose the ability to assess changes of UV radiation at the Earth's surface and associated impacts, to verify satellite UV data with ground-based observations, and to validate model projections.

7.2 Satellite validation

UV radiation at the ground has been estimated from measurements of various space-borne sensors since the late 1970s.[195,196] These estimates are derived from backscattered radiances measured by the sensors in combination with radiative transfer model calculations. Uncertainties of these estimates are typically larger than for direct measurements at the surface because not all model parameters can be adequately quantified from space. For example, absorbing aerosols in the boundary layer are difficult to detect by satellites.[197] In general, sensors on satellites can provide reliable estimates of surface UV irradiance under low-aerosol and clear-sky conditions, but these estimates may be affected by large systematic biases over polluted areas, under overcast skies, or above snow-covered surfaces, as discussed in more detail in the following.

Irradiance estimates are generally less accurate for UV-B than UV-A regions of the spectrum. For example, the irradiance inferred from the Ozone Monitoring Instrument (OMI) onboard NASA's Aura sun-synchronous satellite exceeded clear-sky ground-based measurements at Thessaloniki, Greece, by up to 14% at 305 nm and up to 10% at 310 nm. In contrast, at 324 nm and 380 nm, the OMI data underestimated the UV irradiance by less than 5%.[198] These wavelength-dependent biases indicate that the spectral absorption and scattering pro-

¶¶ http://www.montreal30.io3c.org/sites/montreal30.io3c.org/files/pictures/20%20matin/Braathen-WMO-GAW-Ozone-UV.pdf

perties of aerosols are not correctly addressed by the satellite data-retrieval algorithm.

Comparisons between OMI UV data and ground-based measurements at 13 stations located in the Arctic and Scandinavia from 60°N to 83°N revealed large biases due to incomplete knowledge of the surface albedo.[199] When the surface albedo is known, OMI data typically exceed ground-based measurements by 0–11%. Otherwise, biases are much larger, ranging between +55%, when the albedo assumed by OMI is too high, to −59% when it is too low. These large negative biases are observed when reflections from snow and ice, which ultimately increase downwelling UV irradiance, are misinterpreted as reflections from clouds.

At the Observatoire de Haute Provence (OHP), located in a pristine mountainous region of southeast France, UV data from OMI and the Global Ozone Monitoring Experiment (GOME-2) overestimate the clear-sky noon-time UVI relative to ground-based measurements by only 6% and 2%, respectively. At Saint-Denis (SDR), another pristine site located on La Réunion Island in the Indian Ocean, both OMI and GOME-2 observations are biased high by 4% relative to ground-based observations. These small biases generally increase for all-sky conditions and are 9% at OHP and 11% at SDR.[200]

A new dataset of UVI observations with broadband instruments at six locations in South Africa recently became available.[201] Time records at four of the six sites are as long as 21 years. For clear-sky days, the mean bias between ground-based and OMI measurements at the time of the satellite overpass is less than ±0.6 units of UVI.

At Hoboken, New Jersey, USA, UVI values reported by OMI agree to within ±2% with ground-based measurements with a NILU-UV multifilter radiometer for clear-sky conditions.[202] With increasing cloud cover, OMI overestimates the UVI at the surface, reaching 24% on average for overcast conditions.

UV data products provided by the Tropospheric Emission Monitoring Internet Service (TEMIS) were recently compared with ground-based measurements at Thessaloniki, a moderately polluted site in northern Greece.[203] TEMIS UV data were derived from total ozone measurements provided by the SCanning Imaging Absorption SpectroMeter for Atmospheric CHartographY (SCIAMACHY) up to April 2012 and are based on GOME-2 for later years. Cloud attenuation over Europe is provided by several Spinning Enhanced Visible and InfraRed Imagers (SEVIRI). Because SEVIRI instruments are installed on geostationary satellites, TEMIS data products take changes in cloud cover throughout the day into account, in contrast to OMI UV data, which are based on observations of clouds at the time that the location on the Earth's surface is under the satellite. For cloud-free days, the bias between erythemal daily doses from TEMIS and ground-based measurements at Thessaloniki is less than ±2%. For all-sky conditions, TEMIS overestimates ground observations by 12.5%. Similar positive biases with increasing cloudiness were also reported.[200,202] At highly polluted locations such as Santiago, Chile, satellites may overestimate the UVI at the Earth's surface by up to 47% on average.[23]

Observations of instantaneous total ozone and erythemal irradiance for the entire sunlit globe commenced in June 2015 using data from the Earth Polychromatic Imaging Camera (EPIC) installed on board the Deep Space Climate Observatory (DSCOVR), which is located at the Lagrange Point L1 between the Earth and sun.[204] At L1, the satellite rotates synchronously with the Earth about the sun due to the concurrent action of the gravitational forces of Earth and sun. At this point of equilibrium, DSCOVR is "parked" at a near constant distance of about 1.6 million kilometers from Earth. This vantage point allows unique observations of the sunlit globe from sunrise to sunset that are performed multiple times per day as the Earth rotates in EPIC's field of view. Neither geostationary nor low Earth-orbiting satellites such as OMI can produce similar data or images. Retrieved ozone amounts agree with ground-based measurements and satellite data to within 3%. It has been demonstrated that erythemal irradiance can be calculated from this instrument's data at a nadir resolution of 18 × 18 km^2. These new measurements confirm previous results from satellite data[205] and from ground-based instruments[206–209] that the highest UVI on Earth of greater than 20 occurs in Peru, Bolivia, and Chile at high elevations of the Andes Mountains during summer months (Fig. 9). Solar radiation is less attenuated when reaching such high-altitude locations, compared to sea-level, due to smaller amounts of atmospheric molecules in the column above, resulting in extreme values of the UVI.

UV data from satellite instruments are often provided at a spatial resolution of tens of kilometers. A method has been proposed to scale the UVI data provided by the space-borne Ozone Monitoring Instrument (OMI) down to 1 × 1 km^2 grid. This downscaling was achieved by interpolation of satellite data and other measurements (*e.g.*, surface albedo, aerosol optical depth, cloud cover, dew point, ozone, surface incoming shortwave flux, and sulfur dioxide).[210] Such higher resolution data can be more useful in studies where UV radiation data at specific locations are needed.

By combining ozone data from GOME-2 and cloud data from AVHRR/3 satellite sensors, an improved algorithm was developed to estimate different biological weightings of surface UV radiation, as well as UV-B and UVA, at 0.5° spatial resolution.[211] New global erythemal dose datasets were constructed from OMI measurements and are provided at 0.25° spatial resolution (about 25 km at the equator).[150] Both datasets can be useful for large-scale ecological studies, presuming that possible mismatches between the provided biological weightings and the weighting of interest, as well as the target geometries (*e.g.*, human body or tree shapes), are properly taken into account.

Spectral irradiance is derived from satellite data using, among others, information of the reflectivity of the Earth's surface below. Recent field experiments indicated that when soot, volcanic sand, and glacial silt are deposited on a surface covered by snow, they sink within minutes into the snow. For reflected radiation measured by satellite radiometers at nadir viewing directions (*i.e.*, vertically below the satellite) the

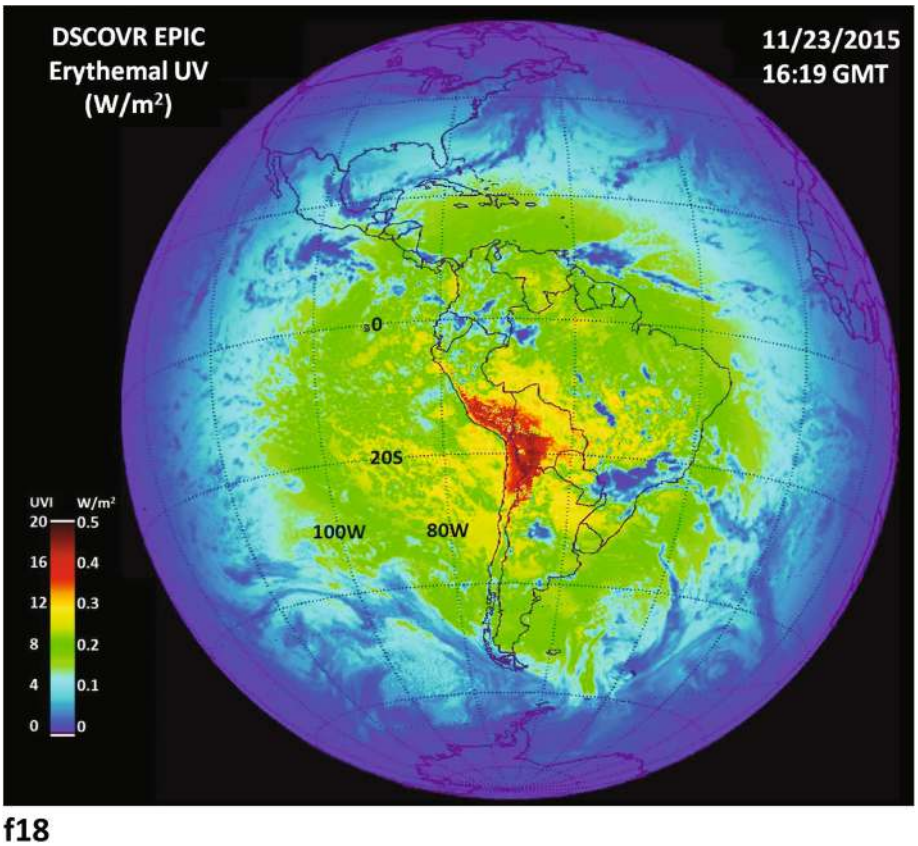

Fig. 9 UVI data over South America derived from DSCOVR on 23 November 2015 at 16:19 UTC. Extremely high values are shown in the Andes Mountains in Peru, Bolivia, and Chile corresponding to a UVI greater than 20. Local solar noon is at 64.75°W and sun is overhead near 20°S. (Adapted from Herman *et al.*[204]).

surface appears darker, but for larger viewing angles it appears brighter, almost as reflective as the natural pristine snow.[212] These discrepancies in the estimated reflectivity may affect the accuracy of satellite-derived spectral irradiance data over snow-covered regions. Ground-based measurements of UV radiation are not prone to this error.

7.3 Personal exposure

The highest-quality measurements of UV radiation from ground-based spectroradiometers are not generally applicable to understanding personal exposure. Firstly, these instruments are generally positioned in locations that are not typical of every-day exposure. Secondly, they typically measure the cosine-weighted irradiance received by a horizontal surface. To more realistically model personal exposure, information on the directional distribution of radiation (radiance) from all directions (*i.e.*, including downwelling and upwelling radiance from the upper and the lower hemisphere, respectively) would be preferable. However, such measurements are not widely available.[213]

For example, the exposure of the human body to UV radiation was calculated with a radiative transfer model by integrating incident radiation over the 3D geometry of the body.[214] When this approach is applied for a snow-free valley and for snow-covered mountain terrain (with albedo of 0.6), an increase in UV exposure by 10% per 100 m increase in altitude was found, which is more than 10 times larger than the usual increase in erythemally weighted UV irradiance with altitude in snow-free conditions.[2,91] The results imply that upwelling radiation is an important source of exposure to UV radiation affecting human health where exposure occurs at higher altitudes (see ref. 27).

A new modelling tool (SimUVEx v2),[215] allows the evaluation of the contribution of the direct, diffuse, and reflected components of UV radiation for different sizes of shade structure. According to this study, although shading can lead to decreases in exposure to direct UV radiation greater than 97% for the upper body areas, such as the head and the neck, a large fraction of the diffuse UV radiation is always present. For example, a subject without adequate protection under a sun umbrella would receive sufficient diffuse radiation for inducing sunburn in 2 hours (12:00–14:00) in the summer.

The radiation field incident on a person is usually obstructed by buildings or trees, including man-made canyons from buildings that reduce the sky view, and can reduce UV amounts appreciably.[216,217] Even if direct sunlight is not obscured, reductions in erythemally-weighted radiation can be substantial because usually at least 50% of unimpeded radi-

ation would be from diffuse skylight. For the same reason, protection from the direct beam alone without obstructing a significant fraction of skylight cannot afford substantial protection from UV radiation. For example, the vitamin D_3-weighted UV exposure of a human with vertical posture was calculated for urban locations to investigate the impact of the orientation of obstructions on the exposure.[218] It was found that, at the spring equinox at a mid-latitude site in Germany, the exposure of a human model with winter clothing in an environment where obstructions cover 40% of the sky varies by up to 25%, depending on the orientation of the human model to the sun. It was also found that for these conditions, the accumulated vitamin D_3-weighted exposure of a human with winter clothing walking during the lunch break is reduced 40% by obstructions from buildings and vegetation.

Total personal exposure also depends critically on the amount of time spent outdoors. On a typical summer's day, the ambient UV dose can exceed 70 SED‖‖,[146] which corresponds to more than 30 MEDs for fair skinned individuals if they are exposed to sunlight throughout the day with no protection. But generally, personal exposure times to sunlight will be much shorter. They are also highly variable from person to person[27] as well as with time and location.

While electronic UV dosimeters can be difficult to use and are more expensive than traditional dosimeters (*e.g.*, spore[219] or polysulfone[220] dosimeters), they have several advantages: firstly, electronic dosimeters can be tuned to more closely match the biological weighting of interest than is the case for polysulfone dosimeters, for which differences between their response function and action spectrum of interest can be large.[221] Secondly, even if there are significant differences between the instrument response and the target weighting, the latter can still be derived from the measurements using radiative transfer models that include ozone and SZA as inputs. This is generally not possible for the older dosimeters because of their long integration periods that include a wide range of SZA.[222] Thirdly, the time series of data from the electronic dosimeters can assist in quality assurance and in verifying compliance of the users to the measurement protocols. For example, if the dosimeter is not actually worn, but left stationary, that can be obvious from the data record. Finally, accuracy will generally be improved from the reusable dosimeters, which generally have a linear response compared with the less precise logarithmic response of older dosimeters. Nevertheless, the accuracy of these devices is still not comparable with that of research-grade spectroradiometers.[223]

Since the last assessment report,[23] there has been some progress in the use of electronic and other types of dosimeters in measuring the exposure to UV radiation in a wide variety of conditions. These include the general public during clinical trials in New Zealand to determine the relationship between UV exposure and vitamin D,[224] members of an Antarctic expedition,[225] high school students in Switzerland,[226] seafarers working on decks of vessels,[227] skiers in Italy,[228] tennis players in Spain,[222] hikers in Spain and France,[222] and runners.[222,229] Dosimeters measure the UV dose at the site where the dosimeter is worn (lapel, wrist, *etc.*), and will have a biological effect only on the fraction of the unprotected skin exposed. For example, skiers expose a small fraction of their body in contrast to swimmers. In most cases, the personal dose was only a small proportion of the available ambient UV dose. The mean exposure for the general public in New Zealand[224] and of students in Switzerland[226] was less than 2% of the ambient dose. The Swiss students received 85% of their cumulative UV dose on weekends and holidays. For outdoor sporting activities, their doses were larger. Measurements with polysulfone detectors showed that skiers in Italy would receive 65% of the ambient dose on average to any exposed skin. The median daily UV exposure of hikers and tennis players typically exceeded 5 SED, according to one study, with maximum exposures being much higher. A recent review of 55 studies on Non-Occupational Personal Solar UV Exposure measurements suggests that knowledge on exposure of humans to UV radiation has clearly increased, especially in the past decade.[230]

The solar UV radiation environment relevant to recreational boaters on oceans was simulated with radiative transfer models that take scattering and absorption processes in the atmosphere and the ocean into account.[231,232] UVI values were calculated for horizontal (pertinent for a sunbather on a boat) and vertical orientation (approximating the face and trunk of an upright person standing on a boat deck), assuming a total ozone column of 332 DU. For overhead sun, the UVI on a horizontal surface was 13.6 with approximately equal contributions from the direct and diffuse components, while the upwelling irradiance (corresponding to lying prone with the considered body surface, such as the head, over the side of the boat) was 0.7 or 5% of the downwelling UV radiation. This indicates that contributions from reflections of the ocean surface and radiation emanating from the ocean (*i.e.*, the water-leaving radiance) are only minor contributors to erythemal irradiance at the sea surface. For a vertical surface, the UV dose rate depends critically on the SZA and its orientation relative to the sun and is obviously highest when facing the sun in azimuth. When facing away from the sun, the surface-reflected contribution is about 16% of the total, showing that radiation originating from below the horizon contributes only little to sunburn at sea.

The studies by Diffey and Mobley and Mobley and Diffey[231,232] also suggest that swimming in the ocean provides little protection from exposure to the sun. Even for depths as large as one meter below the surface, the UVI can be comparable with that at the surface. For example, depending on chlorophyll concentrations (c_{chl}), the UVI one meter below the surface is reduced to about 87%, 85%, and 50% for c_{chl} = 0.05, 1, and 5 mg m^{-3}, respectively. However, the study did not consider attenuation by dissolved organic matter (DOM, see ref. 29) and particulates, and therefore overestimates the UVI at depth for coastal locations.

‖‖SED or Standard Erythemal Dose equals 100 J m^{-2} of erythemally-weighted UV irradiance, which quantifies the effect of UV radiation in the development of sunburn.

7.4 Low-cost, crowd-sourcing sensors (smart phone applications)

The main determinant of personal UV exposure is the time spent outdoors without protection. So, any tool that would help people reduce excess exposure will be beneficial. Forecasts of the peak UVI at any point on the globe are currently available from Google maps (*e.g.*, http://sunburnmap.com/).

New tools are becoming available for monitoring sun exposure. Different approaches include electronic UV dosimeters, films with photosensors that are applied to the skin, and smartphone apps with or without photosensors, or linked devices.

Smartphones offer potential as personal monitors of exposure to solar UV radiation. A low-cost hand-held UVI meter combined with smartphone applications provided accurate estimates of UVI and the duration of the solar exposure to receive 1 MED.[233] Another option is the use of smartphones for UV radiation 'nowcasting'. The UVI derived from this system showed a better match with observations at the site of sunbathing, compared with 24 h forecasts of UV radiation using atmospheric models.[234]

An English and Spanish search in App Store and Google Play Store found 134 apps designed to improve sunscreen use, of which 88 were in English only. The location-based UVI was given in 64 apps, and 16 also informed the user about appropriate sunscreen use.[235] Randomised controlled trials have used smartphone apps that deliver sun protection advice, such as information on the UVI, sun protection strategies, alerts to apply sunscreen, and when to get out of the sun.[236] These interventions resulted in modest improvements in sun-protection behaviour, such as increased use of shade and wide-brimmed hats.[236]

A smartphone app for Android devices has recently been introduced for Poland,[233] providing estimates of the current UVI and duration of skin exposure to get 1 MED. Although there are several smartphone apps that are designed to advise the public about UV risk, few have been validated.[233,237] Their accuracy depends mainly on their ability to forecast changes in ozone, clouds, and aerosols. The relative importance and variability of these three factors can vary widely from place to place, so validation at multiple sites is required.

Images from smartphone cameras have been tested as UV monitoring devices for improved personalisation and public awareness of exposure to UV radiation. Currently the accuracy of these devices is much lower than scientific-grade UV sensors in use, either due to poor technical characteristics and calibration,[238] or due to inappropriate measurement principles.[239]

In the last few years, the possibility of using smartphones to record radiation spectra has emerged, mostly by coupling various classes of entrance optics to these units with data recording achieved using the smartphone camera. UV spectra recorded with these devices have been based on sensors located outside of the smartphone body. However, as some smartphone manufacturers already use UV transmitting optics (*e.g.*, a sapphire lens on the iPhone) and others monochrome sensors (*e.g.*, on some Huawei units), direct recording of UV spectra with smartphones may become a reality in the future.[240] These UV spectra could be weighted with the relevant action spectrum to determine the biologically effective UV for a variety of processes, *e.g.*, in terms of the action spectrum (up to 330 nm) for synthesis of previtamin D_3,[241] and the erythema action spectrum.[242] As has already been illustrated with the iSPEX project,[243] this sort of hardware has great promise for widespread proliferation to broaden current monitoring data, particularly in concert with the citizen science community.

Another recent development is the use of wearable UV-sensitive patches that determine personal exposure from changes in patch colour. Sunscreen can be applied to the patch, which has been designed to have the mechanical properties of skin. Changes in colour can be imaged with a smartphone app which, after skin type input, can indicate a "safe" exposure, set at 0.4 MED. Of note, MED increases with skin type on average, but skin type alone does not predict MED on an individual basis. Thus, there may still be a risk of excessive sun exposure for more sensitive skins. While these are in the early stages of development and use, their low unit cost and automated logging *via* phone networks provides the capability to record UV exposure from large numbers of the general public in everyday settings.[244,245] As such, they show great promise for epidemiological studies. Data from the latter study show high geographical variability in exposure patterns, and large differences between the patterns of personal exposure and ambient UV radiation. In the USA for example, measured personal UV doses in Oregon and Minnesota were much greater than in New Mexico, Texas, or Florida, despite much lower ambient UV in the northern states. Such differences may be expected, in this case, due to deliberate sun-avoidance in the hot conditions. However, the population subsets may not be widely representative (see ref. 27).

Data from such devices should be used with caution for information on actual sun-burning radiation levels, but may be helpful in public health campaigns, pending further evaluation.

8 Action spectra for effects on humans

This section discusses the implications of imprecise knowledge of action spectra for the estimation of effects of UV radiation on humans. Spectral dependence of UV effects on ecosystem processes, such as photosynthesis, viral survival and dissolved organic matter degradation are considered in ref. 28, 29 and 61.

8.1 Action spectrum for damage to skin

The action spectrum for melanoma in humans is still not known. Instead, inferences on risks are usually made from

erythemally-weighted irradiances, assuming the action spectrum for the induction of skin cancer is similar.

In a recent study, the need for blocking of infrared radiation (IR) in sunscreens has been questioned.[246] Some sunscreens incorporate agents that are said to protect against IR damage in the skin. However, evidence for their benefit in the context of normal human behaviour in the sun is lacking. The paper examined typical IR exposure levels to the sun and industrial sources to decide whether there is a need for sunscreens to contain IR-blocking agents. They found that lifetime levels of IR exposure resulting from typical behaviour in the sun are less than those experienced by workers exposed to industrial sources of IR, such as steel and glass furnaces. Yet these workers appear to suffer little in the way of chronic skin damage. The authors concluded that there is no compelling evidence for including IR blockers. Based on this finding, it appears that any IR component of erythema must be small. However, more work in this area would be valuable.

Another study investigated the reasons for sunscreen protection factors determined in the laboratory appearing higher than those determined in natural sunlight.[247] The authors proposed that the discrepancy could be explained if the erythema action spectrum were extrapolated beyond its current limit of 400 nm into the visible, where the component from sunlight is much larger than in the lamps used to test the products in the laboratory. A corollary of this would be that erythema would depend more on the full spectrum of solar irradiance, rather than being dominated by the UV-B component. If that were the case, erythemal irradiance would be less dependent on ozone than previously assumed, and the radiation amplification factor for ozone changes would be smaller than the currently used values of about 1.1. This would reduce the importance of changes in atmospheric ozone as a driver of skin damage. The magnitude of the difference would depend on the weighting at longer wavelengths.

8.2 Action spectrum for synthesis of vitamin D

Recent work has suggested limitations to the present action spectrum for pre-vitamin D_3 synthesis, and a possible need for its revision. As has been noted in recent reports,[2,248] the currently-used CIE action spectrum for pre-vitamin D_3 synthesis in human skin[241] may not be correct, and may also change as a function of exposure. A recent paper discussing chemical modelling of the full set of complex reaction pathways in vitamin D photosynthesis involved in skin chemistry predicts an initial action spectrum that is similar to the CIE action spectrum, but is displaced to shorter wavelengths.[249] Such a displacement would be more consistent with the observation that little vitamin D is produced at latitudes poleward of 40° in winter.[234] Further, this work provides evidence that the shape of the vitamin D action spectrum changes as a function of exposure to UV radiation and will become negative at wavelengths between 315 and 330 nm after exposures of only a few SED. A negative action spectrum means that pre-vitamin D_3 is destroyed rather than produced after absorption of photons in this wavelength range (Fig. 10). If correct, this would have important implications for people who are confined indoors behind glass windows, which transmit only UV-A, but not UV-B radiation. Continued exposure to sunlight through glass windows could even be detrimental to vitamin D status. The study by van Dijk *et al.*[249] also highlighted large differences in the absolute amounts of vitamin D derived by the various action spectra for vitamin D that are currently proposed by the two groups involved. The reason for this factor-of-20 difference is not understood at present, and it highlights a lack of understanding in the photo-synthesis of vitamin D. The action spectrum that is currently recommended by the CIE,[241] is intermediate between the two discussed, and in the absence of further evidence, we recommend its continued usage, despite its obvious limitations.

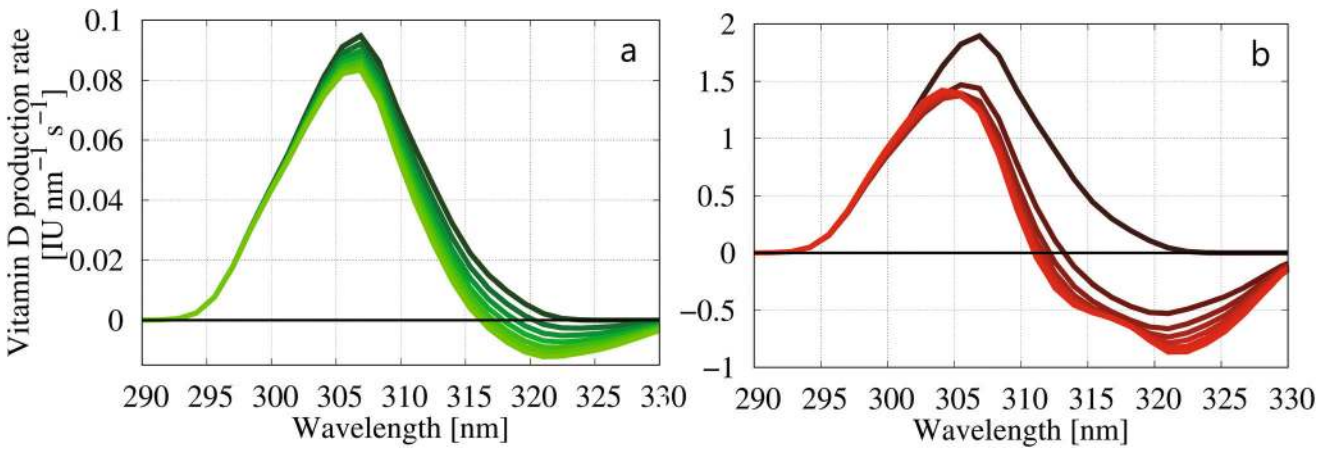

Fig. 10 The decline of vitamin D synthesis (and partly reversal into destruction) due to the formation of other photoactive compounds in the skin, as discussed by van Dijk *et al.*[249] The plots show the deduced spectral synthesis rates for pre-vitamin D3 formation for skin in the lower back/upper leg, for SZA = 30°. Spectra are presented for different stages of exposure, ranging from 0 SED (darkest) to 7.5 SED (brightest). Plot-a is based on an action spectrum from the authors' group at RIVM and plot-b is based on an action spectrum from a group at the Queensland University of Technology (QUT). Results between these two differ by a factor of about 20.

8.3 Action spectrum for phototherapy of psoriasis

Psoriasis is a skin disease that is treated by phototherapy, including sunlight-exposure (*i.e.*, heliotherapy). The action spectrum for clearance of this condition is similar to that for erythema, but with stronger wavelength dependence. An analytic representation of the action spectrum has been developed.[250] A subsequent publication[251] showed that the effective radiation for psoriasis treatment can be estimated from the more widely available erythemally-weighted UV irradiance database. They reported that successful anti-psoriatic heliotherapy would require exposures of 2–3 hours at UVI values of 3–4. Unfortunately, this exposure period is much longer than the maximum time recommended to avoid skin damage (erythema). For example, erythemal damage occurs after exposure times around 1 hour at UVI = 3 in individuals with Fitzpatrick skin-type II. Further work is needed to evaluate the effectiveness of this treatment, and whether the health benefits outweigh the potentially harmful effects. The action spectrum currently used was derived from a small number of measurements made in the 1980s. More detailed knowledge of the action spectrum is needed, because small errors in it would lead to large errors in calculating the doses of sunlight required for effective treatment.

8.4 Risk–benefit analyses

Risk–benefit assessments from exposures to UV radiation are usually based only on the action spectra for erythema (sunburning) and synthesis of vitamin D.[91] In the light of the above findings, calculations of risk–benefit thresholds from exposure to UV radiation may require revision.

In practice, no broad-band detector can perfectly match the biological response (*e.g.*, erythema, vitamin D synthesis, psoriasis treatment, *etc.*) of interest. For meaningful quantitative results, corrections that are functions of ozone and SZA must be applied to measurements with these detectors. However, such corrections have not always been applied in the literature, and without them, the relevance of the UV measurement data is questionable.

Errors also arise from the use of UV irradiance data incident on a horizontal plane, rather than on the surface of interest. There can be appreciable differences between these two quantities. In the case of effects on humans, their attire, posture, and time spent outdoors are also required.

9 Gaps in knowledge

According to ref. 4 and the discussion above, the full recovery of the ozone layer in the mid and high latitudes of the SH will take several decades. It is therefore essential to continue long-term monitoring of total ozone and UV radiation at the Earth's surface without degrading the quality of data.[194] It is concerning that the number of active monitoring stations is declining worldwide, particularly in view of the recently-discovered new emissions of CFC-11.[30,252]

The effects of changes in stratospheric ozone on the UV radiation received at the Earth's surface can be estimated with a very good degree of accuracy. In contrast, and despite progress in recent years, it is still difficult to account for the interactive effects of clouds and aerosols. Over areas with high surface reflectivity (snow- or ice-covered areas) the relevant processes are even more complicated. The estimate of future UV radiation levels is uncertain because of the assumptions in defining the development of these variables over time. All these variables will be affected by anthropogenic changes in GHGs and other species, such as the ODSs. Better understanding of the contribution of changes in ozone and GHGs to changes in the SH climate would improve the predictability of climatic characteristics, such as the variability of atmospheric circulation cells, sea ice, winds, precipitation, and clouds.

Aerosols over the highly polluted areas of south-Eastern Asia and China will dominate changes in UV radiation at these locations in the future. However, these changes depend on the amount and optical properties of aerosols (including the wavelength dependence of their absorption efficiency) both in the present and the future. There are still large uncertainties in quantifying the SSA of aerosols and its wavelength dependence, despite recent new studies that have contributed to our understanding.

Improvement in the understanding of these processes and the availability of higher quality information on the interaction of these factors with UV radiation would strengthen our ability to effectively interpret ongoing projected changes in UV radiation. More accurate projections of UV radiation are essential for accurately assessing effects on human health, ecosystems, materials and related services. Furthermore, quantification of economic and societal impacts resulting either from the projected changes in UV-B radiation or from the avoided changes due to the successful implementation of the Montreal Protocol is still missing.

Concerning the accuracy in estimating biological and health effects of UV radiation, there is incomplete knowledge of the action spectrum for erythema, especially for wavelengths beyond 400 nm in the visible (and possibly IR) regions of the spectrum, as well as of the action spectrum for pre-vitamin D_3. A full understanding of the differences in the action spectra for the various types of skin cancer in humans is also still lacking but will be difficult to obtain.

To more realistically model personal exposure, information on the directional distribution of radiation (radiance) from all directions (*i.e.*, including downwelling and upwelling radiance from the upper and the lower hemisphere, respectively) would be preferable. However, such measurements are not widely available.

Conflicts of interest

There are no conflicts to declare.

Acknowledgements

We acknowledge the contribution of A. Emmanouilidis, MSc student at the University of Thessaloniki, in the modelling of projections of UV radiation. We thank Dr Fiona O'Connor,

Earth System and Mitigation Science, Met Office Hadley Centre, United Kingdom, for providing the model results that were used as inputs in the UV radiation projections. AB's contribution was partly supported by the Research Committee of the Aristotle University of Thessaloniki, Greece. GB's contribution was supported by the U.S. National Science Foundation (grant ARC-1203250), Biospherical Instruments Inc., and the U. S. Global Change Research Program. Richard McKenzie's participation was sponsored by the New Zealand Government's Ministry for the Environment, and supported through the Ministry of Business, Innovation and Employment's research contract C01X1008.

References

1 See the *Photochem. Photobiol. Sci.* themed issue entitled: Environmental effects of ozone depletion and its interaction with climate change: 2018 assessment, *Photochem. Photobiol. Sci.*, 2019, **18**(3).

2 A. F. Bais, R. L. McKenzie, G. Bernhard, P. J. Aucamp, M. Ilyas, S. Madronich and K. Tourpali, Ozone depletion and climate change: Impacts on UV radiation, *Photochem. Photobiol. Sci.*, 2015, **14**, 19–52.

3 G. L. Manney, M. L. Santee, M. Rex, N. J. Livesey, M. C. Pitts, P. Veefkind, E. R. Nash, I. Wohltmann, R. Lehmann, L. Froidevaux, L. R. Poole, M. R. Schoeberl, D. P. Haffner, J. Davies, V. Dorokhov, H. Gernandt, B. Johnson, R. Kivi, E. Kyro, N. Larsen, P. F. Levelt, A. Makshtas, C. T. McElroy, H. Nakajima, M. C. Parrondo, D. W. Tarasick, P. von der Gathen, K. A. Walker and N. S. Zinoviev, Unprecedented Arctic ozone loss in 2011, *Nature*, 2011, **478**, 469–475.

4 WMO, *Scientific Assessment of Ozone Depletion: 2018, Global Ozone Research and Monitoring Project*, Geneva, Switzerland, 2018, in press.

5 M. Weber, M. Coldewey-Egbers, V. E. Fioletov, S. M. Frith, J. D. Wild, J. P. Burrows, C. S. Long and D. Loyola, Total ozone trends from 1979 to 2016 derived from five merged observational datasets – the emergence into ozone recovery, *Atmos. Chem. Phys.*, 2018, **18**, 2097–2117.

6 WMO, *(World Meteorological Organization): Scientific Assessment of Ozone Depletion: 2014, Global Ozone Research and Monitoring Project, Report No. 55*, Geneva, Switzerland, 2014.

7 J. Kuttippurath and P. J. Nair, The signs of Antarctic ozone hole recovery, *Sci. Rep.*, 2017, **7**, 585.

8 S. Solomon, D. J. Ivy, D. Kinnison, M. J. Mills, R. R. Neely and A. Schmidt, Emergence of healing in the Antarctic ozone layer, *Science*, 2016, **353**, 269–274.

9 S. E. Strahan and A. R. Douglass, Decline in Antarctic ozone depletion and lower stratospheric chlorine determined from Aura Microwave Limb Sounder observations, *Geophys. Res. Lett.*, 2018, **45**, 382–390.

10 D. J. Ivy, S. Solomon, D. Kinnison, M. J. Mills, A. Schmidt and R. R. Neely, The influence of the Calbuco eruption on the 2015 Antarctic ozone hole in a fully coupled chemistry-climate model, *Geophys. Res. Lett.*, 2017, **44**, 2556–2561.

11 K. A. Stone, S. Solomon, D. E. Kinnison, M. C. Pitts, L. R. Poole, M. J. Mills, A. Schmidt, R. R. Neely, D. Ivy, M. J. Schwartz, J.-P. Vernier, B. J. Johnson, M. B. Tully, A. R. Klekociuk, G. König-Langlo and S. Hagiya, Observing the impact of Calbuco volcanic aerosols on South Polar ozone depletion in 2015, *J. Geophys. Res.: Atmos.*, 2017, **122**, 11862–11879.

12 E. R. Nash, S. E. Strahan, N. Kramarova, C. S. Long, M. C. Pitts, P. A. Newman, B. Johnson, M. L. Santee, I. Petropavlovskikh and G. O. Braathen, Antarctic ozone hole, in: State of the Climate in 2011, *Bull. Am. Meteorol. Soc.*, 2015, **97**, S168–S172.

13 S. Solomon, D. Ivy, M. Gupta, J. Bandoro, B. Santer, Q. Fu, P. Lin, R. R. Garcia, D. Kinnison and M. Mills, Mirrored changes in Antarctic ozoneand stratospheric temperature in the late 20th versus early 21st centuries, *J. Geophys. Res.: Atmos.*, 2017, **122**, 8940–8950.

14 A. Pazmiño, S. Godin-Beekmann, A. Hauchecorne, C. Claud, S. Khaykin, F. Goutail, E. Wolfram, J. Salvador and E. Quel, Multiple symptoms of total ozone recovery inside the Antarctic vortex during austral spring, *Atmos. Chem. Phys.*, 2018, **18**, 7557–7572.

15 M. P. Chipperfield, S. Bekki, S. Dhomse, N. R. P. Harris, B. Hassler, R. Hossaini, W. Steinbrecht, R. Thiéblemont and M. Weber, Detecting recovery of the stratospheric ozone layer, *Nature*, 2017, **549**, 211–218.

16 S. S. Dhomse, D. Kinnison, M. P. Chipperfield, R. J. Salawitch, I. Cionni, M. I. Hegglin, N. L. Abraham, H. Akiyoshi, A. T. Archibald, E. M. Bednarz, S. Bekki, P. Braesicke, N. Butchart, M. Dameris, M. Deushi, S. Frith, S. C. Hardiman, B. Hassler, L. W. Horowitz, R. M. Hu, P. Jöckel, B. Josse, O. Kirner, S. Kremser, U. Langematz, J. Lewis, M. Marchand, M. Lin, E. Mancini, V. Marécal, M. Michou, O. Morgenstern, F. M. O'Connor, L. Oman, G. Pitari, D. A. Plummer, J. A. Pyle, L. E. Revell, E. Rozanov, R. Schofield, A. Stenke, K. Stone, K. Sudo, S. Tilmes, D. Visioni, Y. Yamashita and G. Zeng, Estimates of ozone return dates from Chemistry-Climate Model Initiative simulations, *Atmos. Chem. Phys.*, 2018, **18**, 8409–8438.

17 W. T. Ball, J. Alsing, D. J. Mortlock, J. Staehelin, J. D. Haigh, T. Peter, F. Tummon, R. Stübi, A. Stenke, J. Anderson, A. Bourassa, S. M. Davis, D. Degenstein, S. Frith, L. Froidevaux, C. Roth, V. Sofieva, R. Wang, J. Wild, P. Yu, J. R. Ziemke and E. V. Rozanov, Evidence for a continuous decline in lower stratospheric ozone offsetting ozone layer recovery, *Atmos. Chem. Phys.*, 2018, **18**, 1379–1394.

18 K. A. Stone, S. Solomon and D. E. Kinnison, On the identification of ozone recovery, *Geophys. Res. Lett.*, 2018, **45**, 5158–5165.

19 M. P. Chipperfield, S. Dhomse, R. Hossaini, W. Feng, M. L. Santee, M. Weber, J. P. Burrows, J. D. Wild,

D. Loyola and M. Coldewey-Egbers, On the cause of recent variations in lower stratospheric ozone, *Geophys. Res. Lett.*, 2018, **45**, 5718–5726.

20 K. Wargan, C. Orbe, S. Pawson, J. R. Ziemke, L. D. Oman, M. A. Olsen, L. Coy and K. E. Knowland, Recent decline in extratropical lower stratospheric ozone attributed to circulation changes, *Geophys. Res. Lett.*, 2018, **45**, 5166–5176.

21 A. H. Butler, J. S. Daniel, R. W. Portmann, A. R. Ravishankara, P. J. Young, D. W. Fahey and K. H. Rosenlof, Diverse policy implications for future ozone and surface UV in a changing climate, *Environ. Res. Lett.*, 2016, **11**, 064017.

22 S. Meul, M. Dameris, U. Langematz, J. Abalichin, A. Kerschbaumer, A. Kubin and S. Oberländer-Hayn, Impact of rising greenhouse gas concentrations on future tropical ozone and UV exposure, *Geophys. Res. Lett.*, 2016, **43**, 2919–2927.

23 A. F. Bais, R. L. McKenzie, G. Bernhard, P. J. Aucamp, M. Ilyas, S. Madronich and K. Tourpali, Ozone depletion and climate change: impacts on UV radiation, *Photochem. Photobiol. Sci.*, 2015, **14**(1), 19–52.

24 R. R. Garcia, D. E. Kinnison and D. R. Marsh, "World avoided" simulations with the Whole Atmosphere Community Climate Model, *J. Geophys. Res.*, 2012, **117**(D23), DOI: 10.1029/2012JD018430.

25 P. A. Newman and R. McKenzie, UV impacts avoided by the Montreal Protocol, *Photochem. Photobiol. Sci.*, 2011, **10**, 1152–1160.

26 M. P. Chipperfield, S. S. Dhomse, W. Feng, R. L. McKenzie, G. J. M. Velders and J. A. Pyle, Quantifying the ozone and ultraviolet benefits already achieved by the Montreal Protocol, *Nat. Commun.*, 2015, **6**, 7233.

27 R. M. Lucas, S. Yazar, A. R. Young, M. Norval, F. R. de Gruijl, Y. Takizawa, L. E. Rhodes and R. E. Neale, Human health in relation to exposure to solar ultraviolet radiation under changing stratospheric ozone and climate, *Photochem. Photobiol. Sci.*, 2019, **19**, DOI: 10.1039/C8PP90060D.

28 J. F. Bornman, P. W. Barnes, T. M. Robson, S. A. Robinson, M. A. K. Jansen, C. L. Ballaré and S. D. Flint, Linkages between stratospheric ozone, UV radiation, and climate change and their implications for terrestrial ecosystems, *Photochem. Photobiol. Sci.*, 2019, **19**, DOI: 10.1039/C8PP90061B.

29 C. E. Williamson, P. J. Neale, S. Hylander, K. C. Rose, F. L. Figueroa, S. A. Robinson, D.-P. Häder, S.-Å. Wängberg and R. C. Worrest, The interactive effects of stratospheric ozone depletion, UV radiation, and climate change on aquatic ecosystems, *Photochem. Photobiol. Sci.*, 2019, **19**, DOI: 10.1039/C8PP90062K.

30 S. A. Montzka, G. S. Dutton, P. Yu, E. Ray, R. W. Portmann, J. S. Daniel, L. Kuijpers, B. D. Hall, D. Mondeel, C. Siso, J. D. Nance, M. Rigby, A. J. Manning, L. Hu, F. Moore, B. R. Miller and J. W. Elkins, An unexpected and persistent increase in global emissions of ozone-depleting CFC-11, *Nature*, 2018, **557**, 413–417.

31 R. Hossaini, M. P. Chipperfield, S. A. Montzka, A. A. Leeson, S. S. Dhomse and J. A. Pyle, The increasing threat to stratospheric ozone from dichloromethane, *Nat. Commun.*, 2017, **8**, 15962.

32 L. Hu, S. A. Montzka, S. J. Lehman, D. S. Godwin, B. R. Miller, A. E. Andrews, K. Thoning, J. B. Miller, C. Sweeney, C. Siso, J. W. Elkins, B. D. Hall, D. J. Mondeel, D. Nance, T. Nehrkorn, M. Mountain, M. L. Fischer, S. C. Biraud, H. Chen and P. P. Tans, Considerable contribution of the Montreal Protocol to declining greenhouse gas emissions from the United States, *Geophys. Res. Lett.*, 2017, **44**, 8075–8083.

33 G. J. M. Velders, D. W. Fahey, J. S. Daniel, S. O. Andersen and M. McFarland, Future atmospheric abundances and climate forcings from scenarios of global and regional hydrofluorocarbon (HFC) emissions, *Atmos. Environ.*, 2015, **123**, 200–209.

34 M. M. Hurwitz, E. L. Fleming, P. A. Newman, F. Li and Q. Liang, Early action on HFCs mitigates future atmospheric change, *Environ. Res. Lett.*, 2016, **11**, 114019.

35 Y. Xu, D. Zaelke, G. J. M. Velders and V. Ramanathan, The role of HFCs in mitigating 21st century climate change, *Atmos. Chem. Phys.*, 2013, **13**, 6083–6089.

36 O. Morgenstern, P. Braesicke, M. M. Hurwitz, F. M. O'Connor, A. C. Bushell, C. E. Johnson and J. A. Pyle, The world avoided by the Montreal Protocol, *Geophys. Res. Lett.*, 2008, **35**, L16811.

37 P. A. Newman, L. D. Oman, A. R. Douglass, E. L. Fleming, S. M. Frith, M. M. Hurwitz, S. R. Kawa, C. H. Jackman, N. A. Krotkov, E. R. Nash, J. E. Nielsen, S. Pawson, R. S. Stolarski and G. J. M. Velders, What would have happened to the ozone layer if chlorofluorocarbons (CFCs) had not been regulated?, *Atmos. Chem. Phys.*, 2009, **9**, 2113–2128.

38 Y. Wu, L. M. Polvani and R. Seager, The importance of the Montreal Protocol in protecting Earth's hydroclimate, *J. Clim.*, 2013, **26**, 4049–4068.

39 L. M. Polvani, S. J. Camargo and R. R. Garcia, The importance of the Montreal Protocol in mitigating the potential intensity of tropical cyclones, *J. Clim.*, 2016, **29**, 2275–2289.

40 W. D. Nordhaus, The economics of hurricanes and implications of global warming, *Climate Change Econom.*, 2010, **01**, 1–20.

41 N. Stern, *Stern Review: The economics of climate change, HM Treasury, UK Report No*, Cambridge University Press, 2006, http://www.cambridge.org/9780521700801.

42 V. Matthias, A. Dörnbrack and G. Stober, The extraordinarily strong and cold polar vortex in the early northern winter 2015/2016, *Geophys. Res. Lett.*, 2016, **43**, 12287–12294.

43 G. H. Bernhard, V. E. Fioletov, J.-U. Grooß, I. Ialongo, B. Johnsen, K. Lakkala, G. L. Manneybron and R. Müller, Ozone and UV radiation, in *State of the Climate in* 2016, *Bull. Am. Meteorol. Soc.*, 2017, S154–S156.

44 U. Langematz, S. Meul, K. Grunow, E. Romanowsky, S. Oberländer, J. Abalichin and A. Kubin, Future Arctic temperature and ozone: The role of stratospheric composition changes, *J. Geophys. Res.: Atmos.*, 2014, **119**, 2092–2112.
45 E. M. Bednarz, A. C. Maycock, N. L. Abraham, P. Braesicke, O. Dessens and J. A. Pyle, Future Arctic ozone recovery: The importance of chemistry and dynamics, *Atmos. Chem. Phys.*, 2016, **16**, 12159–12176.
46 N. Butchart, The Brewer-Dobson circulation, *Rev. Geophys.*, 2014, **52**, 157–184.
47 F. Iglesias-Suarez, P. J. Young and O. Wild, Stratospheric ozone change and related climate impacts over 1850–2100 as modelled by the ACCMIP ensemble, *Atmos. Chem. Phys.*, 2016, **16**, 343–363.
48 IPCC, *Climate Change 2013: The Physical Science Basis. Contribution of Working Group I to the Fifth Assessment Report of the Intergovernmental Panel on Climate Change Report No*, Cambridge, United Kingdom and New York, NY, USA, 2013, p. 1355. http://www.ipcc.ch/.
49 J. Zhang, W. Tian, M. P. Chipperfield, F. Xie and J. Huang, Persistent shift of the Arctic polar vortex towards the Eurasian continent in recent decades, *Nat. Clim. Change*, 2016, **6**, 1094.
50 J. Zhang, W. Tian, F. Xie, M. P. Chipperfield, W. Feng, S.-W. Son, N. L. Abraham, A. T. Archibald, S. Bekki, N. Butchart, M. Deushi, S. Dhomse, Y. Han, P. Jöckel, D. Kinnison, O. Kirner, M. Michou, O. Morgenstern, F. M. O'Connor, G. Pitari, D. A. Plummer, L. E. Revell, E. Rozanov, D. Visioni, W. Wang and G. Zeng, Stratospheric ozone loss over the Eurasian continent induced by the polar vortex shift, *Nat. Commun.*, 2018, **9**, 206.
51 W. J. M. Seviour, Weakening and shift of the Arctic stratospheric polar vortex: Internal variability or forced response?, *Geophys. Res. Lett.*, 2017, **44**, 3365–3373.
52 P. A. Newman, L. Coy, S. Pawson and L. R. Lait, The anomalous change in the QBO in 2015–2016, *Geophys. Res. Lett.*, 2016, **43**, 8791–8797.
53 S. M. Osprey, N. Butchart, J. R. Knight, A. A. Scaife, K. Hamilton, J. A. Anstey, V. Schenzinger and C. Zhang, An unexpected disruption of theatmospheric quasi-biennial oscillation, *Science*, 2016, **353**, 1424–1427.
54 O. V. Tweedy, N. A. Kramarova, S. E. Strahan, P. A. Newman, L. Coy, W. J. Randel, M. Park, D. W. Waugh and S. M. Frith, Response of trace gases to the disrupted 2015–2016 quasi-biennial oscillation, *Atmos. Chem. Phys.*, 2017, **17**, 6813–6823.
55 W. Tian, Y. Li, F. Xie, J. Zhang, M. P. Chipperfield, W. Feng, Y. Hu, S. Zhao, X. Zhou, Y. Yang and X. Ma, The relationship between lower-stratospheric ozone at southern high latitudes and sea surface temperature in the East Asian marginal seas in austral spring, *Atmos. Chem. Phys.*, 2017, **17**, 6705–6722.
56 J. Zhang, W. Tian, Z. Wang, F. Xie and F. Wang, The influence of ENSO on northern midlatitude ozone during the winter to spring transition, *J. Clim.*, 2015, **28**, 4774–4793.
57 WMO, *Scientific Assessment of Ozone Depletion: 2006, World Meteorological Organisation Report No*, Geneva, Switzerland, 2006, p. 572. https://acd-ext.gsfc.nasa.gov/Documents/O3_Assessments/Docs/WMO_2006/scientific-assessment2006.pdf.
58 WMO, *(World Meteorological Organization): Scientific Assessment of Ozone Depletion: 2010, World Meteorological Organisation Report No. 52*, Geneva, Switzerland, 2010, p. 438.
59 R. L. McKenzie, P. J. Aucamp, A. F. Bais, L. O. Björn, M. Ilyas and S. Madronich, Ozone depletion and climate change: Impacts on UV radiation, *Photochem. Photobiol. Sci.*, 2011, **10**, 182–198.
60 UNEP, Environmental effects of ozone depletion and its interactions with climate change: Progress report, 2005, *Photochem. Photobiol. Sci.*, 2006, **5**, 13–24.
61 B. Sulzberger, A. T. Austin, R. M. Cory, R. G. Zepp and N. D. Paul, Solar UV radiation in a changing world: Roles of cryosphere-land-water-atmosphere interfaces in global biogeochemical cycles, *Photochem. Photobiol. Sci.*, 2019, **18**, DOI: 10.1039/C8PP90063A.
62 S. R. Wilson, S. Madronich, J. D. Longstreth and K. R. Solomon, Interactive effects of changing stratospheric ozone and climate on tropospheric composition and air quality, and the consequences for human and ecosystem health, *Photochem. Photobiol. Sci.*, 2019, **18**, DOI: 10.1039/C8PP90064G.
63 A. L. Andrady, K. K. Pandey and A. M. Heikkilä, Interactive effects of solar UV radiation and climate change on material damage, *Photochem. Photobiol. Sci.*, 2019, **18**, DOI: 10.1039/C8PP90065E.
64 A. Solomon, L. M. Polvani, K. L. Smith and R. P. Abernathey, The impact of ozone depleting substances on the circulation, temperature, and salinity of the Southern Ocean: An attribution study with CESM1(WACCM), *Geophys. Res. Lett.*, 2015, **42**, 5547–5555.
65 W. J. M. Seviour, A. Gnanadesikan, D. Waugh and M.-A. Pradal, Transient response of the Southern Ocean to changing ozone: Regional responses and physical mechanisms, *J. Clim.*, 2017, **30**, 2463–2480.
66 S.-W. Son, B.-R. Han, C. Garfinkel, S.-Y. Kim, R. Park, N. L. Abraham, H. Akiyoshi, A. Archibald, N. Butchart, M. Chipperfield, M. Dameris, M. Deushi, S. S. Dhomse, S. Hardiman, P. Jöckel, D. Kinnison, M. Michou, O. Morgenstern, F. M. O'Connor, L. D. Oman, D. A. Plummer, A. Pozzer, L. E. Revell, E. Rozanov, A. Stenke, K. Stone, S. Tilmes, Y. Yamashita and G. Zeng, Tropospheric jet response to Antarctic ozone depletion: An update with Chemistry-Climate Model Initiative (CCMI) models, *Environ. Res. Lett.*, 2018, **13**, 054024.
67 W. J. M. Seviour, D. W. Waugh, L. M. Polvani, G. J. P. Correa and C. I. Garfinkel, Robustness of the simu-

lated tropospheric response to ozone depletion, *J. Clim.*, 2017, **30**, 2577–2585.
68 J. Bandoro, S. Solomon, A. Donohoe, D. W. J. Thompson and B. D. Santer, Influences of the Antarctic ozone hole on southern hemispheric summer climate change, *J. Clim.*, 2014, **27**, 6245–6264.
69 K. Bai, N.-B. Chang and W. Gao, Quantification of relative contribution of Antarctic ozone depletion to increased austral extratropical precipitation during 1979–2013, *J. Geophys. Res.: Atmos.*, 2016, **121**, 1459–1474.
70 S. Brönnimann, M. Jacques-Coper, E. Rozanov, M. F. Andreas, O. Morgenstern, G. Zeng, H. Akiyoshi and Y. Yamashita, Tropical circulation and precipitation response to ozone depletion and recovery, *Environ. Res. Lett.*, 2017, **12**, 064011.
71 B. Liebmann, C. S. Vera, L. M. V. Carvalho, I. A. Camilloni, M. P. Hoerling, D. Allured, V. R. Barros, J. Báez and M. Bidegain, An observed trend in Central South American precipitation, *J. Clim.*, 2004, **17**, 4357–4367.
72 Y. Wu and L. M. Polvani, Recent trends in extreme precipitation and temperature over Southeastern South America: The dominant role of stratospheric ozone depletion in the CESM Large Ensemble, *J. Clim.*, 2017, **30**, 6433–6441.
73 S. M. Kang, L. M. Polvani, J. C. Fyfe, S. W. Son, M. Sigmond and G. J. P. Correa, Modeling evidence that ozone depletion has impacted extreme precipitation in the austral summer, *Geophys. Res. Lett.*, 2013, **40**, 4054–4059.
74 P. L. M. Gonzalez, L. M. Polvani, R. Seager and G. J. P. Correa, Stratospheric ozone depletion: A key driver of recent precipitation trends in South Eastern South America, *Clim. Dyn.*, 2014, **42**, 1775–1792.
75 H. Zhang, T. L. Delworth, F. Zeng, G. Vecchi, K. Paffendorf and L. Jia, Detection, attribution, and projection of regional rainfall changes on (multi-) decadal time scales: A Focus on Southeastern South America, *J. Clim.*, 2016, **29**, 8515–8534.
76 L. Tao, Y. Hu and J. Liu, Anthropogenic forcing on the Hadley circulation in CMIP5 simulations, *Clim. Dyn.*, 2016, **46**, 3337–3350.
77 D. J. Ivy, C. Hilgenbrink, D. Kinnison, R. A. Plumb, A. Sheshadri, S. Solomon and D. W. J. Thompson, Observed changes in the Southern hemispheric circulation in May, *J. Clim.*, 2017, **30**, 527–536.
78 J. Turner and J. Comiso, Solve Antarctica's sea-ice puzzle, *Nature*, 2017, **547**, 275–277.
79 L. L. Landrum, M. M. Holland, M. N. Raphael and L. M. Polvani, Stratospheric ozone depletion: An unlikely driver of the regional trends in Antarctic Sea Ice in Austral fall in the late twentieth century, *Geophys. Res. Lett.*, 2017, **44**, 11062–11070.
80 D. Ferreira, J. Marshall, C. M. Bitz, S. Solomon and A. Plumb, Antarctic Ocean and sea ice response to ozone depletion: A two-time-scale problem, *J. Clim.*, 2015, **28**, 1206–1226.
81 W. J. M. Seviour, A. Gnanadesikan and D. W. Waugh, The transient response of the Southern Ocean to stratospheric ozone depletion, *J. Clim.*, 2016, **29**, 7383–7396.
82 M. M. Holland, L. Landrum, Y. Kostov and J. Marshall, Sensitivity of Antarctic sea ice to the Southern Annular Mode in coupled climate models, *Clim. Dyn.*, 2017, **49**, 1813–1831.
83 G. Chiodo, L. M. Polvani and M. Previdi, Large increase in incident shortwave radiation due to the ozone hole offset by high climatological albedo over Antarctica, *J. Clim.*, 2017, **30**, 4883–4890.
84 T. C. Grenfell, S. G. Warren and P. C. Mullen, Reflection of solar radiation by the Antarctic snow surface at ultraviolet, visible, and near-infrared wavelengths, *J. Geophys. Res.*, 1994, **99**, 18669–18684.
85 A. Y. Karpechko, L. Backman, L. Tholix, I. Ialongo, M. Andersson, V. Fioletov, A. Heikkila, B. Johnsen, T. Koskela, E. Kyrola, K. Lakkala, C. L. Myhre, M. Rex, V. F. Sofieva, J. Tamminen and I. Wohltmann, The link between springtime total ozone and summer UV radiation in Northern Hemisphere extratropics, *J. Geophys. Res.: Atmos.*, 2013, **118**, 8649–8661.
86 G. L. Manney and Z. D. Lawrence, The major stratospheric final warming in 2016: Dispersal of vortex air and termination of Arctic chemical ozone loss, *Atmos. Chem. Phys.*, 2016, **16**, 15371–15396.
87 D. J. Ivy, S. Solomon, N. Calvo and D. W. J. Thompson, Observed connections of Arctic stratospheric ozone extremes to Northern Hemisphere surface climate, *Environ. Res. Lett.*, 2017, **12**, 024004.
88 F. Xie, J. Li, W. Tian, Q. Fu, F.-F. Jin, Y. Hu, J. Zhang, W. Wang, C. Sun, J. Feng, Y. Yang and R. Ding, A connection from Arctic stratospheric ozone to El Niño-Southern oscillation, *Environ. Res. Lett.*, 2016, **11**, 124026.
89 E. A. Barnes and J. A. Screen, The impact of Arctic warming on the midlatitude jet-stream: Can it? Has it? Will it?, *Wiley Interdiscip. Rev. Clim. Change*, 2015, **6**, 277–286.
90 J. A. Francis and S. J. Vavrus, Evidence for a wavier jet stream in response to rapid Arctic warming, *Environ. Res. Lett.*, 2015, **10**, 014005.
91 R. L. McKenzie, P. J. Aucamp, A. F. Bais, L. O. Björn, M. Ilyas and S. Madronich, Ozone depletion and climate change: Impacts on UV radiation, *Photochem. Photobiol. Sci.*, 2011, **10**, 182–198.
92 D. Serrano, M. J. Marín, M. Núñez, M. P. Utrillas, S. Gandía and J. A. Martínez-Lozano, Wavelength dependence of the effective cloud optical depth, *J. Atmos. Sol-Terr. Phys.*, 2015, **130–131**, 14–22.
93 A. Kylling, A. Albold and G. Seckmeyer, Transmittance of a cloud is wavelength-dependent in the UV- range: Physical interpretation, *Geophys. Res. Lett.*, 1997, **24**, 397–400.
94 A. Lindfors and A. Arola, On the wavelength-dependent attenuation of UV radiation by clouds, *Geophys. Res. Lett.*, 2008, **35**, L05806.

95 M. Antón, A. Cazorla, D. Mateos, M. J. Costa, F. J. Olmo and L. Alados-Arboledas, Sensitivity of UV erythemal radiation to total ozone changes under different sky conditions: Results for Granada, Spain, *Photochem. Photobiol.*, 2016, **92**, 215–219.
96 R. McKenzie, B. Liley, M. Kotkamp and P. Disterhoft, Peak UV: Spectral contributions from cloud enhancements, *AIP Conf. Proc.*, 2017, **1810**, 110008.
97 J. Badosa, J. Calbó, R. McKenzie, B. Liley, J.-A. González, B. Forgan and C. N. Long, Two methods for retrieving UV Index for all cloud conditions from sky imager products or total sw radiation measurements, *Photochem. Photobiol.*, 2014, **90**, 941–951.
98 J. Calbó, J.-A. González, J. Badosa, R. McKenzie and B. Liley, How large and how long are UV and total radiation enhancements?, *AIP Conf. Proc.*, 2017, **1810**, 110002.
99 J. Crawford, R. E. Shetter, B. Lefer, C. Cantrell, W. Junkermann, S. Madronich and J. Calvert, Cloud impacts on UV spectral actinic flux observed during the International Photolysis Frequency Measurement and Model Intercomparison (IPMMI), *J. Geophys. Res.: Atmos.*, 2003, **108**, D002731.
100 G. Pfister, R. L. McKenzie, J. B. Liley, A. Thomas and M. J. Uddstrom, Cloud climatology for New Zealand and implications for radiation fields, in *UV Radiation and its Effects Workshop*, RSNZ, 2002.
101 R. D. García, V. E. Cachorro, E. Cuevas, C. Toledano, A. Redondas, M. Blumthaler and Y. Benounna, Comparison of measured and modelled spectral UV irradiance at Izaña high mountain station: Estimation of the underlying effective albedo, *Int. J Climatol.*, 2016, **36**, 377–388.
102 D. Mateos, G. Pace, D. Meloni, J. Bilbao, A. di Sarra, A. de Miguel, G. Casasanta and Q. Min, Observed influence of liquid cloud microphysical properties on ultraviolet surface radiation, *J. Geophys. Res.: Atmos.*, 2014, **119**, D020309.
103 M. O. Andreae, D. Rosenfeld, P. Artaxo, A. A. Costa, G. P. Frank, K. M. Longo and M. A. F. Silva-Dias, Smoking rain clouds over the Amazon, *Science*, 2004, **303**, 1337–1342.
104 J. Mok, N. A. Krotkov, A. Arola, O. Torres, H. Jethva, M. Andrade, G. Labow, T. F. Eck, Z. Li, R. R. Dickerson, G. L. Stenchikov, S. Osipov and X. Ren, Impacts of brown carbon from biomass burning on surface UV and ozone photochemistry in the Amazon Basin, *Sci. Rep.*, 2016, **6**, 36940.
105 S. Kazadzis, P. Raptis, N. Kouremeti, V. Amiridis, A. Arola, E. Gerasopoulos and G. L. Schuster, Aerosol absorption retrieval at ultraviolet wavelengths in a complex environment, *Atmos. Meas. Tech.*, 2016, **9**, 5997–6011.
106 J. Li, B. E. Carlson, O. Dubovik and A. A. Lacis, Recent trends in aerosol optical properties derived from AERONET measurements, *Atmos. Chem. Phys.*, 2014, **14**, 12271–12289.
107 J. P. Putaud, F. Cavalli, S. Martins dos Santos and A. Dell'Acqua, Long-term trends in aerosol optical characteristics in the Po Valley, Italy, *Atmos. Chem. Phys.*, 2014, **14**, 9129–9136.
108 A. R. Attwood, R. A. Washenfelder, C. A. Brock, W. Hu, K. Baumann, P. Campuzano-Jost, D. A. Day, E. S. Edgerton, D. M. Murphy, B. B. Palm, A. McComiskey, N. L. Wagner, S. S. de Sá, A. Ortega, S. T. Martin, J. L. Jimenez and S. S. Brown, Trends in sulfate and organic aerosol mass in the Southeast U.S.: Impact on aerosol optical depth and radiative forcing, *Geophys. Res. Lett.*, 2014, **41**, 7701–7709.
109 D. Mateos, M. Antón, C. Toledano, V. E. Cachorro, L. Alados-Arboledas, M. Sorribas, M. J. Costa and J. M. Baldasano, Aerosol radiative effects in the ultraviolet, visible, and near-infrared spectral ranges using long-term aerosol data series over the Iberian Peninsula, *Atmos. Chem. Phys.*, 2014, **14**, 13497–13514.
110 C. M. Gan, J. Pleim, R. Mathur, C. Hogrefe, C. N. Long, J. Xing, S. Roselle and C. Wei, Assessment of the effect of air pollution controls on trends in shortwave radiation over the United States from 1995 through 2010 from multiple observation networks, *Atmos. Chem. Phys.*, 2014, **14**, 1701–1715.
111 R. Román, M. Antón, A. Valenzuela, J. E. Gil, H. Lyamani, A. De Miguel, F. J. Olmo, J. Bilbao and L. Alados-Arboledas, Evaluation of the desert dust effects on global, direct and diffuse spectral ultraviolet irradiance, *Tellus B*, 2013, **65**, 19578.
112 H. Che, X. Y. Zhang, X. Xia, P. Goloub, B. Holben, H. Zhao, Y. Wang, X. C. Zhang, H. Wang, L. Blarel, B. Damiri, R. Zhang, X. Deng, Y. Ma, T. Wang, F. Geng, B. Qi, J. Zhu, J. Yu, Q. Chen and G. Shi, Ground-based aerosol climatology of China: Aerosol optical depths from the China Aerosol Remote Sensing Network (CARSNET) 2002–2013, *Atmos. Chem. Phys.*, 2015, **15**, 7619–7652.
113 J. Li, Y. Jiang, X. Xia and Y. Hu, Increase of surface solar irradiance across East China related to changes in aerosol properties during the past decade, *Environ. Res. Lett.*, 2017, **13**, 034006.
114 S. Hantson, A. Arneth, S. P. Harrison, D. I. Kelley, I. C. Prentice, S. S. Rabin, S. Archibald, F. Mouillot, S. R. Arnold, P. Artaxo, D. Bachelet, P. Ciais, M. Forrest, P. Friedlingstein, T. Hickler, J. O. Kaplan, S. Kloster, W. Knorr, G. Lasslop, F. Li, S. Mangeon, J. R. Melton, A. Meyn, S. Sitch, A. Spessa, G. R. van der Werf, A. Voulgarakis and C. Yue, The status and challenge of global fire modelling, *Biogeosciences*, 2016, **13**, 3359–3375.
115 M. D. Hurteau, A. L. Westerling, C. Wiedinmyer and B. P. Bryant, Projected effects of climate and development on California wildfire emissions through 2100, *Environ. Sci. Technol.*, 2014, **48**, 2298–2304.
116 M. D. Flannigan, M. A. Krawchuk, W. J. de Groot, B. M. Wotton and L. M. Gowman, Implications of changing climate for global wildland fire, *Int. J. Wildland Fire*, 2009, **18**, 483–507.
117 J. T. Abatzoglou and A. P. Williams, Impact of anthropogenic climate change on wildfire across western US

forests, *Proc. Natl. Acad. Sci. U. S. A.*, 2016, **113**, 11770–11775.

118 R. W. Bergstrom, P. B. Russell and P. Hignett, Wavelength dependence of the absorption of black carbon particles: Predictions and results from the TARFOX experiment and implications for the aerosol single scattering albedo, *J. Atmos. Sci.*, 2002, **59**, 567–577.

119 C. E. Williamson, E. P. Overholt, J. A. Brentrup, R. M. Pilla, T. H. Leach, S. G. Schladow, J. D. Warren, S. S. Urmy, S. Sadro, S. Chandra and P. J. Neale, Sentinel responses to droughts, wildfires, and floods: effects of UV radiation on lakes and their ecosystem services, *Front. Ecol. Environ.*, 2016, **14**, 102–109.

120 D. V. Spracklen, L. J. Mickley, J. A. Logan, R. C. Hudman, R. Yevich, M. D. Flannigan and A. L. Westerling, Impacts of climate change from 2000 to 2050 on wildfire activity and carbonaceous aerosol concentrations in the western United States, *J. Geophys. Res.*, 2009, **114**, D010966.

121 X. Yue, L. J. Mickley, J. A. Logan and J. O. Kaplan, Ensemble projections of wildfire activity and carbonaceous aerosol concentrations over the western United States in the mid-21st century, *Atmos. Environ.*, 2013, **77**, 767–780.

122 J. C. Péré, B. Bessagnet, V. Pont, M. Mallet and F. Minvielle, Influence of the aerosol solar extinction on photochemistry during the 2010 Russian wildfires episode, *Atmos. Chem. Phys.*, 2015, **15**, 10983–10998.

123 M. G. Tosca, J. T. Randerson and C. S. Zender, Global impact of smoke aerosols from landscape fires on climate and the Hadley circulation, *Atmos. Chem. Phys.*, 2013, **13**, 5227–5241.

124 L. Frey, F. A. M. Bender and G. Svensson, Cloud albedo changes in response to anthropogenic sulfate and non-sulfate aerosol forcings in CMIP5 models, *Atmos. Chem. Phys.*, 2017, **17**, 9145–9162.

125 S. Szopa, Y. Balkanski, M. Schulz, S. Bekki, D. Cugnet, A. Fortems-Cheiney, S. Turquety, A. Cozic, C. Déandreis, D. Hauglustaine, A. Idelkadi, J. Lathière, F. Lefevre, M. Marchand, R. Vuolo, N. Yan and J.-L. Dufresne, Aerosol and ozone changes as forcing for climate evolution between 1850 and 2100, *Clim. Dyn.*, 2013, **40**, 2223–2250.

126 J. López-Solano, A. Redondas, T. Carlund, J. J. Rodriguez-Franco, H. Diémoz, S. F. León-Luis, B. Hernández-Cruz, C. Guirado-Fuentes, N. Kouremeti, J. Gröbner, S. Kazadzis, V. Carreño, A. Berjón, D. Santana-Díaz, M. Rodríguez-Valido, V. De Bock, J. R. Moreta, J. Rimmer, A. R. D. Smedley, L. Boulkelia, N. Jepsen, P. Eriksen, A. F. Bais, V. Shirotov, J. M. Vilaplana, K. M. Wilson and T. Karppinen, Aerosol optical depth in the European Brewer Network, *Atmos. Chem. Phys.*, 2018, **18**, 3885–3902.

127 T. Carlund, N. Kouremeti, S. Kazadzis and J. Gröbner, Aerosol optical depth determination in the UV using a four-channel precision filter radiometer, *Atmos. Meas. Tech.*, 2017, **10**, 905–923.

128 M. Zhang, W. Gong, Y. Ma, L. Wang and Z. Chen, Transmission and division of total optical depth method: A universal calibration method for Sun photometric measurements, *Geophys. Res. Lett.*, 2016, **43**, 2974–2980.

129 S. Kazadzis, N. Kouremeti, H. Diémoz, J. Gröbner, B. W. Forgan, M. Campanelli, V. Estellés, K. Lantz, J. Michalsky, T. Carlund, E. Cuevas, C. Toledano, R. Becker, S. Nyeki, P. G. Kosmopoulos, V. Tatsiankou, L. Vuilleumier, F. M. Denn, N. Ohkawara, O. Ijima, P. Goloub, P. I. Raptis, M. Milner, K. Behrens, A. Barreto, G. Martucci, E. Hall, J. Wendell, B. E. Fabbri and C. Wehrli, Results from the Fourth WMO Filter Radiometer Comparison for aerosol optical depth measurements, *Atmos. Chem. Phys.*, 2018, **18**, 3185–3201.

130 G. Bernhard, Trends of solar ultraviolet irradiance at Barrow, Alaska, and the effect of measurement uncertainties on trend detection, *Atmos. Chem. Phys.*, 2011, **11**, 13029–13045.

131 A. Damiani, R. R. Cordero, J. Carrasco, S. Watanabe, M. Kawamiya and V. E. Lagun, Changes in the UV Lambertian equivalent reflectivity in the Southern Ocean: Influence of sea ice and cloudiness, *Rem. Sens. Environ.*, 2015, **169**, 75–92.

132 T. Koenigk, A. Devasthale and K. G. Karlsson, Summer Arctic sea ice albedo in CMIP5 models, *Atmos. Chem. Phys.*, 2014, **14**, 1987–1998.

133 P. Arsenovic, E. Rozanov, J. Anet, A. Stenke, W. Schmutz and T. Peter, Implications of potential future grand solar minimum for ozone layer and climate, *Atmos. Chem. Phys.*, 2018, **18**, 3469–3483.

134 P. Arsenovic, E. Rozanov, A. Stenke, B. Funke, J. M. Wissing, K. Mursula, F. Tummon and T. Peter, The influence of Middle Range Energy Electrons on atmospheric chemistry and regional climate, *J. Atmos. Sol-Terr. Phys.*, 2016, **149**, 180–190.

135 J. R. Norris, R. J. Allen, A. T. Evan, M. D. Zelinka, C. W. O'Dell and S. A. Klein, Evidence for climate change in the satellite cloud record, *Nature*, 2016, **536**, 72–75.

136 S.-Y. Jun, C.-H. Ho, J.-H. Jeong, Y.-S. Choi and B.-M. Kim, Recent changes in winter Arctic clouds and their relationships with sea ice and atmospheric conditions, *Tellus A*, 2016, **68**, 29130.

137 M. Abe, T. Nozawa, T. Ogura and K. Takata, Effect of retreating sea ice on Arctic cloud cover in simulated recent global warming, *Atmos. Chem. Phys.*, 2016, **16**, 14343–14356.

138 D. Perovich, W. Meier, M. Tschudi, S. Farrell, S. Gerland, S. Hendricks, T. Krumpen and C. Haas, Sea ice cover [in State of the Climate in 2016], *Bull. Am. Meteorol. Soc.*, 2017, **98**, S131–S133.

139 J. C. Stroeve, T. Markus, L. Boisvert, J. Miller and A. Barrett, Changes in Arctic melt season and implications for sea ice loss, *Geophys. Res. Lett.*, 2014, **41**, 1216–1225.

140 C. Derksen, R. Brown, L. Mudryk and K. Luojus, Terrestrial snow cover [in State of the Climate in 2016], *Bull. Am. Meteorol. Soc.*, 2017, **98**, S151–S154.

141 J. R. Lee, B. Raymond, T. J. Bracegirdle, I. Chadès, R. A. Fuller, J. D. Shaw and A. Terauds, Climate change

drives expansion of Antarctic ice-free habitat, *Nature*, 2017, **547**, 49–54.

142 R. L. McKenzie, P. V. Johnston and G. Seckmeyer, UV spectro-radiometry in the network for the detection of stratospheric change (NDSC), in *Solar Ultraviolet Radiation. Modelling, Measurements and Effects*, ed. C. S. Zerefos and A. F. Bais, Springer-Verlag, Berlin, 1997, vol. 1.52, pp. 279–287.

143 M. De Mazière, A. M. Thompson, M. J. Kurylo, J. Wild, G. Bernhard, T. Blumenstock, J. Hannigan, J. C. Lambert, T. Leblanc, T. J. McGee, G. Nedoluha, I. Petropavlovskikh, G. Seckmeyer, P. C. Simon, W. Steinbrecht, S. Strahan and J. T. Sullivan, The Network for the Detection of Atmospheric Composition Change (NDACC): History, status and perspectives, *Atmos. Chem. Phys. Disc.*, 2017, **18**, 4935–4964.

144 R. R. Cordero, A. Damiani, J. Jorquera, E. Sepúlveda, M. Caballero, S. Fernandez, S. Feron, P. J. Llanillo, J. Carrasco, D. Laroze and F. Labbe, Ultraviolet radiation in the Atacama Desert, *Antonie van Leeuwenhoek*, 2018, **111**, 1301–1313.

145 A. F. McKinlay and B. L. Diffey, A reference action spectrum for ultra-violet induced erythema in human skin, in *Human Exposure to Ultraviolet Radiation: Risks and Regulations*, ed. W. F. Passchier and B. F. M. Bosnajakovic, Elsevier, Amsterdam, 1987, pp. 83–87.

146 R. McKenzie, UV radiation in the melanoma capital of the world: What makes New Zealand so different?, *AIP Conf. Proc.*, 2017, **1810**, 020003.

147 G. Bernhard, C. Booth and J. Ehramjian, Climatology of ultraviolet radiation at high latitudes derived from measurements of the National Science Foundation's Ultraviolet Spectral Irradiance Monitoring Network, in *UV Radiation in Global Climate Change*, ed. W. Gao, J. Slusser and D. Schmoldt, Springer, Berlin Heidelberg, 2010, pp. 48–72.

148 G. Seckmeyer, C. Mustert, M. Schrempf, R. L. McKenzie, J. B. Liley, M. Kotkamp, A. F. Bais, D. Gillotay, H. Slaper, A.-M. Siani, A. R. D. Smedley and A. Webb, Why is it so hard to gain enough Vitamin D by solar exposure in the European winter?, *Metero. Zeits.*, 2018, **27**, 223–233.

149 G. Bernhard, C. R. Booth and J. C. Ehramjian, Version 2 data of the National Science Foundation's Ultraviolet Radiation Monitoring Network: South Pole, *J. Geophys. Res.: Atmos.*, 2004, **109**, D21207.

150 M. Beckmann, T. Václavík, A. M. Manceur, L. Šprtová, H. von Wehrden, E. Welk and A. F. Cord, glUV: A global UV-B radiation data set for macroecological studies, *Methods Ecol. Evol.*, 2014, **5**, 372–383.

151 S. Madronich and S. Flocke, *Theoretical Estimation of Biologically Effective UV Radiation at the Earth's Surface*, Springer Berlin Heidelberg, Berlin, Heidelberg, 1997, pp. 23–48.

152 K. Eleftheratos, S. Kazadzis, C. S. Zerefos, K. Tourpali, C. Meleti, D. Balis, I. Zyrichidou, K. Lakkala, U. Feister, T. Koskela, A. Heikkila and J. M. Karhu, Ozone and spectroradiometric UV changes in the past 20 years over high latitudes, *Atmos.-Ocean*, 2015, **53**, 117–125.

153 G. Bernhard, C. R. Booth, J. C. Ehramjian and S. E. Nichol, UV climatology at McMurdo station, Antarctica, based on version 2 data of the National Science Foundation's Ultraviolet Spectral Irradiance Monitoring Network, *J. Geophys. Res.: Atmos.*, 2006, **111**, D11201.

154 I. Fountoulakis, A. F. Bais, K. Fragkos, C. Meleti, K. Tourpali and M. M. Zempila, Short- and long-term variability of spectral solar UV irradiance at Thessaloniki, Greece: effects of changes in aerosols, total ozone and clouds, *Atmos. Chem. Phys.*, 2016, **16**, 2493–2505.

155 K. Fragkos, A. F. Bais, I. Fountoulakis, D. S. Balis, K. Tourpali, C. Meleti and P. Zanis, Extreme total column ozone events and effects on UV solar radiation at Thessaloniki, Greece, *Theotet. Appl. Climatol.*, 2016, **126**, 505–517.

156 A. Sanchez-Lorenzo, A. Enriquez-Alonso, M. Wild, J. Trentmann, S. M. Vicente-Serrano, A. Sanchez-Romero, R. Posselt and M. Z. Hakuba, Trends in downward surface solar radiation from satellites and ground observations over Europe during 1983–2010, *Remote Sens. Environ.*, 2017, **189**, 108–117.

157 R. J. Hooke, M. P. Higlett, N. Hunter and J. B. O'Hagan, Long term variations in erythema effective solar UV at Chilton, UK, from 1991 to 2015, *Photochem. Photobiol. Sci.*, 2017, **16**, 1596–1603.

158 V. De Bock, H. De Backer, R. Van Malderen, A. Mangold and A. Delcloo, Relations between erythemal UV dose, global solar radiation, total ozone column and aerosol optical depth at Uccle, Belgium, *Atmos. Chem. Phys.*, 2014, **14**, 12251–12270.

159 A. Lindfors and L. Vuilleumier, Erythemal UV at Davos (Switzerland), 1926–2003, estimated using total ozone, sunshine duration, and snow depth, *J. Geophys. Res.: Atmos.*, 2005, **110**, D02104.

160 M. Posyniak, A. Szkop, A. Pietruczuk, J. Podgórski and J. Krzyścin, The long-term (1964–2014) variability of aerosol optical thickness and its impact on solar irradiance based on the data taken at Belsk, Poland, *Acta Geophys.*, 2016, **64**, 1858–1874.

161 K. Čížková, K. Láska, L. Metelka and M. Staněk, Reconstruction and analysis of erythemal UV radiation time series from Hradec Králové (Czech Republic) over the past 50 years, *Atmos. Chem. Phys.*, 2018, **18**, 1805–1818.

162 R. Román, J. Bilbao and A. de Miguel, Erythemal ultraviolet irradiation trends in the Iberian Peninsula from 1950 to 2011, *Atmos. Chem. Phys.*, 2015, **15**, 375–391.

163 J. W. Krzyścin and P. S. Sobolewski, Trends in erythemal doses at the Polish Polar Station, Hornsund, Svalbard based on the homogenized measurements (1996–2016) and reconstructed data (1983–1995), *Atmos. Chem. Phys.*, 2018, **18**, 1–11.

164 H. Liu, B. Hu, L. Zhang, X. J. Zhao, K. Z. Shang, Y. S. Wang and J. Wang, Ultraviolet radiation over China:

Spatial distribution and trends, *Renewable Sustainable Energy Rev.*, 2017, **76**, 1371–1383.

165 R. L. McKenzie, P. J. Aucamp, A. F. Bais, L. O. Björn and M. Ilyas, Changes in biologically-active ultraviolet radiation reaching the Earth's surface, *Photochem. Photobiol. Sci.*, 2007, **6**(3), 218–231.

166 I. Fountoulakis and A. F. Bais, Projected changes in erythemal and vitamin D effective irradiance over northern-hemisphere high latitudes, *Photochem. Photobiol. Sci.*, 2015, **14**, 1251–1264.

167 O. Morgenstern, M. I. Hegglin, E. Rozanov, F. M. O'Connor, N. L. Abraham, H. Akiyoshi, A. T. Archibald, S. Bekki, N. Butchart, M. P. Chipperfield, M. Deushi, S. S. Dhomse, R. R. Garcia, S. C. Hardiman, L. W. Horowitz, P. Jöckel, B. Josse, D. Kinnison, M. Lin, E. Mancini, M. E. Manyin, M. Marchand, V. Marécal, M. Michou, L. D. Oman, G. Pitari, D. A. Plummer, L. E. Revell, D. Saint-Martin, R. Schofield, A. Stenke, K. Stone, K. Sudo, T. Y. Tanaka, S. Tilmes, Y. Yamashita, K. Yoshida and G. Zeng, Review of the global models used within phase 1 of the Chemistry–Climate Model Initiative (CCMI), *Geosci. Model Dev.*, 2017, **10**, 639–671.

168 V. Eyring, I. Cionni, G. E. Bodeker, A. J. Charlton-Perez, D. E. Kinnison, J. F. Scinocca, D. W. Waugh, H. Akiyoshi, S. Bekki, M. P. Chipperfield, M. Dameris, S. Dhomse, S. M. Frith, H. Garny, A. Gettelman, A. Kubin, U. Langematz, E. Mancini, M. Marchand, T. Nakamura, L. D. Oman, S. Pawson, G. Pitari, D. A. Plummer, E. Rozanov, T. G. Shepherd, K. Shibata, W. Tian, P. Braesicke, S. C. Hardiman, J. F. Lamarque, O. Morgenstern, J. A. Pyle, D. Smale and Y. Yamashita, Multi-model assessment of stratospheric ozone return dates and ozone recovery in CCMVal-2 models, *Atmos. Chem. Phys.*, 2010, **10**, 9451–9472.

169 T. Masui, K. Matsumoto, Y. Hijioka, T. Kinoshita, T. Nozawa, S. Ishiwatari, E. Kato, P. R. Shukla, Y. Yamagata and M. Kainuma, An emission pathway for stabilization at 6 Wm^{-2} radiative forcing, *Clim. Change*, 2011, **109**, 59.

170 K. E. Taylor, R. J. Stouffer and G. A. Meehl, An overview of CMIP5 and the experiment design, *Bull. Am. Meteorol. Soc.*, 2012, **93**, 485–498.

171 B. Mayer and A. Kylling, Technical note: The libRadtran software package for radiative transfer calculations - description and examples of use, *Atmos. Chem. Phys.*, 2005, **5**, 1855–1877.

172 P. J. Crutzen, Albedo enhancement by stratospheric sulfur injections: A contribution to resolve a policy dilemma?, *Clim. Change*, 2006, **77**, 211–220.

173 M. I. Budyko, *Climatic changes*, American Geophysical Society, Washington DC, 1977.

174 M. Boettcher and S. Schäfer, Reflecting upon 10 years of geoengineering research: Introduction to the Crutzen + 10 special issue, *Earth's Future*, 2017, **5**, 266–277.

175 D. G. MacMartin, B. Kravitz, J. C. S. Long and P. J. Rasch, Geoengineering with stratospheric aerosols: What do we not know after a decade of research?, *Earth's Future*, 2016, **4**, 543–548.

176 D. W. Keith and P. J. Irvine, Solar geoengineering could substantially reduce climate risks—A research hypothesis for the next decade, *Earth's Future*, 2016, **4**, 549–559.

177 A. Robock, Albedo enhancement by stratospheric sulfur injections: More research needed, *Earth's Future*, 2016, **4**, 644–648.

178 G. Pitari, V. Aquila, B. Kravitz, A. Robock, S. Watanabe, I. Cionni, N. D. Luca, G. D. Genova, E. Mancini and S. Tilmes, Stratospheric ozone response to sulfate geoengineering: Results from the Geoengineering Model Intercomparison Project (GeoMIP), *J. Geophys. Res.: Atmos.*, 2014, **119**, 2629–2653.

179 S. Tilmes, D. E. Kinnison, R. R. Garcia, R. Salawitch, T. Canty, J. Lee-Taylor, S. Madronich and K. Chance, Impact of very short-lived halogens on stratospheric ozone abundance and UV radiation in a geo-engineered atmosphere, *Atmos. Chem. Phys.*, 2012, **12**, 10945–10955.

180 T. Li, E. Heuvelink, T. A. Dueck, J. Janse, G. Gort and L. F. M. Marcelis, Enhancement of crop photosynthesis by diffuse light: quantifying the contributing factors, *Ann. Bot.*, 2014, **114**, 145–156.

181 L. Xia, A. Robock, S. Tilmes and R. R. Neely Iii, Stratospheric sulfate geoengineering could enhance the terrestrial photosynthesis rate, *Atmos. Chem. Phys.*, 2016, **16**, 1479–1489.

182 A. Redondas, V. Carreño, S. F. León-Luis, B. Hernández-Cruz, J. López-Solano, J. J. Rodriguez-Franco, J. M. Vilaplana, J. Gröbner, J. Rimmer, A. F. Bais, V. Savastiouk, J. R. Moreta, L. Boulkelia, N. Jepsen, K. M. Wilson, V. Shirotov and T. Karppinen, EUBREWNET RBCC-E Huelva 2015 Ozone Brewer Intercomparison, *Atmos. Chem. Phys.*, 2018, **18**, 9441–9455.

183 G. Hülsen and J. Gröbner, *Second International UV Filter Radiometer Intercomparison UVC-II (GAW Report- No. 240), Report No*, Geneva, 2018, p. 212. https://library.wmo.int/doc_num.php?explnum_id=4557.

184 P. Gies, R. Hooke, R. McKenzie, J. O'Hagan, S. Henderson, A. Pearson, M. Khazova, J. Javorniczky, K. King, M. Tully, M. Kotkamp, B. Forgan and S. Rhodes, International intercomparison of solar UVR Spectral Measurement Systems in Melbourne in 2013, *Photochem. Photobiol.*, 2015, **91**, 1237–1246.

185 G. Hülsen, J. Gröbner, S. Nevas, P. Sperfeld, L. Egli, G. Porrovecchio and M. Smid, Traceability of solar UV measurements using the Qasume reference spectroradiometer, *Appl. Opt.*, 2016, **55**, 7265–7275.

186 J. Gröbner, J. Schreder, S. Kazadzis, A. F. Bais, M. Blumthaler, P. Gorts, R. Tax, T. Koskela, G. Seckmeyer, A. R. Webb and D. Rembges, Traveling reference spectroradiometer for routine quality assurance of spectral solar ultraviolet irradiance measurements, *Appl. Opt.*, 2005, **44**, 5321–5331.

187 L. Egli, J. Gröbner, G. Hülsen, L. Bachmann, M. Blumthaler, J. Dubard, M. Khazova, R. Kift,

K. Hoogendijk, A. Serrano, A. Smedley and J. M. Vilaplana, Quality assessment of solar UV irradiance measured with array spectroradiometers, *Atmos. Meas. Tech.*, 2016, **9**, 1553–1567.

188 S. Nevas, J. Gröbner, L. Egli and M. Blumthaler, Stray light correction of array spectroradiometers for solar UVmeasurements, *Appl. Opt.*, 2014, **53**, 4313–4319.

189 R. Zuber, P. Sperfeld, S. Riechelmann, S. Nevas, M. Sildoja and G. Seckmeyer, Adaption of an array spectroradiometer for total ozone column retrieval using direct solar irradiance measurements in the UV spectral range, *Atmos. Meas. Tech.*, 2018, 2477–2484.

190 R. Zuber, M. Ribnitzky, M. Tobar, K. Lange, K. Dimitri, M. Schrempf, A. Niedzwiedz and G. Seckmeyer, Global spectral irradiance array spectroradiometer validation according to WMO, *Meas. Sci. Technol.*, 2018, **29**, 105801.

191 J. F. Bornman, P. W. Barnes, S. A. Robinson, C. L. Ballaré, S. D. Flint and M. M. Caldwell, Solar ultraviolet radiation and ozone depletion-driven climate change: Effects on terrestrial ecosystems, *Photochem. Photobiol. Sci.*, 2015, **14**, 88–107.

192 N. A. Cabrol, U. Feister, D.-P. Häder, H. Piazena, E. A. Grin and A. Klein, Record solar UV irradiance in the tropical Andes, *Front. Environ. Sci.*, 2014, **2**, 19.

193 R. L. McKenzie, B. Liley and S. Madronich, Critical appraisal of data used to infer record UVI in the tropical Andes, *Photochem. Photobiol. Sci.*, 2017, **16**, 785–794.

194 WMO, *(World Meteorological Organization): Report of the 10th Meeting of the Ozone Research Managers of the Parties to the Vienna Convention for the Protection of the Ozone Layer, Global Ozone Research and Monitoring Project, Report No. 57*, Geneva, Switzerland, 2017.

195 J. R. Herman, N. Krotkov, E. Celarier, D. Larko and G. Labow, Distribution of UV radiation at the Earth's surface from TOMS-measured UV-backscattered radiances, *J. Geophys. Res.*, 1999, **104**, 12059–12076.

196 A. Tanskanen, N. A. Krotkov, J. R. Herman and A. Arola, Surface ultraviolet irradiance from OMI, *IEEE Trans. Geosci. Remote Sens.*, 2006, **44**, 1267–1271.

197 A. Arola, S. Kazadzis, N. Krotkov, A. Bais, J. Gröbner and J. R. Herman, Assessment of TOMS UV bias due to absorbing aerosols, *J. Geophys. Res.*, 2005, **110**, D23211.

198 M.-M. Zempila, M.-E. Koukouli, A. Bais, I. Fountoulakis, A. Arola, N. Kouremeti and D. Balis, OMI/Aura UV product validation using NILU-UV ground-based measurements in Thessaloniki, Greece, *Atmos. Environ.*, 2016, **140**, 283–297.

199 G. Bernhard, A. Arola, A. Dahlback, V. Fioletov, A. Heikkilä, B. Johnsen, T. Koskela, K. Lakkala, T. Svendby and J. Tamminen, Comparison of OMI UV observations with ground-based measurements at high northern latitudes, *Atmos. Chem. Phys.*, 2015, **15**, 7391–7412.

200 C. Brogniez, F. Auriol, C. Deroo, A. Arola, J. Kujanpää, B. Sauvage, N. Kalakoski, M. R. A. Pitkänen, M. Catalfamo, J. M. Metzger, G. Tournois and P. Da Conceicao, Validation of satellite-based noontime UVI with NDACC ground-based instruments: influence of topography, environment and satellite overpass time, *Atmos. Chem. Phys.*, 2016, **16**, 15049–15074.

201 J.-M. Cadet, H. Bencherif, T. Portafaix, K. Lamy, K. Ncongwane, G. Coetzee and C. Wright, Comparison of ground-based and satellite-derived solar UV Index levels at six South African sites, *Int. J. Environ. Res. Public Health*, 2017, **14**, 1384.

202 L. Fan, W. Li, A. Dahlback, J. J. Stamnes, S. Stamnes and K. Stamnes, Long-term comparisons of UV index values derived from a NILU-UV instrument, NWS, and OMI in the New York area, *Appl. Opt.*, 2015, **54**, 1945–1951.

203 M. M. Zempila, J. H. G. M. van Geffen, M. Taylor, I. Fountoulakis, M. E. Koukouli, M. van Weele, R. J. van der A, A. Bais, C. Meleti and D. Balis, TEMIS UV product validation using NILU-UV ground-based measurements in Thessaloniki, Greece, *Atmos. Chem. Phys.*, 2017, **17**, 7157–7174.

204 J. Herman, L. Huang, R. McPeters, J. Ziemke, A. Cede and K. Blank, Synoptic ozone, cloud reflectivity, and erythemal irradiance from sunrise to sunset for the whole earth as viewed by the DSCOVR spacecraft from the earth–sun Lagrange 1 orbit, *Atmos. Meas. Tech.*, 2018, **11**, 177–194.

205 J. B. Liley and R. L. McKenzie, *Where on Earth has the highest UV?, National Institute of Water and Atmospheric Research (NIWA) Report No. not provided*, Lauder, Central Otago, New Zealand, 2006, vol. 2006, p. 2.

206 R. L. McKenzie, S. Madronich, G. Bernhard and F. Zaratti, Comment on "Record solar UV irradiance in the tropical Andes, by Cabrol *et al.*", *Front. Environ. Sci.*, 2015, **3**, 00026.

207 R. R. Cordero, G. Seckmeyer, A. Damiani, S. Riechelmann, J. Rayas, F. Labbe and D. Laroze, The world's highest levels of surface UV, *Photochem. Photobiol. Sci.*, 2014, **13**, 70–81.

208 A. Cede, E. Luccini, L. Nunez, R. D. Piacentini and M. Blumthaler, Monitoring of erythemal irradiance in the Argentine ultraviolet network, *J. Geophys. Res.: Atmos.*, 2002, **107**, D001206.

209 F. Zaratti, R. D. Piacentini, H. A. Guillen, S. H. Cabrera, J. Ben Liley and R. L. McKenzie, Proposal for a modification of the UVI risk scale, *Photochem. Photobiol. Sci.*, 2014, **13**, 980–985.

210 T. VoPham, J. E. Hart, K. A. Bertrand, Z. Sun, R. M. Tamimi and F. Laden, Spatiotemporal exposure modeling of ambient erythemal ultraviolet radiation, *Environ. Health*, 2016, **15**, 111.

211 J. Kujanpää and N. Kalakoski, Operational surface UV radiation product from GOME-2 and AVHRR/3 data, *Atmos. Meas. Tech.*, 2015, **8**, 4399–4414.

212 J. Peltoniemi, M. Gritsevich, T. Hakala, P. Dagsson-Waldhauserová, Ó. Arnalds, K. Anttila, H.-R. Hannula, N. Kivekäs, H. Lihavainen and O. Meinander, Soot on snow experiment: bidirectional reflectance factor measurements of contaminated snow, *Cryosphere*, 2015, **9**, 2323–2337.

213 G. Seckmeyer, S. Riechelmann, M. Schrempf, A. Stuhrmann and A. Niedzwiedz, Solar simulators for a

healthy vitamin D synthesis, *Anticancer Res.*, 2015, **35**, 3607–3607.

214 M. Schrempf, D. Haluza, S. Simic, S. Riechelmann, K. Graw and G. Seckmeyer, Is multidirectional UV exposure responsible for increasing melanoma prevalence with altitude? A hypothesis based on calculations with a 3D-human exposure model, *Int. J. Environ. Res. Public Health*, 2016, **13**, 961.

215 A. Religi, C. Backes, L. Moccozet, L. Vuilleumier, D. Vernez and J.-L. Bulliard, Body anatomical UV protection predicted by shade structures: A modeling study, *Photochem. Photobiol.*, 2018, **27**, 1289–1296.

216 M. Hess and P. Koepke, Modelling UV irradiances on arbitrarily oriented surfaces: Effects of sky obstructions, *Atmos. Chem. Phys.*, 2008, **8**, 3583.

217 R. Carrasco-Hernandez, A. R. D. Smedley and A. Webb, Fast calculations of the spectral diffuse-to-global ratios for approximating spectral irradiance at the street canyon level, *Theotet. Appl. Climatol.*, 2015, **124**, 1065–1077.

218 M. Schrempf, N. Thuns, K. Lange and G. Seckmeyer, Impact of orientation on the vitamin D weighted exposure of a human in an urban environment, *Int. J. Environ. Res. Public Health*, 2017, **14**, 920.

219 P. Setlow and L. Li, Photochemistry and photobiology of the Spore Photoproduct: A 50-year journey, *Photochem. Photobiol.*, 2015, **91**, 1263–1290.

220 A. M. Siani, G. R. Casale, S. Modesti, A. V. Parisi and A. Colosimo, Investigation on the capability of polysulphone for measuring biologically effective solar UV exposures, *Photochem. Photobiol. Sci.*, 2014, **13**, 521–530.

221 G. R. Casale, M. Borra, A. Colosimo, M. Colucci, A. Militello, A. M. Siani and R. Sisto, Variability among polysulphone calibration curves, *Phys. Med. Biol.*, 2006, **51**, 4413–4427.

222 M.-A. Serrano, J. Canada, J. C. Moreno and G. Gurrea, Personal UV exposure for different outdoor sports, *Photochem. Photobiol. Sci.*, 2014, **13**, 671–679.

223 G. Seckmeyer, M. Klingebiel, S. Riechelmann, I. Lohse, R. L. McKenzie, J. Ben Liley, M. W. Allen, A.-M. Siani and G. R. Casale, A critical assessment of two types of personal UV dosimeters, *Photochem. Photobiol.*, 2012, **88**, 215–222.

224 R. K. R. Scragg, A. W. Stewart, R. L. McKenzie, A. I. Reeder, J. B. Liley and M. W. Allen, Sun exposure and 25-hydroxyvitamin D3 levels in a community sample: Quantifying the association with electronic dosimeters, *J. Expos. Anal. Envion. Epid.*, 2017, **27**, 471–477.

225 A. Russell, M. Gohlan, A. Smedley and M. Densham, The ultraviolet radiation environment during an expedition across the Drake Passage and on the Antarctic Peninsula, *Antarct. Sci.*, 2015, **27**, 307–316.

226 M. Gröbner, J. Gröobner and G. Hulsen, Quantifying UV exposure, vitamin D status and their relationship in a group of high school students in an alpine environment, *Photochem. Photobiol. Sci.*, 2015, **14**, 352–357.

227 U. Feister, G. Meyer, G. Laschewski and C. Boettcher, Validation of modeled daily erythemal exposure along tropical and subtropical shipping routes by ship-based and satellite-based measurements, *J. Geophys. Res.: Atmos.*, 2015, **120**, 4117–4131.

228 G. R. Casale, A. M. Siani, H. Diémoz, G. Agnesod, A. V. Parisi and A. Colosimo, Extreme UV index and solar exposures at Plateau Rosà (3500 m a.s.l.) in Valle d'Aosta Region, Italy, *Sci. Total Environ.*, 2015, **512–513**, 622–630.

229 V. Nurse, C. Y. Wright, M. Allen and R. L. McKenzie, Solar ultraviolet radiation exposure of South African marathon runners during competition marathon runs and training sessions: A feasibility study, *Photochem. Photobiol.*, 2015, **91**, 971–979.

230 A. W. Schmalwieser and A. M. Siani, Review on nonoccupational personal solar UV exposure measurements, *Photochem. Photobiol.*, 2018, **94**, 900–915.

231 C. D. Mobley and B. L. Diffey, The solar ultraviolet environment at the ocean, *Photochem. Photobiol.*, 2018, **94**, 611–617.

232 B. L. Diffey and C. D. Mobley, Sunburn at the seaside, *Photodermatol., Photoimmunol. Photomed.*, 2018, **34**, 298–301.

233 J. Guzikowski, A. E. Czerwińska, J. W. Krzyścin and M. A. Czerwiński, Controlling sunbathing safety during the summer holidays - The solar UV campaign at Baltic Sea coast in 2015, *J. Photochem. Photobiol., B*, 2017, **173**, 271–281.

234 J. Guzikowski, J. Krzyścin, A. Czerwińska and W. Raszewska, Adequate vitamin D3 skin synthesis versus erythema risk in the Northern Hemisphere midlatitudes, *J. Photochem. Photobiol., B*, 2018, **179**, 54–65.

235 W. A. Tellez, W. Nieto-Gutierrez and A. Taype-Rondan, Sunscreen mobile apps: A content analysis, *Eu. Res. Telemed.*, 2017, **6**, 157–163.

236 D. B. Buller, M. Berwick, K. Lantz, *et al.*, Evaluation of immediate and 12-week effects of a smartphone sun-safety mobile application: A randomized clinical trial, *JAMA Dermatol.*, 2015, **151**, 505–512.

237 J. Burke and R. L. McKenzie, Story behind the two UVI Apps: uv2Day and GlobalUV, in *NIWA UV Workshop*, ed. R. L. McKenzie, Wellington, Zew Zealand, 2018, p. 2.

238 D. P. Igoe, A. Amar, A. V. Parisi and J. Turner, Characterisation of a smartphone image sensor response to direct solar 305 nm irradiation at high air masses, *Sci. Total Environ.*, 2017, **587**, 407–413.

239 B. Mei, R. Li, W. Cheng, J. Yu and X. Cheng, Ultraviolet radiation measurement via smart devices, *IEEE Internet of Things Journal*, 2017, **4**, 934–944.

240 A. McGonigle, T. Wilkes, T. Pering, J. Willmott, J. Cook, F. Mims and A. Parisi, Smartphone Spectrometers, *Sensors*, 2018, **18**, 223.

241 R. Bouillon, J. Eisman, M. Garabedian, M. Holick, J. Kleinschmidt, T. Suda and K. Lucas, *Action spectrum for the production of previtamin D3 in human skin*, CIE Report No. 174:2006, Vienna, 2006.

242 CIE, *Erythema reference action spectrum and standard erythema dose, Commission Internationale de l'Eclairage Report No. S 007/E-1998*, Vienna, Austria, 1998, p. 4.

243 F. Snik, J. H. H. Rietjens, A. Apituley, H. Volten, B. Mijling, A. D. Noia, S. Heikamp, R. C. Heinsbroek, O. P. Hasekamp, J. M. Smit, J. Vonk, D. M. Stam, G. Harten, J. Boer and C. U. Keller, Mapping atmospheric aerosols with a citizen science network of smartphone spectropolarimeters, *Geophys. Res. Lett.*, 2014, **41**, 7351–7358.

244 H. Araki, J. Kim, S. Zhang, A. Banks, K. E. Crawford, X. Sheng, P. Gutruf, Y. Shi, R. M. Pielak and J. A. Rogers, Materials and device designs for an epidermal UV colorimetric dosimeter with near field communication capabilities, *Adv. Funct. Mater.*, 2017, **27**, 1604465.

245 Y. Shi, M. Manco, D. Moyal, G. Huppert, H. Araki, A. Banks, H. Joshi, R. McKenzie, A. Seewald, G. Griffin, E. Sen-Gupta, D. Wright, P. Bastien, F. Valceschini, S. Seité, J. A. Wright, R. Ghaffari, J. Rogers, G. Balooch and R. M. Pielak, Soft, stretchable, epidermal sensor with integrated electronics and photochemistry for measuring personal UV exposures, *PLoS One*, 2018, **13**, e0190233.

246 B. Diffey and B. Cadars, An appraisal of the need for infrared radiation protection in sunscreens, *Photochem. Photobiol. Sci.*, 2016, **15**, 361–364.

247 B. Diffey and U. Osterwalder, Labelled sunscreen SPFs may overestimate protection in natural sunlight, *Photochem. Photobiol. Sci.*, 2017, **16**, 1519–1523.

248 M. Norval, L. O. Björn and F. R. D. Gruijl, Is the action spectrum for the UV-induced production of previtamin D3 in human skin correct?, *Photochem. Photobiol. Sci.*, 2009, **9**, 11–17.

249 A. van Dijk, P. den Outer, H. van Kranen and H. Slaper, The action spectrum for vitamin D3: initial skin reaction and prolonged exposure, *Photochem. Photobiol. Sci.*, 2016, **15**, 896–909.

250 J. W. Krzyścin, J. Jarosławski, B. Rajewska-Więch, P. S. Sobolewski, J. Narbutt, A. Lesiak and M. Pawlaczyk, Effectiveness of heliotherapy for psoriasis clearance in low and mid-latitudinal regions: A theoretical approach, *J. Photochem. Photobiol., B*, 2012, **115**, 35–41.

251 J. W. Krzyścin, J. Guzikowski, A. Czerwińska, A. Lesiak, J. Narbutt, J. Jarosławski, P. S. Sobolewski, B. Rajewska-Więch and J. Wink, 24 hours forecast of the surface UV for the antipsoriatic heliotherapy in Poland, *J. Photochem. Photobiol., B*, 2015, **148**, 136–144.

252 X. Fang, A. R. Ravishankara, G. J. M. Velders, M. J. Molina, S. Su, J. Zhang, J. Hu and R. G. Prinn, Changes in emissions of ozone-depleting substances from China due to implementation of the Montreal Protocol, *Environ. Sci. Technol.*, 2018, **52**, 11359–11366.

